

Multiple-Parametric Imaging of Tumour Angiogenesis in Colorectal Cancer

Shih-Hsin Chen

Institute of Nuclear Medicine, Division of Medicine, UCL

This dissertation is submitted for the PhD degree

I, Shih-Hsin Chen, confirm that the work presented in this thesis is my own. Where information has been derived from other sources, I confirm that this has been indicated in the thesis.

Abstract

Angiogenesis is an important aspect in tumour growth. The effectiveness of anti-angiogenic drugs in metastatic colorectal cancer implies importance of this hallmark in the third most common cancer type worldwide. Exosomes, cell-secreted vesicles of approximately 50-150 nm consisting of proteins and microRNAs that are known to affect the behaviours of recipient cells, may be important for tumour cells modulating their environment such as angiogenesis in response to hypoxia. In this study, FDG-PET, CT perfusion and texture analysis performed on the FDG-PET/CT and CT perfusion images were analysed in a cohort of prospectively-recruited colorectal cancer patients. The predictive value of these image parameters on patients' outcome was tested. Correlation between image parameters and angiogenesis markers as demonstrated by immunohistochemical staining on available surgical specimens was also sought. The relationship between exosomal proteins related to hypoxia and proliferation isolated from patient's serum and these parameters was also put to the test.

364 patients were recruited into this ethically approved study from 2007 to mid-2017. CT perfusion was successfully performed in 293 patients. Histology specimen were collected in 153 patients. The follow-up time was 0.3-116 months (median: 33.4 months), during which time there were 96 deaths.

CT perfusion parameters were not predictive of survival. On the FDG-PET/CT images, those with higher TLG had worse survival in patients with colon cancer. Kurtosis of the finely and intermediately-filtered CT images were stable prognosticators in addition to stage when dividing the patients into testing and validating groups in a 2:1 ratio.

On the histology specimens, CD105 was positively correlated with VEGF, while negatively correlated with HIF-1 α . VEGF expression was found to be positively correlated with mean transit time and negatively correlated with mean slope of increase from the CT perfusion scans.

We found P4HA1 in the exosomes increased after hypoxia treatment in cell lines. In exosomes isolated from 54 colorectal cancer patients, we found patients with higher P4HA1 had higher EGFR. The exosomal EGFR signal intensity was negatively correlated with mean slope of increase from CT perfusion scans. However, no difference was found between those with metastatic or localized disease, nor did the exosomal protein expressions affect patient survival.

In summary, a prognosticator, kurtosis of CT images, was found in addition to the clinical stage. Mean slope of increase from the CT perfusion was found to be negatively correlated with VEGF expression on histology specimens and exosomal EGFR intensity. Angiogenesis could be reflected on CT perfusion confirmed by relevant protein expressions in the tumour tissue and exosomes, but not necessarily affect patients' outcome.

Impact Statement

Angiogenesis is essential to tumour development. How it affects clinical images and how it affects patient outcome are not clear. We analysed CT perfusion and FDG-PET images and compared the parameters to proteins associated with angiogenesis and hypoxia on patient tumour tissues and serum exosomes. We demonstrated a method to investigate the protein contents of exosomes isolated from patients' blood. Mean slope of increase from the CT perfusion was found to be negatively correlated with VEGF expression on histology specimens and exosomal EGFR intensity. We also found a prognosticator from texture analysis of the clinical images in addition to clinical stage. It seems angiogenesis could be reflected on CT perfusion scans as confirmed by relevant protein expressions in the tumour tissue and exosomes, but not necessarily affect patients' outcome.

These data are being written for peer review publication

The method we used to analyse the exosome contents could be adopted by the research community to look into many different research questions such as protein interactions within the exosomes, whether certain proteins affect an outcome in a certain group of patients. As exosomes are implicated in cancers, cardiac diseases, neurodegenerative disorders, the potential application could be arched through different specialities. Refinement of our methods on exosome works could lead to

commercialization of blood tests that give hints to various disease status or prognosis stratification.

From the perspective of clinical practice, we found a feature on CT perfusion scans that could reflect angiogenesis. That is useful for monitoring the treatment of anti-angiogenic therapies. Based on our findings, further trials on anti-angiogenic drugs could be designed to incorporate the CT perfusion parameter that could reflect the drugs' effects on angiogenesis. The identified prognostic factor from further analysis of a routine clinical image might help decision making such as whether to give adjuvant treatment without exposing the patients to further radiation or additional time and expense associated with another exam in the hospitals.

Table of Content

Abstract	3
Impact Statement.....	5
Table of Content	7
List of Tables	10
Table of Figures	12
List of Abbreviations	16
Acknowledgements	20
1 Introduction.....	21
1.1 Angiogenesis and hypoxia	21
1.2 Colorectal cancer	23
1.2.1 Epidemiology	23
1.2.2 Diagnosis & staging.....	23
1.2.3 Treatment.....	24
1.2.4 Prognosis	25
1.2.5 Molecular subtypes	25
1.3 Selected proteins involved in tumourigenesis	27
1.3.1 ErbB family	27
1.3.2 cMET	29
1.3.3 HIF-1 α	31
1.3.4 Collagen prolyl-4-hydroxylase (P4HA)	32
1.3.5 S100A8/9	33
1.3.6 VEGF.....	34
1.3.7 CA-IX.....	36
1.4 Exosome	36
1.4.1 As transporters of RNA, proteins	37

1.4.2	As non-invasive markers of malignant diseases.....	39
1.4.3	More than one type of exosomes could be released from colorectal cells.....	41
1.4.4	Exosomes are also implicated in angiogenesis and metastasis	41
1.4.5	Exosomes as immunosuppression signals	42
1.4.6	Exosome contents change with pharmacologic treatment.....	43
1.5	Medical images as a source of biomarkers	43
1.5.1	FDG-PET.....	43
1.5.2	Perfusion images	54
1.5.3	Texture analysis	58
1.6	Summary.....	59
2	Materials & Methods.....	61
2.1	Cell Line Works	61
2.1.1	Hypoxia treatment.....	61
2.1.2	Exosome isolation from culture media.....	61
2.1.3	Western blot.....	62
2.2	Recruitment of Patients	64
2.3	Patient exosome work	64
2.3.1	Exosome isolation from serum.....	64
2.3.2	Nanoparticle tracking analysis	65
2.3.3	Dotblot	65
2.4	CT Perfusion imaging.....	66
2.5	FDG-PET/CT images.....	67
2.6	Texture analysis	68
2.7	Immunohistochemical staining	69
2.8	Statistical methods.....	72
3	Colorectal cancer imaging pertinent to angiogenesis as sources of biomarkers: FDG-PET, CT perfusion and texture analysis in predicting outcome of colorectal cancer patients	73
3.1	Methods	73
3.2	Results	75
3.2.1	Reproducibility of image parameters	75
3.2.2	Image parameters as prognosticators	77
3.2.3	Subgroup analysis by site	81
3.2.4	Subgroup analysis by staging	83

3.2.5	Subgroup analysis by treatment modalities	86
3.3	Discussion	90
4	What do these imaging parameters mean: Correlation with immunohistochemical staining results	95
4.1	Results	95
4.1.1	Associations between IHC parameters	96
4.1.2	Associations between CT perfusion and IHC	97
4.1.3	Associations between PET parameters and IHC	98
4.1.4	Associations between textural parameters (CT and PET) and IHC	99
4.2	Discussion	100
5	What messages are there in seral exosomal proteins	106
5.1	Introduction	106
5.2	Results	108
5.2.1	Antibody specificity test	108
5.2.2	Cell line results	113
5.2.3	Patient data	114
5.3	Discussion	124
6	Summary and Conclusion	131
6.1	FDG PET	131
6.2	CT Perfusion	132
6.3	Texture	132
6.4	Exosomes	133
6.5	Conclusion	135
7	Bibliography	136
8	Appendix	156

List of Tables

Table 1: Summaries of FDG-PET parameters and genetic associations	47
Table 2: Summaries of literatures on FDG-PET parameters and outcome	51
Table 3: Patients' demographics	74
Table 4: Distribution of the stage at subsites.....	74
Table 5: Intra-class correlation coefficient (ICC) and coefficient of variation (CV) of image parameters. *not reliable as some values were negative	75
Table 6: Significant prognosticators from the Kaplan-Meier estimator & Log-Rank test. The texture parameters were listed as “texture parameter_filter level_image modality”. For example, skewness_6_VE meant the skewness calculated from the venous phase of contrast-enhanced CT after filtration with the 6-mm spatial scale filter.	79
Table 7: Cox regression analysis examined the interaction between stage and CT kurtosis. Both parameters were significantly influence patients' survival.	81
Table 8: Significant prognosticators from Kaplan-Meier mean survival & Log-Rank test in colon cancer patients.....	81
Table 9: Significant prognosticators from Kaplan-Meier mean survival & Log-Rank test in rectum cancer patients.....	82
Table 10: Significant prognosticators from Kaplan-Meier mean survival & Log-Rank test in patients with localized diseases.....	83
Table 11: Significant prognosticators in patients with stage 1 disease. No median survival was listed as the three dead patients were distributed in the same side when dichotomized by the median value of these parameters.....	84
Table 12: Significant prognosticators from Kaplan-Meier mean survival & Log-Rank test in patients with stage 2 diseases	84
Table 13: Significant prognosticators from Kaplan-Meier mean survival & Log-Rank test in patients with stage 3 diseases	85
Table 14: Significant prognosticators from Kaplan-Meier mean survival & Log-Rank test in patients with metastatic diseases.....	86
Table 15: Significant prognosticators from Kaplan-Meier mean survival & Log-Rank test in patients treated with primary surgery.....	87
Table 16: Significant prognosticators from Kaplan-Meier mean survival & Log-Rank test in patients treated with only primary surgery without adjuvant treatments	88

Table 17: Significant prognosticators from Kaplan-Meier mean survival & Log-Rank test in patients treated with curative-intended chemoradiotherapy	89
Table 18: Significant prognosticators from Kaplan-Meier mean survival & Log-Rank test in patients treated with palliation	89
Table 19: Summary of significant correlations between IHC & image parameters	95
Table 20: Spearman's correlation coefficient and p-values of the histopathologic staining. Bold font denotes significant correlation after Bonferroni correction ($p < 0.004$).	96
Table 21: Kaplan-Meier mean survival & Log-Rank test of the histopathologic staining results	96
Table 22: Spearman's correlation coefficient and p-values of the histopathologic staining and CT perfusion parameters. Bold font denotes significant correlation after Bonferroni correction ($p < 0.00167$).	98
Table 23: Spearman's correlation coefficient and p-values of the histopathologic staining and FDG-PET parameters. None had the significance level below 0.0025 (the significance level after Bonferroni correction).....	99
Table 24: Correlations between texture parameters and IHC results with p-value less than 0.01	99
Table 25: Significant different parameters between localized and metastatic tumours and their p-value by Mann-Whitney U test. Those with p-value < 0.05 were listed here.....	122
Table 26: Mean survival from the Kaplan-Meier estimator & results of Log-Rank test. The texture parameters were listed as "texture parameter_filter level_image modality". For example, skewness_6_VE meant the skewness calculated from the venous phase of contrast-enhanced CT after filtration with the 6-mm spatial scale filter.	159
Table 27: Spearman's correlation between histopathological results and texture analysis of the PET images. * $p < 0.05$; ** $p < 0.01$	165
Table 28: Spearman's correlation between histopathological results and texture analysis of the non-contrast CT images. * $p < 0.05$; ** $p < 0.01$	167
Table 29: Spearman's correlation between histopathological results and texture analysis of the contrast-enhanced CT images. * $p < 0.05$; ** $p < 0.01$	169
Table 30: Correlation between protein signal intensities from the exosomes and texture parameters from the PET images. * $p < 0.05$; ** $p < 0.01$	171
Table 31: Correlation between protein signal intensities from the exosomes and texture parameters from the non-contrast CT images. * $p < 0.05$; ** $p < 0.01$	173
Table 32: Correlation between protein signal intensities from the exosomes and texture parameters from the contrast-enhanced CT images. * $p < 0.05$; ** $p < 0.01$	175

Table of Figures

- Figure 1. The positions of aorta (arterial input, short arrow) and tumour (long arrow) were selected on the CT images (A). The software would then calculate the CT perfusion parameters such as permeability surface (B), blood volume (C), blood flow (D), time to peak (E), mean transit time (F) as shown here on parametric maps. The average values of each pixel within the tumour were recorded.67
- Figure 2. The PET/CT images were loaded onto the Advantage Workstation. The left was the PET image, and the right was the fusion PET/CT image. After identifying the tumour location, the highest SUV and average SUV within the volume of interest were calculated automatically, as shown in numbers at the right lower corners of each picture.68
- Figure 3. TexRAD analysis of the non-contrast CT image from one patient. The largest section of the tumour was loaded into TexRAD, and the ROI was drawn on the tumour manually (left upper). The software applied filters to extract features of different sizes (fine, medium, coarse as shown in the right upper, left lower, right lower images). A histogram was formed in each filtered image, and the mean, standard deviation, entropy, mean positive pixels, skewness, kurtosis were calculated from the histogram..... 69
- Figure 4. After antigen retrieval by Leica antigen retrieval solution ER2 for 20 minutes, CD105 was stained with Leica NCL-CD105 with the final concentration of 1 mg/ml for 15 minutes, followed by 8 minutes each post primary and polymer, before incubating in DAB for 10 minutes and counterstained with haematoxylin for 2 minutes. (A) showed a field of high microvascular density, in contrast with (B) of low microvascular density. 71
- Figure 5. After antigen retrieval by Leica antigen retrieval solution ER1 for 30 minutes, CA-IX was stained with Leica NCL-L-CAIX with the final concentration of 1 mg/ml for 15 minutes, followed by 8 minutes each post primary and polymer, before incubating in DAB for 10 minutes and counterstained with haematoxylin for 2 minutes. (A) showed a sample with high intensity and extent of CAIX staining whereas (B) showed a sample negative for CAIX.71
- Figure 6. Kaplan-Meier survival curves comparing patients with high (1.0, lower curve) and low (.0, higher curve) CD105. Patients with higher

- microvascular density as counted by CD105 had worse outcome (mean survival 81.96 ± 5.34 versus 64.33 ± 2.26 months, $p = 0.035$).....97
- Figure 7. This work was done by Dr. James Monypenny of Pitmilley. Western blot of the cell lysates of HCC1954 cells treated with control and ALIX shRNA respectively confirmed the knock-down of ALIX (left, upper row); tubulin control confirmed equal protein loading (left, lower row). Dotblot of the exosome confirmed there was little unspecific signals (right, upper row); despite equal protein loading, EpCAM was also decreased in exosomes derived from HCC1954 cells treated with ALIX shRNA as compared to those treated with control shRNA (right, lower row).109
- Figure 8. This work was done by Dr. James Monypenny of Pitmilley. Exosomes from the EGFR knock-down H1975 cell line had little signals from the anti-EGFR antibody on the dotblot (left, upper row), while the presence of exosome proteins was confirmed by CD63 staining (left, lower row). EGFR knock-down was confirmed by western blot (not shown). Those cells treated with EGFR shRNA had around 60% of the EGFR protein expression compared to those treated with control shRNA (right).110
- Figure 9. Western blots and dotblots of anti-HER2 antibody on the HER2 negative cell line MCF7 and HER2 positive cell line HCC1954 confirmed the specificity of anti-HER2 antibody. The presence and absence of HER2 proteins in HCC1954 and MCF7 cells were confirmed by western blot (left). On the dotblot of the anti-HER2 antibody, the exosomes from MCF7 had no signals, while those from HCC1954 were positive. GADPH confirmed the loading of exosome proteins.....110
- Figure 10. Western blot and dotblot of the anti-HER3 antibody on the HER3 negative cell line PC3 and HER3 positive cell line LNCaP confirmed the specificity of anti-HER3 antibody. The western blot done by Dr. Myria Galazi confirmed little HER3 expression in PC3 cells (left). Dotblot of the exosomes derived from the PC3 revealed almost invisible signals, confirming good specificity of the anti-HER3 antibody.111
- Figure 11. Exosomes from cMET knock-down H1975 cells had no visible signals from the anti-cMET antibody on the dotblot, while the presence of exosome proteins was confirmed by tubulin staining. The knock-down was confirmed by the western blot (not shown). The cells treated with cMET shRNA had less than 10% of cMET protein expression compared to those treated with control shRNA (right).112
- Figure 12. Western blot and dotblots of the anti-S100A9 antibody on THP1 and H1975 lysates and exosomes. Western blots revealed S100A9 signals in THP1 lysate, while little signals were detected in the lysate of H1975 (left). The dotblots showed strong signals from THP1 exosomes, but weak signals from H1975 exosomes were also detected (right). The weak signals might be the result of concentration of S100A9 in the exosomes.....112
- Figure 13. Western blot and dotblot of the anti-P4HA1 antibody. On the western blot, P4HA1 signals increased with the concentration of treated cobalt chloride (left). The exosomes from 0.2 mM cobalt chloride treated SW48

- cells had a clear P4HA1 signals on the dotblot; while little signals were detected from the exosomes of control SW48 cells (right)..... 113
- Figure 14. Several colorectal cell lines were cultured in McCoy's 5a Medium Modified supplemented with 10% fetal bovine serum, 1% glycine and penicillin/streptomycin. The normoxic control cells ('N') were incubated at 37 °C in a 5% CO₂ air atmosphere, while the hypoxia treated cells ('H') were incubated in a hypoxic incubator with 5% CO₂ and 1% O₂ at 37 °C overnight. Immunoblotting of cell lysates was performed for the detection of HIF-1 α and P4HA1, along with loading control (GAPDH). 114
- Figure 15. A sample of the nanoparticle tracking analysis result, showing the majority of the isolated particle was less than 100 nm in diameter. ... 115
- Figure 16. Dotblots of patient serum exosomes. Isolated exosomes from a total of 54 patients were stained with EGFR, HER2, HER3, cMET, Alix, S100A9 and P4HA1. Each dot contained 5 μ l of exosomes in PBS from a single patient. Every membrane was dotted in the same fashion, namely, the same position representing the exosome from the same patient. The signal intensities were quantified with a digital imaging platform (GE ImageQuant LAS 4000)..... 115
- Figure 17. Separation correlation of the exosomal protein signals. The signals were normalized by the intensity of ALIX, a protein involved in the exosome synthesis. The correlation coefficients were listed above each bar. Significance level was adjusted by Bonferroni correction ($p < 0.00333$). There was a positive correlation between HER1/HER3, HER2/HER3, HER1/S100A9, HER2/cMET and HER3/cMet..... 116
- Figure 18 (A). Exosomes were isolated from the colorectal cancer cell line HCT116. The upper row showed the dotblots from the normoxic control exosomes. The lower row was from exosomes of cells subjected to 1% oxygen in a hypoxic incubator for 16 hours. Immunoblotting with anti-CD63, an exosomal marker, revealed similar loading of exosomes in each condition. P4HA1 was more than double (as indicated by the P4HA1/CD63 ratio) in exosomes after hypoxic treatment (H = hypoxia, N = normoxia). (B-F) Serum exosomes were isolated from 54 pre-treatment colorectal cancer patients (13 of whom were shown subsequently to have metastasis on staging images). The boxplot shows the median (the middle thick line), interquartile range (IQR, the difference between 75th and 25th percentile, the box), and 1.5x IQR above and below the box (the T-bars). The difference in the amount of exosomal EGFR/HER1, HER2, HER3, c-Met and S100A9 between patients whose exosomal marker for hypoxia (P4HA1) was $>$ vs \leq median, was compared for each of the proteins. The significance level by Mann-Whitney U test is indicated. 117
- Figure 19. Scatter plot of HIF-1 α and GLUT-1 showed negative correlation between these two proteins on tumour specimens ($\rho = -0.710$, $p = 0.001$). No correlation was found between HIF-1 α on the tumour specimen and P4HA1 intensity in the exosomes ($\rho = 0.009$, $p = 0.973$), nor between GLUT1 on the tumour specimen and P4HA1 intensity in the exosomes ($\rho = 0.348$, $p = 0.157$)..... 118

- Figure 20. The boxplot shows the median (the middle thick line), interquartile range (IQR, the difference between 75th and 25th percentile, the box), and 1.5x IQR above and below the box (the T-bars). The difference in the CT perfusion parameter “mean slope of increase” between patients whose exosomal markers for hypoxia (P4HA1) and HER1 was $>$ vs \leq median, was compared. The significance level by Mann-Whitney U test is indicated.119
- Figure 21. Heatmap of Spearman's correlation between image parameters and exosome protein intensities. The correlation coefficients were denoted by the color key as shown on the left upper corner. None of these were significant after Benferroni correction for multiplicity. The exact numbers are shown in the Appendix (Table 27-32).....121
- Figure 22. Radiomic analysis of image parameters from patients. The histogram shows Principal Component (PC)1 of 122 radiomic features. SD & MPP of CT, as well as entropy of PET were among the most weighted parameters constituting PC1, which was able to distinguish metastatic from non-metastatic patients ($p = 0.041$)......123

List of Abbreviations

5-FU	fluorouracil
ALIX	ALG-2 interacting protein X
APC	adenomatous polyposis coli
ATSM	diacetyl-bis(N4-methylthiosemicarbazone)
BF	blood flow
BOLD	Blood oxygenation level-dependent
BRAF	V-raf murine sarcoma viral oncogene homolog B1
BV	blood volume
CA-IX	carbonic anhydrase IX
CEA	carcino-embryonic antigen
CMS	consensus molecular subtype
COX-2	cyclooxygenase-2
CRC	colorectal cancer
CRP	C-reactive protein
CT	computer tomography
CV	coefficient of variation
DCE	dynamic contrast enhanced
EGFR	epidermal growth factor receptor

EpCAM	epithelial cell adhesion molecule
FAP	familial adenomatous polyposis
FDG	fluorodeoxyglucose
F-MISO	fluoromisonidazole
GDP	guanosine-5'-diphosphate
GLUT	glucose transporter
GTP	guanosine-5'-triphosphate
HER2	human epidermal growth factor receptor 2
HER3	human epidermal growth factor receptor 3
HER4	human epidermal growth factor receptor 4
HGF	hepatocyte growth factor
HIF	hypoxia inducible factor
HNPCC	hereditary non-polyposis colorectal cancer
HRAS	Harvey rat sarcoma viral oncogene homolog
HRE	hypoxia response elements
ICC	intra-class correlation coefficient
IHC	immunohistochemistry
KRAS	Kirsten rat sarcoma viral oncogene homolog
LV	leucovorin
MAPK	mitogen-activated protein kinase
MMP	matrix metalloproteinase
MMR	DNA mismatch repair
MPP	mean positive pixels
MRI	magnetic resonance imaging

MTT	mean transit time
MTV	metabolic tumour volume
MVD	microvascular density
MVE	multivesicular endosomes
MV	microvesicles
NRAS	neuroblastoma rat sarcoma viral oncogene homolog
NTA	nanoparticle tracking analysis
P4HA1	prolyl 4-hydroxylase subunit alpha 1
PBS	phosphate buffered saline
PD-L1	programmed death-ligand 1
PET	positron emission tomography
PI3K	phosphoinositide 3-kinase
PKC	protein kinase C
PS	permeability surface area product
RNA	ribonucleic acid
RECIST	Response Evaluation Criteria In Solid Tumors
ROC	receiver operating characteristic
ROI	region of interest
SD	standard deviation
SDS	sodium dodecyl sulfate
shRNA	short hairpin ribonucleic acid
siRNA	small interfering ribonucleic acid
SUV	standard uptake value
TBST	Tris-buffered saline with Tween

TLG	total lesion glycolysis
TNF	tumour necrosis factor
VEGF	vascular endothelial growth factor
VHL	von Hippel-Lindau tumour suppressor

Acknowledgements

This PhD study would not have been possible without the sponsorship of Chang Gung Memorial Hospital, Taiwan. I am indebted to my colleagues in the Department of Nuclear Medicine, Chang Gung Memorial Hospital for their support and share my clinical duties while I performed this thesis. I wish to show my appreciation to my supervisors Prof. Ashley Groves and Prof. Tony Ng. I could not complete the thesis without the help of staff members in the Institute of Nuclear Medicine, UCL Cancer Institute and the School of Cancer at KCL. In particular I would like to name Dr. Simon Wan, Dr. Kjell Erlandsson, Dr. Balaji Ganeshan, Dr. Manuel Rodriguez-Justo, Dr. Sanjay Dindyal, Dr. Jose Miguel Vicencio Bustamante, Dr. James Monypenny, Dr. James Barrett, Dr. Valenti Gomez, Dr. Gregory Weitsman, Dr. Hanna Milewicz, and other members of Prof. Groves team at UCL. I had Yu-Jung Tsai, Drs. Fanfei Gao and Myria Galazi together in the quest of PhD study. Prof. Tim Meyer, Prof. Massimo Pinzani, Prof. John Bridgewater, Dr. Tan Arulampalam and Mr. Daren Francis gave me warm encouragement along the way. A special thanks to Pam O'Donoghue for her enthusiasm and support of the project. Finally, thanks to my family to tolerate my absence.

1 Introduction

1.1 Angiogenesis and hypoxia

Angiogenesis – defined as the formation of new blood vessels by a process of sprouting from pre-existing vessels – is a hallmark of malignant tumour progression [1]. It is an early step in tumourigenesis. Cells require oxygen and nutrients feeding from the vessels. Tumours without vessel supply could not grow more than 2-3 mm [2]. Tumours of that size have less than 1 million cells [3]. Generally, tissues become more hypoxic as further away they sit from the vessel [4]. Under hypoxic conditions, cells have not enough oxygen to conduct oxidative phosphorylation to produce ATP. Instead, they produce ATP in a less efficient way, glycolysis [5]. To match the energy requirement, this consumption of much more glucose results in the accumulation of intermediate products, which ultimately could be used to synthesize biomass such as nucleotides, amino acids and lipids, via anabolic reactions [6]. Interestingly, the accumulation of lactate, an end product of anaerobic glycolysis, increases angiogenesis by promoting endothelial VEGF expression and cell migration [7]. Hypoxia also upregulates pro-survival pathways. In a colorectal cancer cell line, treatment with 1% oxygen upregulated Wnt/ β -catenin pathway, as well as stem cell markers such as c-Myc, SOX2, CD44 [8]. Hypoxia additionally drives the proliferation of a subpopulation of cancer stem-cells, which is known to be resistant to radiation and chemotherapy, as

well as involving in metastases [9]. In this way, tumour cells revert the challenging conditions triggered by hypoxia, utilising hypoxia-induced adaptive mechanisms that facilitate tumour progression.

In the clinical practice of metastatic colorectal cancer, the effectiveness of anti-angiogenic drugs such as bevacizumab and aflibercept illustrates the importance of both angiogenesis and hypoxia as mechanisms driving cancer progression [10] [11]. Because angiogenesis and hypoxia are tightly linked, we can take advantage of this and investigate the blood supply to tissues by CT perfusion. Increased glycolytic activity can be demonstrated on fluorodeoxyglucose positron emission tomography (FDG-PET) scans.

Interestingly as well, for our purposes in this PhD thesis, it has been observed that under hypoxic conditions, there is increase in exosome release in certain tumour models including breast cancer [12] and prostate cancer cell lines [13]. The role of exosomes in cancer progression and signalling will be explained in detail further along. Briefly here, exosomes are nanometric vesicles secreted by virtually all cell types, which carry proteins, nucleic acids and are involved in inter-cellular signalling. Exosomes therefore offer a prognostic value in liquid biopsies as they can be extracted from sera and analysed [14].

In this study, we investigated whether angiogenesis affected patient outcome by applying pertinent clinical images to a large prospectively recruited patient cohort. We also collected exosomes from the sera of the patients recruited later in the cohort. We linked the image parameters to protein expressions of tumour specimens and to exosome profiling. In this way, we combined for the first time clinical imaging and

exosome biopsies to fathom how underlying biologic processes cross-talk with other pathways contributing to tumour proliferation and metastasis.

1.2 Colorectal cancer

1.2.1 Epidemiology

Worldwide, colorectal cancer is the third most common cancer in men and the second in women [15]. In the UK, it is the fourth most common cancer (13% of all new cases). The European Age-Standardised (AS) Incidence Rates is 47.0 per 100,000 population. The incidence rate is increasing since early 1990s. In 2015, there were 41804 new bowel cancer cases in the UK, approximately 110 new diagnosed each day [16].

1.2.2 Diagnosis & staging

When colorectal malignancy is suspected, a colonoscopy should be performed except for those patients with major comorbidity. It allows direct visualization of the lesions, performing biopsy, tattooing and even polypectomy. Once colon cancer is confirmed, computer tomography (CT) is the next staging tool to evaluate the disease extension. After surgery, the T-staging and N-staging could be ascertained. For rectal cancer, the modality of choice is magnetic resonance imaging (MRI) for T-staging and N-staging. CT is used for M-staging [17]. FDG-PET is reserved for equivocal findings on CT or MR, for those contraindicated for contrast medium injection or unable to

tolerate MR, and to evaluate those with potentially resectable metastatic disease to exclude other disease sites that might render surgery ineffective [18].

1.2.3 Treatment

Surgery is the curative method. For early colon cancers such as Tis or T1 disease, endoscopic polypectomy could replace surgical resection in case of no lymphovascular invasion and clear margins. For those with positive lymph nodes, adjuvant chemotherapy is recommended. Adjuvant chemotherapy is additionally recommended for those with stage III and high-risk stage II colon cancer patients.

For clinical T1-2 rectal cancers, trans-anal endoscopic microsurgery (TEM) could be considered. Adjuvant chemo/chemoradiotherapy should be administered if there are positive lymph nodes. For T3 and T4 disease and above, pre-operative radiotherapy or chemoradiotherapy is given before surgery. Adjuvant chemotherapy might be needed [17].

For distant metastasis, systemic treatment is the standard. The possibility of local ablative therapies could be evaluated after 6-8 weeks of systemic therapies. For liver metastasis, complete resection should be attempted. It could be treated by upfront surgical resection and adjuvant chemotherapy for 6 months; another option is three-month chemotherapy followed by surgery and three-month adjuvant chemotherapy.

The systemic therapy is usually fluoropyrimidine-based plus oxaliplatin (FOLFOX) or irinotecan (FOLFIRI). Anti-epidermal growth factor receptor antibodies such as cetuximab and panitumumab are used in patients with RAS wild-type diseases. In patients with RAS mutation, anti-angiogenic drugs could be used [19].

Bevacizumab, a monoclonal antibody against vascular endothelial growth factor (VEGF) has been used in combination with standard chemotherapy regimens [11]. Another anti-angiogenic drug, aflibercept, was also shown to increase overall survival when combined with FOLFIRI [10].

1.2.4 Prognosis

The prognosis of colorectal cancer patients is determined by the stage. In England, 24% of colorectal cancer patients were diagnosed at stage 4 in 2015. The 1-year survival rate for stage 1-3 patients is around 90%; it is around 40% for stage 4 patient. The overall 5-year survival is around 60% for patients diagnosed between 2011 to 2015 and followed up to 2016 [20].

1.2.5 Molecular subtypes

The traditional view of the pathogenesis of colorectal cancer is accumulation of mutations transforming the epithelial cells into benign polyps before progressing to full-blown malignancy [21].

It is estimated that 3-5% of colorectal cancer are hereditary [17]. The most common form is hereditary non-polyposis colorectal cancer (HNPCC) or Lynch syndrome, which is caused by defects in DNA mismatch repair (MMR) genes including MLH1, MSH2, MSH6, and PMS2. Familial adenomatous polyposis (FAP) results from the mutation of adenomatous polyposis coli (APC) gene.

In 2015, Guinney *et al.* [22] defined four consensus molecular subtypes based on gene expression. "CMS1 (microsatellite instability immune 14%), hypermutated, microsatellite unstable, and strong immune activation". They had lower chromosomal

instability as compared to other subtypes. They had less DNA methylation. BRAF mutation is more frequent in this subtype. They are more often right-sided. Once relapsed, the survival is dismal. They do not respond well to anti-EGFR therapies [23].

“CMS2 (Canonical 37%), epithelial, chromosomally unstable, with marked WNT and MYC signalling activation”. They tend to have higher copy number gains of oncogenes, and copy number losses of tumour suppressor genes. miR-17-92 cluster, a MYC target, is upregulated. They are often left-sided. Even after relapse, they tend to have good survival rate. They had good responses to anti-EGFR therapies [23].

“CMS3 (Metabolic 13%), epithelial, with evident metabolic dysregulation”. They have intermediate level of somatic copy number alterations and DNA methylation. KRAS mutation is more common in this subtype than others. They show lower let-7 miR family expression.

“CMS4 (Mesenchymal 23%), prominent TGF- β activation, stromal invasion and angiogenesis”. Their survival is the worst amongst the 4 subtypes. Irinotecan-based chemotherapy had better responses than oxaliplatin-based in this subtype [23].

Microsatellite instability arises from defective DNA mismatch repair. Germline mutation of the MMR genes results in Lynch syndrome. While some cases are sporadic. The sporadic cases are often resulted from methylation of MLH1 gene, associated with serrated polyps and BRAF V600E mutation [21]. Patients with microsatellite instability have better response to immune check-point therapy pembrolizumab [24].

Another mechanism of tumourigenesis is epigenetic instability, demonstrated as hypermethylation of CpG islands and global hypomethylation. These could be caused by overexpression of DNA methyltransferases DNMT3B or DNMT1, as well as genes relating to chromatin remodeling such as CHD8 [21]

Chromosomal instability resulted in aneuploidy or polyploidy, recognizable by changes in chromosome numbers or structural aberrations [21].

1.3 Selected proteins involved in tumourigenesis

1.3.1 ErbB family

This family includes EGFR, HER2, HER3, and HER4. They form dimers with each other and their resultant phosphorylation transmit signals to downstream RAS-RAF-MEK-ERK-MAPK and PI3K-AKT-mTOR pathways promoting cell survival and proliferation [25].

As the EGFR antibodies cetuximab and panitumumab improved progression-free survival of metastatic colorectal patients, the importance of this pathway is beyond doubt [26, 27].

Kountourakis *et al.* reported membranous/cytoplasmic expression of EGFR in 47/30%, membranous/cytoplasmic expression of HER2 in (6/17%), positive HER3 (membranous, cytoplasmic: 17%, 28%) and HER4 (19%, 30%) of colorectal patients. HER4 positivity is correlated with lymph node metastasis [28, 29]. The expression of EGFR or HER2 did not correlate with clinical outcomes [28, 30].

Sun *et al.* meta-analysed 30 studies comprising 4942 patients. They found HER2 was increased in CRC patients, more common in Duke C/D than A/B, and higher in those with lymph node metastasis than without [31].

Richman *et al.* analysed 1914 patients from the QUASAR stage II-III trial and 1342 patients from stage IV trials (FOCUS and PICCOLO). They found only 1.3% & 2.2% patients harbouring HER2 overexpression. It was more common in KRAS/BRAF wild

type patients than in KRAS/BRAF mutated patients. HER2 overexpression was not associated with survival or 5-FU/LV responses [32].

Loree *et al.* retrospectively analysed the tissues of 1038 CRC patients for HER2 & HER3 mutation; additional circulating tumour DNA from 1623 patients were analysed for HER2 mutation. They found HER2 and HER3 mutation in 4.1-5.8% and 5.7% of patients. Both mutations were associated with microsatellite instability and CMS1 subtype. They were not associated with TP53, APC, KRAS, NRAS, BRAF mutations, but ERBB2 mutation was associated with PIK3CA mutation. HER2 mutation was associated with worse survival, while HER3 was not [33].

Jeong *et al.* retrospectively investigated HER2 amplification and outcome in 142 metastatic colorectal patients with wild-type KRAS, NRAS and BRAF treated with cetuximab. 7 patients harboured HER2 amplification and their progression-free survival was worse [34]. Similarly, Sawada *et al.* retrospectively analysed 359 patients with metastatic colorectal cancer and primary tumour resection. Only 15 patients with HER2 amplification, 11 of which harboured wild-type RAS and BRAF. The overall survival was worse in these patients compared to those with wild-type RAS/BRAF without HER2 amplification. When given anti-EGFR treatment, the progression-free survival was also shorter [35].

HER3 was overexpressed in 69% of patients from a retrospective study of 364 patients by Seo *et al.* [36] Ledel *et al.* reported high HER3 expression in 80% of patients. HER3 expression correlated with lymph node and liver metastasis [37]. The same group found it is more commonly associated with distal colon cancer and low-grade tumour. In distal colon cancer patients, the upregulation of HER3 is associated with shorter disease-free survival [38]. Scartozzi *et al.* retrospectively analysed HER3

expression in 84 KRAS wild-type patients treated with irinotecan and cetuximab. They found 52% had HER3 overexpression, and these patients had worse survival than HER3-negative patients [39].

Stahler *et al.* did not find survival difference among HER2 or HER3 expression level in 208 CRC patients treated with first line chemotherapy (either 5-FU/LV + irinotecan or irinotecan + oxaliplatin). However, those with low neuregulin expression had better survival [40].

In summary, HER2 expression is less common in colorectal cancers than HER1 and HER3. Some reports suggested the expression of HER2 or HER3 is associated with metastasis and sometimes indicated worse outcome.

1.3.2 cMET

c-MET is a tyrosine kinase surface receptor activated by hepatocyte growth factor (HGF). On binding of HGF, c-MET dimerizes and activates downstream signals through RAS-MAPK and PI3K/AKT pathways among others [41].

In colorectal cancer, Raghav *et al.* found only 1-2% cMET amplification in 4 cohorts patients (n=795). However, in one cohort (Cohort 4), the amplification rate reached 22.6% in EGFR target therapy refractory patients [42].

Gayyed *et al.* found c-MET was over-expressed in 66.7% of their 102 primary CRC tumours. There was positive correlation between c-MET expression and higher TNM staging. The expression of c-MET is higher in metastatic tissues than in primary tumours [43].

c-MET expression is associated with poor overall and progression-free survival. Lee *et al.* retrospectively studied 255 stage IV CRC patients. C-MET overexpression was

found in 15.3% of their patients. Although c-MET overexpression did not correlate with primary site, differentiation or metastatic sites, it denoted worse overall survival and progression-free survival for bevacizumab treatment [44]. Shoji *et al.* reported higher c-MET expression in primary CRC conferred a shorter relapse-free survival after liver metastectomy [45]. Al-Maghrabi *et al.* reported high c-MET expression is associated with larger tumour and left-sided tumour; also conferring higher local recurrence rate [46].

Senetta *et al.* in 81 rectal cancer patients treated with neoadjuvant CCRT found the expression of c-MET and YKL-40 predicted higher risk of non-complete response [47]. Schweiger *et al.* found overexpression of c-MET or phosphorylated signal transducer and activator of transcription 3 (pSTAT3) worsened survival after lung metastectomy from CRC [48].

c-MET activation is involved in the resistance to anti-EGFR therapy. KRAS wild-type cells could resist anti-EGFR therapy by c-MET activation [49]. Takahashi *et al.* found KRAS wild-type colorectal patients treated with anti-EGFR antibody had shorter survival time if they had elevated serum level of the ligand of c-MET, HGF [50].

The c-MET pathway is also involved in angiogenesis. After anti-angiogenic therapy, HGF promoted GLUT1 for glycolysis and autophagy, thus evading CRC cell death, suggesting additional resistance mechanisms driven by c-MET [51]. The ligand of c-MET, HGF, could induce HIF-1 α mRNA expression and VEGF expression in a different model [52]. Jia *et al.* found that inhibition of c-MET by shRNA in SW620 cells increased apoptosis and decreased HIF-1 α expression after exposure to irradiation [53].

Cancer-associated fibroblasts secrete HGF to enhance the proliferation and invasiveness of colonic epithelial cancer cells by activation of PKC-cMET-ERK1/2-COX-2

signalling [54]. These findings illustrate the relevance of the HGF/c-MET axis in driving tumorigenesis and resistance to chemotherapy/radiotherapy.

1.3.3 HIF-1 α

Hypoxia in tumours leads to HIF-1 α stabilization and allows dimerization with HIF-1 β to bind to hypoxia response elements (HRE) on the target genes. This induces epithelial-mesenchymal transition via loss of E-cadherin, increase of vimentin and transcription suppressors of E-cadherin including SNAIL and TWIST. Matrix metalloproteinases (MMP) 2 and 9 were also regulated by HIF-1 α and HIF-2 α , allowing tumour cells to cross basement membrane for invasion and metastasis [55]. Other targets of HIF include VEGF, carbonic anhydrase IX (CA-IX), glucose transporters (GLUTs), hexokinases (HKs), transforming growth factor (TGF), C-MYC, amongst others. Thus HIF-1 impacts on a wide range of pro-tumorigenic responses involving angiogenesis, glucose metabolism, cell proliferation, invasion and metastasis [56]. The hypoxia status of tissues can be interrogated by positron emission tracers, such as fluoromisonidazole (F-MISO). It is a nitroimidazole compound that can be reduced by tissue reductase and covalently binds to thiol groups of intracellular proteins, thus being trapped inside hypoxic cells [57].

Cao *et al.* retrospectively reviewed the paraffin-embedded samples of 71 resected colorectal cancers. They found expression of HIF-1 α and VEGF in 54.9% and 56.3% patients. Their expressions were correlated and associated with tumour stage and overall survival of these patients [58]. Rasheed *et al.* found that in 90 rectal cancer patients treated with surgery, HIF-1 α , but not HIF-2 α correlated with staging, vascular invasion, recurrence and survival [59]. Shiyoma *et al.* in 50 rectal cancer patients

treated with hyperthermo-chemoradiotherapy followed by surgery, found those with positive HIF-1 α expression had worse survival than negative ones [60]. Shimomura *et al.* also found high HIF-1 α expression was a risk factor for tumour recurrence after liver metastases from colorectal cancers treated with liver transplant [61].

One retrospective study by Saka *et al.* consisting of 186 CRC patients found 94.0% and 15.6% of the cases were positive for HIF-1 α and CA-IX staining. There was no correlation between HIF-1 α or CA-IX staining intensity and patients' survival or clinicopathologic features [62].

Kaidi *et al.* found that in the CRC cell line HT-29 HIF-1 α bound to the promoter of cyclooxygenase-2 (COX-2). Thus in hypoxic conditions, COX-2 upregulation increased prostaglandin E2 (PGE2), which induced ERK phosphorylation of the MAPK pathway leading to cell proliferation. Activation of the MAPK pathway also increased HIF-1 α transcription, forming a positive feedback loop [63].

Ahn *et al.* showed HIF-1 α , not HIF-2 α , promoted VEGF and S100/A8 expression in monocytes; these two proteins cooperatively enhanced neovascularization [64].

Utilizing siRNA of HIF-1 α and HIF-2 α , Imamura *et al.* showed in SW480 cell line, HIF-1 α promoted tumour growth and migration, while HIF-2 α restrained growth [65].

1.3.4 Collagen prolyl-4-hydroxylase (P4HA)

(2S,4R)-4-hydroxyproline is required for stabilization of the collagen triple helix structure at physiologic temperature. Proline on procollagen is hydroxylated by prolyl-4-hydroxylase. Prolyl-4-hydroxylase is a $\alpha_2\beta_2$ tetramer. Its α subunit (P4H α) weighs 59-kDa, consisting of a peptide-substrate binding site and an enzymatic site. There are three isoforms of the P4H α subunit in vertebrates, α (I) being the most prevalent. The β

subunit is 55-kDa, functioning independently as protein disulfide isomerase (PDI). It helps retain the α subunit in a soluble active form in the endoplasmic reticulum [66].

Under hypoxia, HIF-1 induces expression of collagen prolyl (P4HA1 and P4HA2) and lysyl (PLOD2) hydroxylases in fibroblasts, mediating ECM remodeling, promoting breast cancer invasion and metastasis [67, 68].

The increase of type I collagen prolyl-4-hydroxylase also leads to prolyl-hydroxylation of Argonaute2 (Ago2), which inhibits Ago2 degradation as well as increases the association of Ago2 with heat shock protein 90 (Hsp90), leading to the loading of microRNAs (miRNAs) into the RNA-induced silencing complex (RISC), and translocation to stress granules. This leads to increase of miRNA production [69]. On the other hand, hypoxia could potentiate the association between EGFR and Ago2 leading to the phosphorylation of Ago2 at Tyr 393 which inhibits miRNA processing from precursor miRNAs to mature miRNAs by reduces the binding of Dicer to AGO2 [70].

1.3.5 S100A8/9

The heterodimer S100A8/9 is a ligand for the receptor for advanced glycation end products (RAGE) and for Toll-like receptor 4 (TLR4). They are found to be abundant in places rich in myeloid-derived suppressor cells (MDSC), which provide environment for cancer cell growth in the pre-metastatic niches [71].

Burke *et al.* showed exosomes released from myeloid-derived suppressor cells contain S100A8/9. They can induce a macrophage switch into the M2 type (pro-tumorigenic) and are also chemotactic for myeloid-derived suppressor cells [72].

S100A8 and S100A9 are controlled by HIF-1. HRE was identified on promoters of S100A8 and S100A9. Grebhardt *et al.* found HIF-1 α increased the expression of S100A8/A9 in prostate epithelial cell line BPH-1. They also found in 165 prostate cancer samples that HIF-1 α expression was correlated with both S100A8 and S100A9 [73]. Using mice deficient for VHL (thus stabilizing HIF-1), Ahn *et al.* found increased angiogenesis mediated by increased VEGF and S100A8 production from monocytes through HIF-1 α , not HIF-2 α [64].

Bassorgun *et al.* found higher S100A8/9 positive inflammatory cells in the colorectal tumours or peritumour regions correlated with higher tumour grade and presence of metastasis [74]. S100A8/9 could promote colorectal cell line survival and migration via β -catenin and its downstream targets c-Myc and MMP7 [75]. S100A8 and S100A9 were increased in exosomes from SW620 as compared to SW480. SW620 is derived from the lymph node metastasis of the SW480 primary tumour. These results suggested the importance of S100A8/9 in CRC metastasis [76].

1.3.6 VEGF

The vascular endothelial growth factor family consists of VEGF-A, VEGF-B, VEGF-C, VEGF-D and placental growth factor. There are three main receptors, VEGFR-1-3. VEGF signalling is augmented by hypoxia, promoting endothelial proliferation, as well as monocyte and macrophage migration. Bevacizumab, an antibody against VEGF-A, and aflibercept, binding to VEGF-A, VEGF-B and PlGF, have been approved for the treatment of metastatic colorectal cancer [77].

As a first-line treatment of metastatic colorectal cancer, the addition of bevacizumab to oxaliplatin-based treatment (capecitabine + oxaliplatin (XELOX) or

fluorouracil + leucovorin + oxaliplatin (FOLFOX)) prolonged the progression-free survival by 3.1 months (17.9 vs 14.6 months, $p = 0.008$) [78]. In another trial as a second-line treatment, the addition of bevacizumab to FOLFOX significantly improved the response rate from 8.6% to 22.7% [79].

In metastatic colorectal cancer patients previously treated with oxaliplatin, the addition of aflibercept to FOLFIRI (fluorouracil + leucovorin + irinotecan) prolonged overall survival (median 13.50 vs 12.06 months) and progression-free survival (6.9 vs 4.67 months) [10].

VEGF expression in the CRC tissue sample was correlated with outcome as shown by Cao *et al.*, who retrospectively reviewed the paraffin-embedded samples of 71 resected colorectal cancers and found the expressions of VEGF and HIF-1 α were correlated and were associated with tumour stage and overall survival of these patients. The expression of HIF-1 α and VEGF were shown in 54.9% and 56.3% patients [58].

Anti-VEGF treatment can increase EGFR activities as well as result in hypoxia. Mesange *et al.* found that bevacizumab treatment increased EGFR activities in CRC cell lines, which could be blocked by erlotinib regardless of the RAS status [80]. Rahbari *et al.* found anti-VEGF treatment resulted in hypoxia and leading to increased expression of hyaluronic acid (HA) sulfated glycosaminoglycans (sGAGs) in the extracellular matrix of the tumour, which prevented entry of chemotherapy. Decreased microvascular density could be found after 3 days of bevacizumab. The area of increased hyaluronic acid deposition corresponded to areas of hypoxia [81].

1.3.7 CA-IX

Carbonic anhydrase IX converts carbonic dioxide and water to bicarbonate and proton. It is activated by HIF-1, along with MCT4 (monocarboxylate transporter 4) which transports lactate out of cells, and NHE1 (sodium-hydrogen exchanger 1) which take sodium into the cell in exchange of proton [82]. These proteins maintain an intracellular alkaline pH while increasing the acidity of the extracellular space. This acid-resistant phenotype was associated with tumour invasiveness [83].

1.4 Exosome

Exosomes are extracellular vesicles enclosed by lipid-bilayers. They are nanometric, of approximately 50-150 nm in diameter, produced by most cell types and released into various body fluids such as serum, saliva, urine, cerebrospinal fluid amongst others. The contents of exosomes include lipids, nucleic acids and proteins [84]. They were first described in 1984 by Harding *et al.* as they found that rat reticulocytes were able to endocytose gold-labelled transferrin (Tf) receptors and accumulate them inside a pre-lysosomal endosome containing multiple vesicles (MVE, from multivesicular endosomes). After the endocytosis of Tf receptors and their incorporation into the limiting membrane of inclusion vesicles inside the MVE, these vesicles were discharged by MVE exocytosis [85].

It is now widely accepted that MVE fuse with the plasma membrane to release exosomes to the extracellular space [86]. The contents of exosomes include some common proteins, such as chaperones (Hsp70 and Hsp90), proteins associated with the endosomal complex required for transport (ESCRT) pathway (TSG 101, ALIX),

proteins involved in transport and fusion (Rab proteins, annexins), and the classic exosomal markers that span the lipid bilayers four times, hence called tetraspanins (CD9, CD63, CD81, CD82) [87, 88]. Other proteins are cell-type specific. Exosomes can transfer their contents from parental cells to specific targets via tetraspanin–integrin complex [89]. They have been implicated in cell proliferation, metastases, angiogenesis and immunosuppression [14]. Currently exosomes are viewed and accepted as a type of inter-cellular communication.

Exosomes differ from other types of extracellular vesicles in their release mechanism and also in their size. The larger cousins of exosomes are microvesicles (MV), which range between 200-1000 nm in size. Unlike exosomes, MVs are not produced inside an organelle and they are not released in mass via MVE exocytosis. Instead, MVs are produced by viable cells via budding and shedding off from the plasma membrane. Therefore all MVs contain surface markers from their parental cells, whereas in exosomes this is not the case, and thus their origin can be more difficult to track [90]. For similar reasons, exosomes reflect more of a full intracellular profile rather than a surface-restricted profile of their parental cells, and it is one of the reasons why we are interested in them. Another type of extracellular vesicles are apoptotic bodies, which are larger (1-2 μm) and are released by dying cells via blebbing off from the plasma membrane.

1.4.1 As transporters of RNA, proteins

Chiba *et al.* found that exosomes from three colorectal cell lines HCT-15, SW480 and WiDr contained RNA and could be taken up into other cells including the hepatocellular carcinoma cell line HepG2 and the lung cancer cell line A549 [89].

Demory Beckler *et al.* found exosomes from KRAS-mutant cell lines could transfer the mutant KRAS to wild-type cell line and promoting its growth [91].

Cha *et al.* compared miRNA profiles of CRC cell lines different only in their KRAS mutation status. While the whole-cell miRNA profiles were similar, the exosomal miRNA profiles were different on principal component analysis. Exosomes from wild-type KRAS cells were enriched with miR-10b, while miR-100 was increased in the KRAS mutant exosomes [92].

Soldevilla *et al.* found Δ Np73, a TP73 gene-derived isoform that lacks the amino terminal transactivation domain, in exosomes from the colon cancer cell line HCT116. Not all the cell lines tested could receive the Δ Np73 from exosomes. In the positive recipient cell lines, the proliferation rate was increased after incubation with Δ Np73-containing exosomes. The level of exosomal Δ Np73 in patient blood correlated with serum CEA level [93].

Wang *et al.* found that exosomes from a colorectal cancer cell line (HT-29) with high metastatic potential to the liver could increase the originally low metastatic potential cell line, Caco-2 in mice, in both metastatic volume and distribution to the liver [94].

Hu *et al.* reported that exosomes from fibroblasts could promote the growth of cancer stem cells even when treated with 5-FU or oxaliplatin, and this effect was mediated via Wnt pathway [95].

Wang *et al.* found CD44v6 (cancer initiating cell marker) cooperates with other CIC marker such as Tspan8 to interact with integrins and proteases, promoting cell invasion and metastases. In CD44v6 knock-out cells, these properties were suppressed,

but could be partially rescued by transferring exosomes from the wild type CIC which contains CD44v6 [96].

Lugini *et al.* found exosomes from CRC cells could induce phenotypic changes of mesenchymal stromal cells into more proliferative, invasive cells. Their vacuolar H⁺-ATPase expression was increased, promoting an acidic environment. CEA expression was also increased [97].

Song *et al.* found after 2 Gy radiation, bronchial epithelial cells exported miR-7-5p into their exosomes, which was able to induce autophagy through the EGFR/AKT/mTOR pathway in recipient cells [98]. These findings illustrate how exosomes can mediate the transfer of pro-tumorigenic functions from parental cells to recipient cells via shuttling both RNA molecules and proteins.

1.4.2 As non-invasive markers of malignant diseases

In addition to carrying pro-tumorigenic molecules, the identification of certain exosomal proteins and microRNAs derived from tumours has led insight into the potential use of exosomes as biomarkers. This is particularly useful in liquid biopsies, as blood from patients at different stages of disease/treatment allows the obtention of serum, plasma and immune cells. Using serum exosomes or immune cells allows a deeper layer for understanding patient phenotypes and possibly stratification. Combining the exosomal information with the patients' imaging data is one of the main interests of our study. The following examples illustrate how exosome levels, or the abundance of different molecules that have been identified in exosomes from cancer patients, can correlate with patient outcomes.

Silva *et al.* quantify the number of exosomes by cytometry in the plasma of 91 colorectal patients. They found high level of exosomes associated with carcinoembryonic antigen level and poorly differentiated tumours [99].

In an exploratory study utilizing microfluid chips to isolate exosomes, Fang *et al.* captured EpCAM-positive exosomes from the blood and found that 6 patients with breast cancer had more of these EpCAM-positive exosomes than 3 control subjects [100].

Menck *et al.* isolated exosomes from patients with various cancer. They noted matrix metalloproteinase inducer EMMPRIN was increased throughout the cancer types. Higher EMMPRIN expression correlated with worse survival. Other proteins such as MUC1, EGFR and EpCAM were tumour type specific [101].

Matsumura *et al.* found elevated serum exosomal miR-19a in colorectal patients. Those with higher serum exosomal miR-19a had worse survival than those with lower level [102].

Ogata-Kawata *et al.* analysed the miRNA of serum exosomes from 88 colorectal patients and 11 healthy controls. They found elevated level of 7 miRNA (let-7a, miR-1229, miR-1246, miR-150, miR-21, miR-223, and miR-23a) in colorectal patients. The level decreased with removal of primary surgery. This could be used as a non-invasive diagnostic tool [103]. Similarly, Ostenfeld *et al.* look for EpiCAM positive extracellular vesicles in the blood of CRC patients before and after surgery. They found (miR-16-5p, miR-23a-3p, miR-23b-3p, miR-27a-3p, miR-27b-3p, miR-30b-5p, miR-30c-5p and miR-222-3p) were increased as compared to healthy controls but decreased after surgery [104].

1.4.3 More than one type of exosomes could be released from colorectal cells

Using immunoaffinity beads, Tauro *et al.* isolated A33 and EpCAM containing exosomes from LIM1863 colorectal cancer cell lines. Analysis of the protein contents by mass-spectroscopy found differential enrichment of proteins. Basolateral trafficking molecules such as early endosome antigen 1, the Golgi membrane protein ADP-ribosylation factor, and clathrin were enriched in A33-containing exosomes. While classic apical trafficking molecules such as CD63 (LAMP3), mucin 13, the apical intestinal enzyme sucrase isomaltase, dipeptidyl peptidase IV and the apically restricted pentaspan membrane glycoprotein prominin 1 were identified in EpCAM-containing exosomes. Colocalization of EpCAM, claudin-7, and CD44 was also observed [105].

Exosomes released from cell lines established from the primary tumour (SW480) and metastatic site (SW620) of the same patient were also shown to be different in their contents. Exosomes released from the metastatic cell line were proportionally enriched with metastatic factors (MET, S100A8, S100A9, TNC), signal transduction molecules (EFNB2, JAG1, SRC, TNK1), lipid raft and lipid raft-associated components (CAV1, FLOT1, FLOT2, PROM1) [76].

1.4.4 Exosomes are also implicated in angiogenesis and metastasis

Hong *et al.* found that exosomes from colorectal cancer cell lines could increase the proliferation capabilities of endothelial cells. mRNA associated with cell-cycle related processes, especially M phase, were enriched in these exosomes. This implies

that exosomes released from colorectal cancer cells might promote angiogenic proliferation in neighbouring endothelium [106].

Yoon *et al.* also found that exosomes from the SW480 cell line promoted endothelial cell proliferation and migration. This action was blocked by siRNA-mediated silencing of early growth response-1 (Egr-1), as well as by inhibition of ERK1/2 (by PD98059) and JNK (by SP600125) [107].

Huang *et al.* found that exosomes secreted from hypoxic CRC cell lines were enriched with Wnt4, which induced β -catenin translocation in endothelial cells. Wnt4- β -catenin pathway promoted angiogenesis of the tumour [108].

In addition to angiogenesis, tumour-related exosomes also contribute to tumour metastasis. Breast cancer cells could take up exosomes secreted by stromal fibroblast, enhancing the WNT signalling for increased invasiveness and metastasis [109].

Exosomes from melanoma cells can promote vascular leakage at pre-metastatic sites and promote bone-marrow progenitors to form the niche via MET expression [110].

Exosomes from renal cancer stem cells can activate endothelial cells to form capillary-like structures and promote the formation of a premetastatic niche via MMP2, MMP9 and VEGFR1 [111].

1.4.5 Exosomes as immunosuppression signals

Several immunomodulatory signals have been detected in exosomes including TNF and PD-L1 [112]. Huber *et al.* found microvesicles released by human colorectal cancer cells and those found in plasma of colorectal cancer patients contained Fas ligand (FasL) and TNF-related apoptosis-inducing ligand (TRAIL), inducing dose-dependent apoptosis

(annexin V/propidium iodide) in activated human T cells. The apoptosis could be blocked by anti-Fas or TRAIL antibody and pan-caspase inhibitor [113].

Yamada *et al.* found extracellular vesicles from colorectal cells were rich in TGF- β and were able to transform T-cells into T-reg to promote tumour growth by activating TGF- β /Smad signalling and suppressing SAPK signalling [114].

Recently, our group identified a correlation between ALIX and PD-L1 exposure, spreading further the relationship between exosome production and the immunogenicity of tumours [115].

1.4.6 Exosome contents change with pharmacologic treatment.

Ragusa *et al.* found exosome contents of Caco-2 (cetuximab-sensitive) and HCT-116 (cetuximab-resistant) CRC cell lines changed after cetuximab treatment. The changes in Caco-2 cells included those related to proliferation and inflammation; while changes in HCT-116 cells related to cell to cell signalling. Adding exosomes from cetuximab-treated Caco-2 into HCT-116 increased the viability of HCT-116, but not vice versa [116].

1.5 Medical images as a source of biomarkers

1.5.1 FDG-PET

FDG is a glucose analogue. It can be transported into the cells by glucose transporters and phosphorylated by hexokinase into FDG-6-phosphate. FDG-6-phosphate cannot go further into the metabolic pathways and is trapped inside the

cells unless dephosphorylated by phosphatases. Cancer cells often have high glycolysis activities [117]. With increased glucose transporter and hexokinase, cancer cells accumulate FDG-6-phosphate and can be visualized by the PET scanners. FDG-PET has been therefore widely utilized for cancer detection. High FDG uptake often denotes worse prognosis [118]. In addition, hypoxia was shown to increase FDG uptake through an increase of glucose transporters [119].

In colorectal cancer staging, FDG-PET is used when there are uncertainties after CT or MR, especially for suspicious liver lesions found on CT as FDG-PET has higher sensitivity and specificity for hepatic lesions [120].

Lubezky *et al.* analyzed 27 patients for hepatectomy and 48 patients receiving hepatectomy after neoadjuvant therapy. They found decreased sensitivity of both CT and FDG in detecting metastatic lesions after neoadjuvant therapy. FDG was worse than CT in the neoadjuvant setting, especially in those that received bevacizumab therapy [121]. A similar report by Carnaghi *et al.* [122] evaluated 65 liver lesions in 19 patients who received pre-operative chemotherapy. The sensitivity of FDG-PET and CT was 62% and 70% respectively. FDG performed better in lesions larger than 1 cm (74% vs 18%). Metser *et al.* compared FDG-PET performance with CT for detection of other metastasis before liver resection of metastatic CRC tumours. 50 patients received chemotherapy within 90 days, and 37 were responders. They found that in those patients who responded to chemotherapy, the FDG-PET and CT performance was similar. However, in all other patients, FDG-PET found more extrahepatic disease (in 11.7%) or significantly more liver lesions (18.3%) than CT [123].

1.5.1.1 Association with gene expression or mutation

1.5.1.1.1 EGFR

Choi *et al.* reviewed the records of 132 patients who underwent FDG-PET before surgical resection of the primary colorectal cancers. They found the SUVmax was higher in EGFR-positive tumours (N=86, 65.2%) than negative ones (12.1 ± 2.1 vs. 10.0 ± 4.2 ; $p = 0.012$) [124]

1.5.1.1.2 KRAS

Oner *et al.* reported that simple parameters such as SUVmax, or MTV could not differentiate KRAS mutation status (of codon 12, 13) in a retrospective study consisting of 55 CRC patients. There was no difference between 20 KRAS mutant and 35 KRAS wild type patients in these FDG-PET parameters [125]. Similarly, Krikelis *et al.* failed to find correlation between FDG uptake and KRAS codon 12, and 13 mutation status in a retrospective study consisting of 44 metastatic colorectal cancer patients. The SUVmax was not different in 27 KRAS mutant patients and 17 KRAS wild type patients [126].

Kawada *et al.* found higher SUVmax in the primary tumour of KRAS/BRAF mutated group in 51 patients. They noted GLUT-1 but not hexokinase II expression was associated with FDG uptake [127]. In 55 metastatic lesions, they found higher SUVmax in the KRAS mutated group only if lesions > 10mm was considered [128].

Chen *et al.* in 103 patients found TP53, KRAS, APC, PIK3CA, BRAF mutation in 41/103 (40%), 34/103 (33%), 27/103 (26%), 5/103, 4/103 patients. They found higher

SUVmax in TP53 mutated tumours, as well as higher lesion glycolysis with a SUV40% threshold in KRAS mutated tumours [129].

Another report by Cho *et al.* in 93 metastatic CRC patients found higher SUVmax, SUVmean, TLG of the primary tumours in KRAS mutant cases. They also found lung metastases were more frequent in patients with mutant KRAS while liver metastasis were more frequent in patients with KRAS wild type [130]. Lovinfosse *et al.* genotyped KRAS on codons 12, 13, 61, 117 and 146, NRAS on codons 12, 13 and 61 and BRAF on codon 600 in 151 rectal cancer patients. They found 74 patients had a KRAS mutation, 9 NRAS, and none had BRAF mutation. Higher SUVmax (p-value = 0.002), SUVmean were noted in RAS mutated group. There was significant difference between RAS mutated and wild-type groups in skewness (p-value = 0.049), SUV standard deviation (p-value = 0.001) and SUV coefficient of variation (SUVcov) (p-value = 0.001). No correlation was found by metabolic tumour volume, total lesion glycolysis or other local/regional texture parameters [131].

Lee *et al.* in 179 CRC patients treated with surgery found those with elevated c-reactive protein (CRP, > 6 mg/L) had higher tumour volume, SUVmax, SUVmean. In those with normal CRP (< 6 mg/L, N=132), higher SUVmax was associated with KRAS mutation [132].

Iwamoto *et al.* using cell line work found GLUT-1, HK-II were higher in KRAS mutant cells. HIF-1 α induction was higher in KRAS mutant cells, thus inducing higher GLUT-1 expression. They found positive correlation between KRAS mutation, GLUT-1 and HIF-1 α expression in clinical samples [133].

Miles *et al.* in 33 CRC patients treated with primary surgery found a decision-tree consisting of SUVmax of FDG-PET, mean-positive-pixels from histogram analysis of the

non-contrast CT images (MPP), and blood flow (BF) from perfusion CT determined the KRAS mutation status with an accuracy of 90.1%. In addition, two distinct phenotypes were found among KRAS mutant tumours; those with high SUVmax and low MPP tended to be hypoxic (HIF-1 +), while those with low SUVmax, high MPP and high BF tended to be proliferative (mcm2 +) [134].

1.5.1.1.3 VEGF

Kocael *et al.* in 63 CRC patients found higher serum VEGF and VEGFR in FDG-PET positive than in FDG-PET negative patients. VEGF-D, VEGF-A, VEGF-C, VEGF-E, and VEGFR-3 were higher in patients with metastasis than without [135].

These results are summarized in Table 1.

Table 1: Summaries of FDG-PET parameters and genetic associations

Gene	FDG-PET parameter	Finding	Reference
EGFR	SUVmax	Higher in EGFR(+) tumours	123
KRAS	SUVmax	not associated with KRAS mutation status	124, 125, 128
	SUVmax	Higher in KRAS mutant tumours	126, 127, 129, 130
	SUVmax	Higher in KRAS mutant tumours in patients with normal CRP	131
	Glycolysis	Higher in KRAS mutant tumours	128, 129
	Glycolysis	not associated with KRAS mutation status	130
VEGF	Positivity	Higher serum VEGF in FDG(+) patients	134

1.5.1.2 Correlation with patient outcome

Shi *et al.* reviewed 107 prospectively-recruited CRC patients treated with surgery. Univariate analysis found prognosticators including tumour size, TNM stage, nodal metastasis, the ratio of metastasized nodes to retrieved nodes, cyclin D1 immunostaining and SUVmax. In multivariate analysis, only TNM stage and SUVmax remained prognosticators [136].

Ogawa *et al.* retrospectively compared the overall survival of 325 patients undergoing surgery. They found MTV and TLG could differentiate the survival of these patients. In multivariate regressions, high TLG, age ≥ 65 years old, rectal tumours and positive lymph node metastases were independent poor prognosticators [137].

Lee *et al.* followed 163 surgical patients. They found SUVmax did not differ between patients with recurrence and without. After dividing the patient group with the median value of SUVmax, both groups did not show different disease-free survival either [138].

In 73 rectal patients undergoing surgical resection, Jo *et al.* found advanced stage, higher MTV, TLG, and positive surgical margins were associated with worse overall survival. However, only surgical margin was the independent prognosticator in Cox regression [139].

Nakajo *et al.* investigated the prognostic impact of clinicopathologic factors and image parameters in 32 surgically-treated CRC patients. They found those with high stage ($p = 0.004$), high ^{18}F -FDG-intensity variability [IV] ($p = 0.015$), high ^{18}F -FDG-size-zone variability ($p = 0.013$) and high ^{18}F -FLT-entropy ($p = 0.015$) had significantly worse progression free survival by log rank test [140].

Bone marrow SUV [141] and tumour-to-liver ratio [142] were claimed to be prognosticator in CRC patients treated with surgery. Lee *et al.* reviewed 226 CRC patients treated with surgery and found higher SUV of the bone marrow was correlated with worse recurrence-free survival [141]. Hunag *et al.* found tumour-to-liver ratio was a prognosticator independent of lymphovascular/neural invasion in 118 stage II CRC patients [142].

Bang *et al.* in 74 rectal cancer patients undergoing neoadjuvant chemoradiotherapy followed by resection found higher metabolic tumour volume and gradient-kurtosis were associated with worse 3-year disease free survival. Multivariate analysis found gradient-kurtosis remained significant. No parameters were associated with tumour regression grade (TRG) in the multivariate analysis [143]. Kim *et al.* performed FDG-PET before and after 45 Gy of radiotherapy with concurrent oral capecitabine chemotherapy in 64 rectal cancer and found high MTV of the first PET and smaller changes of TLG were associated with worse outcome in multivariate Cox regression [144].

In a prospective study, 27 metastatic CRC patients received cetuximab as third-line therapy. After one week of therapy, the increase of metabolic activity denoted poor progression-free survival and overall survival. At 4 weeks after therapy initiation, both PERCIST 1.0 (PET response criteria in solid tumours) and change in metabolic activity predicted survival [145].

In another prospective study, Lim *et al.* followed 40 patients treated with regorafenib. They found those with higher TLG40% had worse overall survival. The change of TLG40% after 2-weeks of treatment predicts both progression-free survival

and overall survival, and could further stratify patients with stable disease on RECIST 1.1 [146].

In 105 biopsy-confirmed recurrent CRC patients, age, tumour grade, median TLG, and median MTV were independently prognosticators in the multivariate Cox regression analysis. Cut by median values, SUVmax, MTV, TLG were all significant on Kaplan-Meier and Log Rank tests. Patients with higher values had worse prognosis [147].

In 23 patients with multiple liver metastases treated with liver transplant, Grut *et al.* found lower total MTV & TLG were associated with better overall survival & disease-free survival while SUVmax, SUVmean, SUVpeak and tumour to background ratio were not [148].

Samim *et al.* retrospectively reviewed 54 patients with CRC liver metastases treated with thermal ablation. They found SUVpeak, SUVmean, SUVmax, partial volume corrected SUVmean and total lesion glycolysis (TLG) were not associated with local tumour recurrence time, but lower SUVpeak, SUVmean, SUVmax, partial volume corrected SUVmean had better new intrahepatic recurrence free survival [149].

These results are summarized in Table 2.

Table 2: Summaries of literatures on FDG-PET parameters and outcome

study type	patient number	Patient population	treatment	FDG-PET parameter	Findings	Reference
P	107	CRC	OP	SUVmax	higher the value, worse the outcome	135
R	163	CRC	OP	SUVmax	not associated with survival	137
R	325	CRC	OP	TLG	higher the value, worse the outcome	136
R	73	rectal	OP	MTV, TLG	higher the value, worse the outcome, but not independent of surgical margin	138
R	32	CRC	OP	intensity variability, size-zone variability	associated with progression-free survival	139
R	226	CRC	OP	bone marrow SUV	higher the value, worse the recurrence-free survival	140
R	118	CRC, stage II	OP	tumour-to-liver ratio	higher the value, worse the outcome	141
R	74	rectal	neoadjuvant + OP	MTV, kurtosis	higher the value, worse the outcome. Only kurtosis was an independent prognosticator to perineural invasion	142
R	64	rectal	neoadjuvant + OP	MTV	higher the value, worse the outcome	143
P	40	mCRC	regorafenib	TLG	higher the value, worse the outcome	145
R	105	recurrent CRC	various	MTV, TLG	higher the value, worse the outcome. Independent to age and tumour grade.	146
R	23	CRC liver mets	liver transplant	MTV, TLG	higher the value, worse the outcome.	147
R	54	CRC liver mets	thermal ablation	SUVmax, SUVmean, SUVpeak, TLG	not associated with local recurrence-free survival, but except TLG, lower values correlated with longer time to develop new lesions	148

CRC = colorectal cancer, mCRC = metastatic colorectal cancer, mets = metastases, MTV = metabolic tumour volume, OP = operation, P = prospective, R = retrospective, SUV = standard uptake value, TLG = total lesion glycolysis

1.5.1.3 Predicting treatment response

Skougaard *et al.* conducted a prospective study treating metastatic CRC patients with irinotecan and cetuximab. FDG-PET/CT was done every fourth cycle until progression. There were 61 patients for response evaluation. There was poor correlation between CT and PET response evaluation. That is, many patients deemed with stable disease by CT RECIST had partial metabolic response (PMR) by PET evaluation. By RECIST, those with progressive disease had worse overall survival than those with partial response or stable disease. By PET evaluation, those with PMR had better overall survival than those with either progressive metabolic disease or stable metabolic disease [150].

In a prospective setting in which 64 high-risk rectal cancer treated with neoadjuvant chemoradiotherapy followed by surgery, Li *et al.* found difference in pre-treatment MTV, both pre-treat & post-treat CEA as well as CEA reduction in pathologic complete response and non-CR patients [151].

Kawai analyzed 148 rectal cancer patients treated with neoadjuvant chemoradiotherapy followed by surgery and found post-treatment SUVmax, but not pre-treatment SUVmax, correlated with pathologic response. Furthermore, the PET performed later than 7 weeks after chemoradiotherapy had better accuracy in predicting pathologic response than those performed early (area under curve: 0.879 vs 0.669) [152].

Goshen *et al.* studied 7 patients with 20 liver lesions treated with neoadjuvant bevacizumab. FDG-PET was done after 4 cycles (before surgery). There were 17 lesions with pathologic results. FDG-PET predicted necrosis in 70% of the lesions, while CT

only predicted 35%. It seemed FDG-PET is a better evaluation tool for bevacizumab treatment response [153].

De Bruyne *et al.* evaluated 19 patients who received neoadjuvant FOLFOX/FOLFIRI with bevacizumab before hepatectomy in a prospective trial. DCE-MRI and FDG were done at baseline and after 5 cycles. They found a larger decrease in Ktrans, low pre-OP SUVmax and low microvascular density were good prognostic factors [154]. The same group found low pre-surgical SUVmax, low standardized total lesion glycolysis (sTLG, defined as lesion TLG minus background activity), and large decrease in sTLG were good prognosticators [155].

Despite the inability to predict pathologic responses, Lastoria *et al.* evaluated 33 patients in a prospective study testing FOLFIRI + bevacizumab before CRC liver metastasis resection, FDG-PET was performed at baseline and after 1 cycle of treatment (7 days). RECIST was assessed with CT after three months of treatment. They found metabolic response as defined by more than 50% reduction of SUVmax or more than 50% reduction of TLG predicted better overall survival and progression-free survival after surgery, while RECIST did not. In multivariate analysis, the addition of PET parameters to either RECIST or pathologic responses after surgery increased the predictive power of the models [156].

Bystrom *et al.* evaluated 51 patients treated with irinotecan-based chemotherapy in a prospective trial. FDG was performed after 2 cycles. They found baseline SUV was higher in radiologic non-responders than responders. Metabolic response as qualitatively evaluated by the NM physician was correlated with subjective response, but not with survival [157].

Maisonobe *et al.* evaluated 40 patients with FDG at 14-day after chemotherapy and compared with RECIST by CT 6 - 8 weeks after. They found SUV parameters without partial volume correction could be used to predict RECIST [158].

Similarly, Hendlisz *et al.* evaluated 41 metastatic CRC patients treated with biweekly chemotherapy. FDG-PET was done at 2-wk (after 1 cycle). Metabolic non-responder was defined as a decrease in SUVmax less than 15%. They found 100% sensitivity and 57% specificity, 43% PPV and 100% NPV for metabolic response to predict RECIST response. Thus a lack of FDG response after 1 cycle might denote absence of response of that treatment [159]. Similar results were reported by Woff *et al.* on sorafenib-capecitabine. The lack of response on early FDG-PET after one cycle of treatment predicted subsequent treatment failure in 19 out of 20 patients [160].

1.5.2 Perfusion images

Quantitative perfusion images utilize dynamic images to assess various aspects of the hemodynamic status of a given tissue via the use of an intravenous contrast agent. The concentration of contrast agent in the tissue changes with time via the blood supply and then diffusing into the extravascular space. The rate is determined by blood flow and vascular leakiness. Different algorithms can be applied to model the dynamics of the contrast medium. The derived parameters are different in each model. Generally, blood flow and volume are correlated with microvascular density; permeability surface area product or flow extraction product are representative of vascular leakage [161, 162].

The technique could be performed by positron emission tomography, computer tomography or magnetic resonance images. PET uses intravenous radioactive tracers.

CT perfusion study utilizes iodinated intravenous contrast medium. Dynamic contrast MRI utilizes intravenous gadolinium chelated contrast medium. Gadolinium shortens the longitudinal relaxation time of the tissues, and thus causing increased signal in T1-weighted images [163].

As for CT perfusion studies, quantitative measures such as blood volume (BV), blood flow (BF), mean transit time (MTT) and permeability surface area product (PS) are stable against different amount of contrast medium injected. However, semi-quantitative measurements such as peak enhancement and time to peak enhancement are higher in response to increased injected volume [164]. As for timing, 45-seconds is long enough for the calculation of blood flow, blood volume, mean transit time, but inadequate to calculate permeability [165].

Previous studies of CT perfusion on colorectal cancer revealed acceptable repeatability of the technique [166, 167]. Increase of z-axis coverage did not improve repeatability [168]. Of note, different software can produce different results, including updates of the same software packages [169, 170]. Furthermore, lesion movement such as originated by respiration or peristalsis poses difficulties that introduce measurement errors and variability [171].

Attempts have been made to correlate CT perfusion parameters with angiogenesis reflected by microvascular density, and compare CT perfusion parameters to tumour grading. Dighe *et al.* put two small ROIs in each tumour (invasive & luminal) in 29 CRC patients. No correlation was found between CT perfusion parameters and microvascular density (MVD) by CD105 or factor VIII (von Willebrand factor, vWF) [172]. Although their method of putting two small ROIs might be challenged by the results of Goh *et al.*, who reported that larger ROI outlining the whole tumour were

more reproducible [173]. Using the ROIs contouring the whole tumour, Goh *et al.* in 23 patients [174] revealing moderate correlation between blood volume ($r = 0.59$, $P = 0.002$), permeability surface-area product ($r = 0.46$, $P = 0.03$) and CD34. No correlation between CD34, and blood flow ($r = 0.27$, $P = 0.22$) or transit time ($r = -0.18$, $P = 0.44$) was found. In 35 patients, they found mild correlation between blood flow and CD105; no correlation was found between SUVmax or SUVmean and CD105 [175]. In this patient cohort, SUVmax and blood flow were correlated in later stage (III/IV, $r = 0.47$, $p = 0.03$) but not in early stage (I/II, $r = 0.09$, $p = 0.65$) tumours. The ratio BF/SUVmax was lower in patients with high VEGF and HIF-1 expression (3.65 vs. 5.98; $P = 0.01$ for VEGF) (3.63 vs. 5.48; $P = 0.04$ for HIF-1 α) [176]. Taxier *et al.* found a positive correlation between blood flow from CT perfusion and PET parameters such as metabolic active tumour volume (MATV), intensity variability (IV) and local homogeneity in 13 stage III/IV patients, but none found in 17 stage I/II patients [177].

Kim *et al.* in 27 CRC patients found no correlation between CT perfusion parameters and CD34. They found higher BF, shorter MTT in moderately-differentiated (MD) tumours ($n=15$) compared to well-differentiated (WD) ($n=8$) or poorly-differentiated (PD) ($n=4$) tumours. CD34 was highest in the PD group [178]. Sun *et al.* using the software from Philips (CT Perfusion; Philips Healthcare Systems, The Netherlands) in 37 CRC patients found no correlation between CT perfusion parameters and CD105. CD105 was not different in WD, MD, PD groups. BF, BV were higher in the WD groups.; while time to peak (TTP) was longer in the PD group. [179].

Similarly, Xu *et al.* using the Philips software (CT Perfusion; Philips Healthcare Systems, The Netherlands) in 53 CRC patients reported BF was higher in well-differentiated tumours, and TTP was longer in PD cancers [180]. In 44 rectal patients

treated with only surgery, Hayano et al. found higher BF in WD groups. Low BF showed the tendency for lymphovascular invasion and metastases. Those with high blood flow had better survival than these with low BF [181]. Goh et al. reported higher blood flow in patients of disease-free status than those with subsequent metastasis after surgery in 52 patients [182].

These reports indicated wide variation of correlation between CT perfusion parameters and microvascular density. Different antibodies and quantifying methods exist for indication of microvascular density. This might account for the discordancy between the findings of different investigators. With respect to tumour grading, CT perfusion seems to suggest well-differentiated tumours have higher blood flow. In turn those tumours with higher blood flow might be indicative of better survival.

Qi *et al.* used a rat glioma model to demonstrate that BF and BV from the CT perfusion images negatively correlated with hypoxia volume as calculated by immunohistochemical staining with pimonidazole [183], a marker for tumour hypoxia[184]. Another report by Spira *et al.* claimed no correlation between blood volume, blood flow or Ktrans derived from the Patlak model on the CT perfusion images and HIF-1/2 staining in 72 lung cancer patient samples. However, the manuscript did not specify how the staining was performed or quantified, nor the exact value of these correlations [185]. Perfusion images can also be used to monitor the effectiveness of anti-angiogenic therapy in a patient. Monitoring the treatment effect could be performed by perfusion imaging. Willett *et al.* demonstrated decrease in tumour blood flow and blood volume after a single dose of bevacizumab in 6 rectal cancer patients [186].

1.5.3 Texture analysis

In addition to perfusion parameters and conventional measurements such as extension of disease and changes in tumour size, additional image features can be extracted from routine medical images. One such method is to perform textural analysis. A simple method called a filtration-histogram method can be used to extract texture parameters from the images. This method measures the value of each pixel in a defined area of the image, and lists mean, standard deviation, kurtosis, and skewness of the histogram. Image features of different sizes are enhanced by applying filters of various sizes to the original images [187]. These additional features might be able to provide useful information. For example, using portal-phase CT images from colorectal patients without liver metastases, Ganeshan *et al.* showed entropy from the hepatic region or normalized uniformity of the hepatic region at coarse filter was correlated with patients' survival [188, 189]. Ng *et al.* revealed the fine texture parameters derived from CT images of primary colorectal cancer including entropy, uniformity, kurtosis, skewness, and standard deviation were predictive of overall survival [190]. Texture parameters also depicted underlying physiologic properties. As Ganeshan *et al.* showed the mean correlated negatively with SUV from FDG-PET and positively with hepatic blood flow [191]. Miles *et al.* showed texture parameter from the primary colorectal patients in combination with FDG-PET scan and blood flow from CT perfusion could predict the status of KRAS mutations [134].

1.6 Summary

Colorectal cancer is an increasingly common cancer and represents a heavy burden for health care systems. New drugs targeting the EGFR family and the process of angiogenesis have been used against colorectal cancer, highlighting the importance of both pathways in the tumorigenesis of colorectal cancer. Tumour cells can release exosomes into their microenvironment for modulating different biological responses such as immunosuppression, angiogenesis, and metastasis. Clinical imaging of patients using CT perfusion investigates the perfusion status of tumours, and FDG-PET is linked to their hypoxic status. Both image modalities provide prognostic values and are linked to expression of proteins such as EGFR, KRAS, VEGF. Texture analysis of these clinical images can provide additional information on patient survival and the underlying biology processes involved in disease. However, at present there are no studies that have conducted correlations between the exosomal profile of patients, with data derived from the imaging of their tumours

Here we present a prospective cohort of colorectal cancer patients with clinical images investigating angiogenesis and hypoxia. We investigated these images and their extended features from texture analysis and associated them with the patients' overall survival. We additionally performed studies on the underlying biology of tumours by profiling exosomes from liquid biopsies. These correlations allowed us to hypothesise biological association by combining imaging features to immunohistochemical staining and proteins related to proliferation, angiogenesis and hypoxia in the exosomes.

Our hypotheses are that CT perfusion scans could visualize angiogenesis in vivo; the image parameters acquired including those from texture analysis could provide prognostic information for colorectal cancer patients; and there could be biologic meanings in these image texture parameters.

2 Materials & Methods

2.1 Cell Line Works

2.1.1 Hypoxia treatment

The colorectal cell line HCT-116 was maintained in our lab and was authenticated yearly via external sequencing service (see Appendix 1 for authentication certificate). It was cultured in McCoy's 5a Medium Modified supplemented with 10% fetal bovine serum, 1% glycine and penicillin/streptomycin. The normoxic control was incubated at 37 °C in a 5% CO₂ air atmosphere, while the hypoxia treated cells were incubated in a hypoxic incubator with 5% CO₂ and 1% O₂ at 37 °C overnight.

2.1.2 Exosome isolation from culture media

Culture medium was collected in Falcon tubes and underwent centrifugation at 300 g for 10 min. The supernatant was transferred to Beckman Coulter capped polycarbonate bottles (#3118-0050), and centrifuged at 12,200 g for 45 minutes using a JA25.50 rotor in an Avanti J-26 XPI centrifuge. The supernatant was transferred to Beckman Coulter thick wall ultracentrifuge tubes (#355631), topped with filtered-PBS up to tube maximum capacity (i.e. 16.5 ml) and ultra-centrifuged at 100,000 g for 2 hours using a Beckman Coulter 70Ti Rotor in an Optima L-100 XP Ultracentrifuge. The

supernatant was discarded, and the pellet was resuspended with 1.5 ml of 0.45 μ m-filtered phosphate-buffered saline (PBS), and put into ultracentrifuge tubes (1,5 ml capacity; Beckman Coulter No 357448) for ultracentrifugation for 90 min at 100,000 \times g, 4 $^{\circ}$ C using a TIA 55 Rotor in an Optima MAX XP Ultracentrifuge. After discarding the supernatant, the exosome pellets were resuspended in 200 μ l of 0.45 μ m-filtered PBS and aliquoted to 20 μ l replicates, and store at -80 $^{\circ}$ C [115].

2.1.3 Western blot

At the end of hypoxic treatments, adherent cells were washed with PBS and lysed on ice using ice-cold lysis buffer (300 mM NaCl, 100 mM Tris, 0.5% NP40, proteinase inhibitor cocktail (Complete-Mini, Roche #04693124001), phosphatase inhibitor cocktail (PhosStop, Roche #04693124001), and adjusted to pH 7.4). After scrapping the cells from the culture dish along with the lysis buffer, lysates were transferred to Eppendorf tubes and kept on ice for 20 minutes with periodic agitation. After centrifugation at 13000 g for 10 minutes, the supernatant was collected and either stored at -20 $^{\circ}$ C or processed immediately for protein quantification.

Protein quantification was performed using Thermo Scientific Pierce BCA Protein Assay Kit (#23225). 5 μ l of samples were diluted 5 times by adding into 20 μ l of lysis buffer, and 5 μ l of this were transferred to a 96-well plate. A serial of diluted bovine serum albumin protein standards of 0, 0.5, 0.75, 1, 1.5, 2.0 mg/ml in concentration were also pipetted to the microplate. Working solution (Kit reagent A and B in 50:1 ratio) was added into each well to a final volume of 200 μ l. After shaking for 30 seconds, the microplate was incubated at 37 $^{\circ}$ C for 30 minutes, and then read in the

Thermo Varioskan LUX reader at 562 nm. The protein concentration was calculated by fitting the blank-subtracted absorbance to the standard concentration.

After quantification, protein concentrations were equalized with pure water and added into 4x sample buffer (final concentration 2 % sodium dodecyl sulfate (SDS), 5 % 2-beta-mercaptoethanol, 10 % glycerol, 0.002 % bromophenol blue and 0.0625 M Tris HCl, pH 6.8). After heating the samples for 10 minutes at 95 °C, 25 µg of protein were loaded for electrophoresis onto 10 % NuPAGE Bis-Tris gels and run at 100 V for approximately 2 hours in MOPS SDS running buffer. The proteins were then transferred onto PVDF membranes (0.45 µm, Millipore) under 300 mA for 1 hour. Membranes were then blocked with 5 % milk for 1 hour, followed by incubation with primary antibodies overnight at 4 °C and secondary antibodies for 1 hour at room temperature. Blots were imaged after incubation with ECL reagent using a digital camera acquisition system (GE ImageQuant LAS 4000). Band intensities were quantified using standard ImageJ protocols for densitometry.

2.1.3.1 Antibody list

HER1: rabbit IgG monoclonal, cell signaling #4267 (D38B1) (0.029 µg/ml)

HER2: rabbit IgG monoclonal, cell signaling #2165 (29D8) (0.25 µg/ml)

HER3: rabbit IgG monoclonal, cell signaling #12708 (D22C5) (0.059 µg/ml)

cMET: rabbit IgG monoclonal, cell signaling #8198 (D1C2) (1:1000)

ALIX: mouse IgG1 monoclonal, cell signaling #2171 (3A9) (0.05 µg/ml)

P4HA1: rabbit IgG polyclonal, protein tech 12658-1-AP (0.59 µg/ml)

S100A9: rabbit IgG polyclonal (MRP14;IV), provided by Prof. Thomas Vogl of University of Muenster (0.55 µg/ml)

2nd anti-rabbit: Dako polyclonal goat anti-rabbit immunoglobulins/HRP (P0448)

(0.0125 mg/L)

2nd anti-mouse: Dako polyclonal goat anti-mouse immunoglobulins/HRP (P0447)

(0.05 mg/L)

2.2 Recruitment of Patients

Patients with suspected colorectal cancer either by sigmoidoscopy, colonoscopy or CT images were prospectively recruited into the study after informed consent under The Tumour Angiogenesis:Radiology-Pathology and Prognostic Correlation project approved by the research ethic committee (05/Q0505/34). Patients from several hospitals in the London region were approached. These hospitals included UCLH, Colchester, Broomfield, Barnet, Chase Farm, Queens, King George, Whipps Cross, Welwyn Garden City and are members of the Molecular Imaging in Colorectal Cancer (MiC) Consortium. Patients were offered FDG-PET, CT perfusion, and optional MR images. After the scans, the patients were treated as decided by the local multi-disciplinary team, and followed-up at the referring hospitals.

2.3 Patient exosome work

2.3.1 Exosome isolation from serum

Before the image scan, 10mls of blood was drawn into Yellow Top Vacutainer (SST tubes). After standing at room temperature for 30 minutes, it was centrifuged for 10 minutes at 1,000 x g. The supernatant (serum) was aliquoted into cryovials, and stored

in a -80°C freezer until time of isolation. The storage time was between 18.8 to 34.7 months (median: 29.3 months).

The isolation began by defrosting 2mls of serum, and diluting the serum with equal volume of PBS. After centrifuge for 45 minutes at $12,000 \times g$, 4°C , the supernatant was transferred to ultracentrifuge tubes (Beckman Coulter #357448) to be centrifuged for 120 minutes at $100,000 \times g$, 4°C using TIA 55 Rotor in Optima MAX XP Ultracentrifuge. The supernatant was discarded, and the exosome pellets were resuspended in 1.5ml PBS, and underwent another centrifuge for 60 minutes at $100,000 \times g$, 4°C . After discarding the supernatant, the exosome pellets were resuspended in 200 μl PBS and aliquoted into 10, 20, 50, 100 μl , stored at -80°C [192].

2.3.2 Nanoparticle tracking analysis

10 μl of isolated exosomes in PBS was diluted with reverse osmosis water into 1 ml. The sample was run through Nanosight LM10 system (Malvern Panalytical, Malvern, UK) with a speed of 50 by an automatic syringe pump. Five 30-second videos were taken and the results were analysed by the NTA software (version 2.3). There would be further dilution to keep the concentration around 10^8 particles/ml. The camera level was set automatically, while the detection level was adjusted manually.

2.3.3 Dotblot

5 μl of exosomes in PBS was spotted onto the nitrocellulose membrane and air-dried. Non-specific binding was blocked by 5% bovine serum albumin (BSA) in Tris-buffered saline with Tween (TBS-T: 0.02mM Tris, 0.05M NaCl, 0.01M KCl, 0.1% Tween-20, pH 7.4) in room temperature for 1 hour. Then the membrane was incubated with

primary antibody in TBS-T at 4°C overnight. In the second day, after washing with TBS-T for 5 minutes 3 times, the membrane was incubated with secondary antibody for 1 hour at room temperature. The membrane was washed again with TBS-T for 5 minutes 3 times, and incubated with ECL reagent for 1 min. The signal intensities were quantified with a digital imaging platform (GE ImageQuant LAS 4000), and were normalized to the signal intensities of the ALIX protein.

2.4 CT Perfusion imaging

Perfusion CT was added to the FDG-PET/CT acquisition. After the PET acquisition, 50ml of intravenous iodinated contrast was given at a rate of 5 ml/sec (350 mg/mL iodine Omnipaque, GE Healthcare; Chalfont St Giles, UK), followed by 50ml of saline chaser also at a rate of 5 ml/sec. After a delay of 10 seconds, CT was acquired with a 2-second interval for 20 frames, then 5-second interval for 22 frames. Total acquisition time was 150 seconds. The images were acquired with rotation time of 1 seconds, 120 kVp, 60 mAs using 64 x 0.6mm detectors (4cm coverage). The slice thickness was 5mm, scan field of view 50cm, matrix size 512 x 512.

The perfusion CT images were assessed using a commercial software based on a distributed parameter analysis (Perfusion 4D; GE Healthcare, Chalfont St Giles, UK). The processing threshold was set between 0 to 120HU. The arterial time-enhancement curve was derived by placing a circular region of interest within the best-visualized artery. Tumour region of interest (ROI) was defined by depicting the contour of tumour in all images where the tumour was visible. “Base” was the average CT number (Hounsfield Unit) of each pixels in the ROI at the baseline (i.e. before contrast medium

injection); “Average” was the average of CT number of each pixels in the ROI across the whole perfusion scan sequence. Tumour blood flow, blood volume, mean transit time and permeability surface were derived from the generated parametric maps. Time to peak and mean slope of increase were calculated from the time-density curve. The mean values of these parameters were recorded.

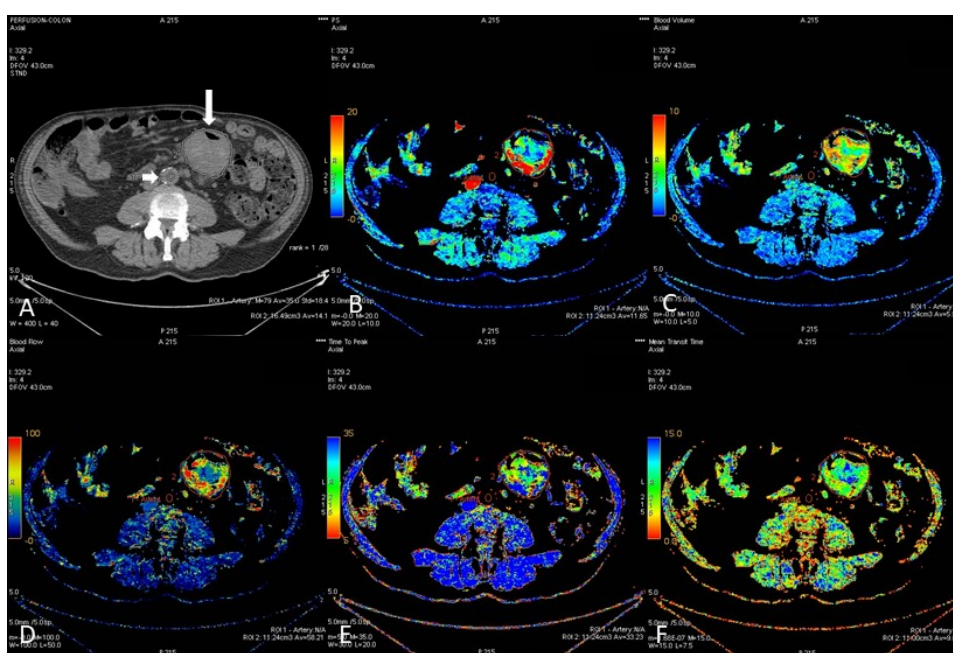


Figure 1. The positions of aorta (arterial input, short arrow) and tumour (long arrow) were selected on the CT images (A). The software would then calculate the CT perfusion parameters such as permeability surface (B), blood volume (C), blood flow (D), time to peak (E), mean transit time (F) as shown here on parametric maps. The average values of each pixel within the tumour were recorded.

2.5 FDG-PET/CT images

FDG-PET was performed on a PET/64-detector-CT (Discovery VCT, GE Healthcare, Amersham, UK). Patients were requested to fast for at least 6 hours, and injected with 250 ± 50 MBq of FDG. Scans began at 60 ± 7 min after injection. Attenuation CT was acquired with 64×3.75 mm detectors, a pitch of 1.5 and 5-mm collimation (140 kVp, 40mAs, in 0.8 sec). PET was acquired in 2D mode, with 3 minutes/bed position from skull to upper thigh. Images were reconstructed using ordered subsets expectation

maximization (OSEM) with two iterations and 28 subsets, with slice thickness of 3.27 mm. The reconstructed field of view was 50 cm, matrix size 128 x 128. The tracer uptake was quantified using the standardized uptake value (SUV) calculated as tissue concentration (Bq/g)/[injected dose (Bq)/body weight (g)]. The maximal SUV and mean SUV within the volume of interest were calculated automatically on the GE Advantage Workstation (version 4.2, GE Healthcare, Amersham, UK) (Figure 2).

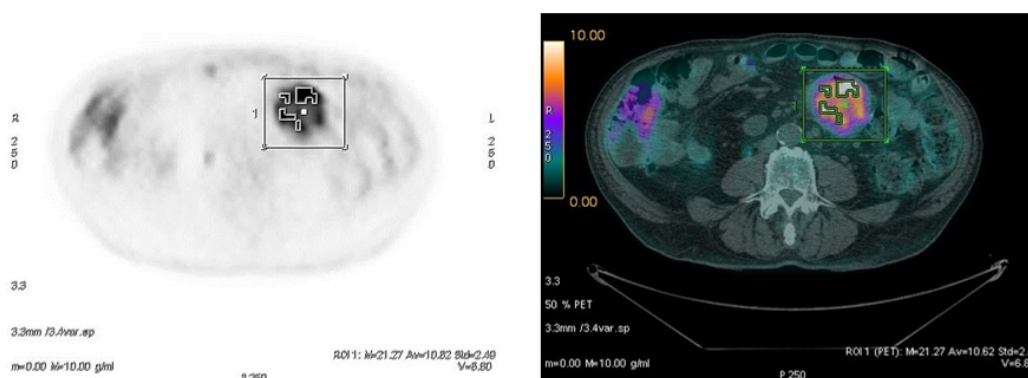


Figure 2. The PET/CT images were loaded onto the Advantage Workstation. The left was the PET image, and the right was the fusion PET/CT image. After identifying the tumour location, the highest SUV and average SUV within the volume of interest were calculated automatically, as shown in numbers at the right lower corners of each picture.

2.6 Texture analysis

Texture analysis was performed using a proprietary software package (TexRAD, Feedback PLC, Cambridge, UK). A single slice with largest tumour dimension was selected, and a region of interest (ROI) was drawn manually to contour the tumour. Laplacian of gaussian spatial band-pass filters of different spatial scale filters were applied to the ROI, to extract features of different sizes (from 2mm to 6mm in radius). The histogram parameters including mean, standard-deviation, kurtosis, skewness and mean positive pixels were then calculated.

The textural analysis was performed on the images derived from FDG-PET, non-contrast CT, perfusion CT (at 80-second post injection, venous phase).

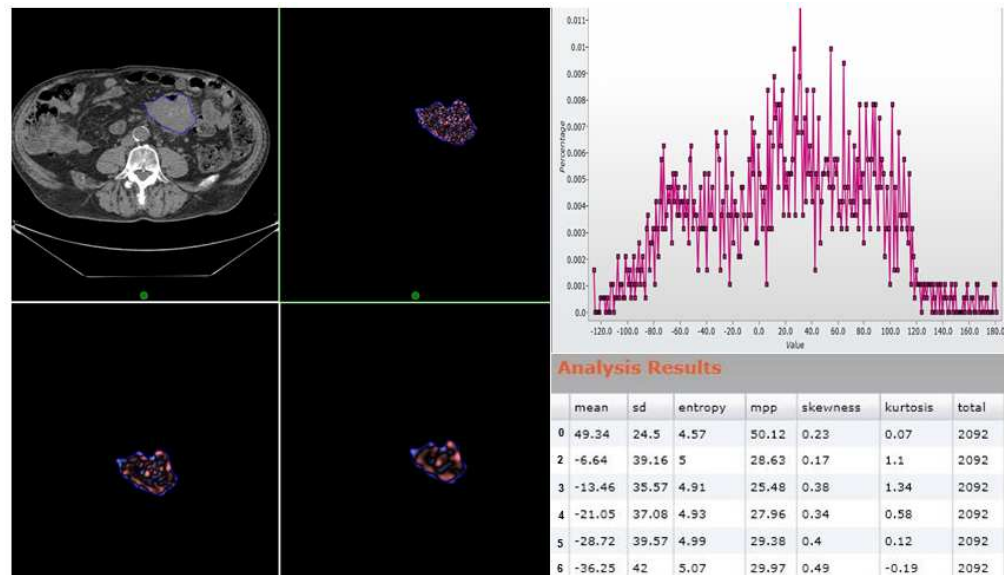


Figure 3. TexRAD analysis of the non-contrast CT image from one patient. The largest section of the tumour was loaded into TexRAD, and the ROI was drawn on the tumour manually (left upper). The software applied filters to extract features of different sizes (fine, medium, coarse as shown in the right upper, left lower, right lower images). A histogram was formed in each filtered image, and the mean, standard deviation, entropy, mean positive pixels, skewness, kurtosis were calculated from the histogram [187].

2.7 Immunohistochemical staining

Formalin-fixed paraffin-embedded tumour samples were obtained from the surgical specimens of those treatment-naïve patients who received primary surgery (i.e. without neoadjuvant therapies) after the CT perfusion and FDG-PET scans. Some of these patients also had their blood drawn for exosome isolation at the time of their image scans.

The FFPE specimens were cut at a thickness of 4 μm using Leica Microtome RM2235. Slides were stained on the Leica Bond Max Auto-stainer using Bond Polymer

Refine Detection Kit. Epitopes for CAIX were exposed by antigen retrieval solution ER1 (Leica) for 30 minutes. Epitopes for HIF1 α and CD105 were exposed by antigen retrieval solution ER2 (Leica) for 20 minutes. Epitopes for VEGF were exposed by antigen retrieval solution ER2 for 20 minutes. GLUT1 did not require antigen retrieval. Non-specific endogenous peroxidase activity was blocked by incubation with 3-4% hydrogen peroxide included in the kit.

Following this, antibodies were diluted in Leica Bond Diluent. Staining protocol of 15 minutes primary antibody, 8 minutes post primary and 8 minutes polymer was used for GLUT-1, VEGF, CD105 and CAIX. Staining protocol of 30 minutes primary antibody, 20 minutes post primary and 20 minutes polymer was used for HIF1 α . Slides were incubated for 10 minutes in substrate chromogen, 3,3'-Diaminobenzidine tetrahydrochloride hydrate (DAB) and counterstained with haematoxylin for 2 minutes.

Afterwards, slides were removed from the Bond-max and rehydrated by immersion in increasing concentrations of ethanol (70%, 90% and 100%). Finally, slides were immersed in xylene three times prior to cover-slipping.

CD105 was used to quantify microvascular density. Four most vascular areas each patient sample were identified under low magnification of CD-105 stained sections. The vessels were identified with a clearly defined lumen or with a well-defined linear vessel shape that was not a single endothelial cell. Vessels were counted on a field of 0.62 mm² (200x on an Olympus microscope) [193]. A high count of vessels is shown in Figure 4A and a low count of vessels is shown in Figure 4B.

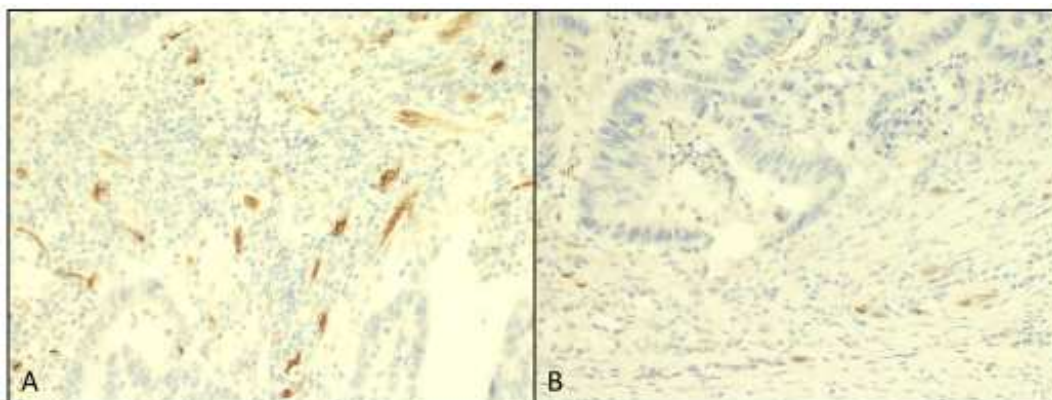


Figure 4. After antigen retrieval by Leica antigen retrieval solution ER2 for 20 minutes, CD105 was stained with Leica NCL-CD105 with the final concentration of 1 mg/ml for 15 minutes, followed by 8 minutes each post primary and polymer, before incubating in DAB for 10 minutes and counterstained with haematoxylin for 2 minutes. (A) showed a field of high microvascular density, in contrast with (B) of low microvascular density.

Scores for other proteins were based on staining intensity and percentage of positively-stained cells. The intensity was score from 0-3 (no staining/weak/medium/strong), and the extent of staining was scored from 0-4 (<5%/5-25%/26-50%/51-75%/>75%) [176]. Figure 5A shows a sample with high intensity and extent of CAIX staining whereas Figure 5B shows a sample negative for CAIX.

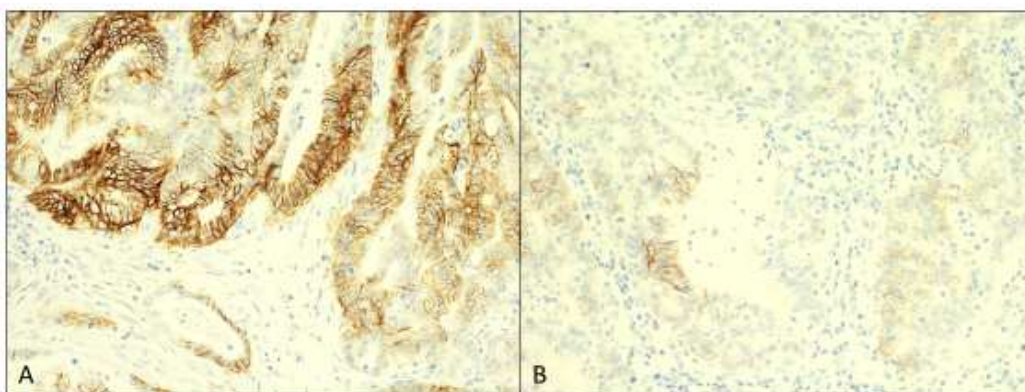


Figure 5. After antigen retrieval by Leica antigen retrieval solution ER1 for 30 minutes, CA-IX was stained with Leica NCL-L-CAIX with the final concentration of 1 mg/ml for 15 minutes, followed by 8 minutes each post primary and polymer, before incubating in DAB for 10 minutes and counterstained with haematoxylin for 2 minutes. (A) showed a sample with high intensity and extent of CAIX staining whereas (B) showed a sample negative for CAIX.

Antibody list:

CD105: Leica NCL-CD105 (1 mg/ml)

HIF-1 α : Abcam AB51608 (1 mg/ml)

VEGF: Dako M7273 (1 mg/ml)

GLUT-1: Millipore 07-1401 (1 mg/ml)

CA-IX: Leica NCL-L-CAIX (1 mg/ml)

2.8 Statistical methods

The correlation between different parameters were calculated by Spearman's rank correlation coefficient. The distribution of parameters was compared by non-parametric Mann-Whitney U test. Parameters were dichotomized by the median value and their effects on survival was tested by the log-rank test. P-value less than 0.05 were considered statistically significant. All the calculation was done in IBM SPSS Statistics Version 22.0 (Armonk, NY: IBM Corps).

3 Colorectal cancer imaging pertinent to angiogenesis as sources of biomarkers: FDG-PET, CT perfusion and texture analysis in predicting outcome of colorectal cancer patients

In this chapter, the aim was to analyse a large cohort of patients that underwent CT perfusion and texture analysis of the FDG-PET/CT to evaluate these modalities in predicting patient outcome.

3.1 Methods

364 patients were recruited into the colorectal angiogenesis study from 2007 to mid-2017. 20 patients were found later to be of benign pathology (N=6), malignancy already removed during biopsy polypectomy (N=10), anal squamous cell carcinoma (N=3), or neuroendocrine tumour (N=1), and were excluded from the analysis. Among the remaining 344 patients, 335 patients underwent FDG-PET/CT scans and CT perfusion was successfully performed in 293 patients. Texture analysis by histogram method was done on the FDG-PET/CT images as well as the perfusion CT at 80-second post injection (venous phase). The follow-up time was 0.3-116 months (median: 33.4

months), during which there were 96 deaths. The patient demographics are listed in Table 3 and Table 4.

Table 3: Patients' demographics

Sex	N	percentage			
Male	224	65.1%			
Female	120	34.9%			
Site					
Caecum	33	9.5%			
Ascending	26	7.6%			
Transverse	26	7.6%			
Descending	22	6.4%			
Sigmoid	103	29.9%			
Rectum	134	39.0%			
Overall Clinical Stage and primary treatment			OP	CRT	Palliation
Colonic					
I	24		24	0	0
II	69		69	0	0
III	65		57	5	3
IV	52		28	7	17
Rectal					
I	18		10	6	2
II	21		11	10	0
III	69		13	52	4
IV	26		1	11	14

CRT = chemoradiotherapy, OP = operation

Table 4: Distribution of the stage at subsites

Site \ Stage	Stage				Overall
	1	2	3	4	
Caecum	4	14	6	9	33
A-colon	4	8	10	4	26
T-colon	0	12	10	4	26

D-colon	4	4	5	9	22
Sigmoid	12	31	34	26	103
Rectum	18	21	69	26	134

3.2 Results

3.2.1 Reproducibility of image parameters

The reproducibility of image parameters was tested by deriving the parameters from 25 patients randomly picked from our cohort by another operator and compare the results by intra-class correlation coefficient (ICC) for agreement using a two-way random effect model [194]. Coefficient of variation was also listed in Table 5.

Table 5: Intra-class correlation coefficient (ICC) and coefficient of variation (CV) of image parameters. *not reliable as some values were negative

parameters	ICC	95% confidence interval	CV (%)
CT sizes	0.677	0.577-0.756	26.55
FDG-PET			
SUVmax	0.997	0.993-0.999	2.94
SUVmean	0.833	0.668-0.920	20.89
TLG	0.968	0.939-0.983	25.78
CT Perfusion			
Average	0.916	0.832-0.959	15.18
Base	0.862	0.739-0.929	19.92
Time to Peak	0.700	0.453-0.848	15.87

Mean slope of increase	0.728	0.478-0.868	22.82
Blood volume	0.794	0.647-0.885	27.43
Blood flow	0.933	0.860-0.969	15.35
Mean transit time	0.740	0.497-0.875	14.67
PS	0.893	0.784-0.948	18.77
PET Texture analysis			
Mean	0.845	0.793-0.885	30.43
SD	0.709	0.621-0.780	12.83
MPP	0.887	0.849-0.917	15.71
Skewness	0.709	0.621-0.780	36.73*
Entropy	0.753	0.676-0.813	6.53
Kurtosis	0.739	0.657-0.803	223.40*
CT Texture analysis			
Mean	0.867	0.780-0.916	23.01
SD	0.798	0.719-0.855	7.23
MPP	0.963	0.947-0.974	5.09
Skewness	0.759	0.647-0.834	111.24*
Entropy	0.897	0.774-0.944	1.99
Kurtosis	0.757	0.669-0.824	148.92*

The results confirmed moderate to good reproducibility with different observers.

SUVmax from the FDG-PET images was the most reproducible in keeping with the results of Goh *et al.*[167]

3.2.2 Image parameters as prognosticators

Within the entire cohort, older patients and patients with lymph node or distant metastases had the worse survival. CT perfusion parameters were not predictive of survival. On the FDG-PET/CT images, those with higher glycolysis, MTV, TLG, CT size had worse survival. Using the median value as cut-off, unfiltered mean and skewness of the PET, standard deviation and mean-positive-pixels of intermediately-filtered CT image, as well as kurtosis of the CT images were all prognosticators. Standard deviation, mean-positive pixels, and kurtosis of the coarsely-filtered contrast-enhanced CT images were also prognosticators (Table 6).

After calculating the results from the whole cohort, two third of the patients were chosen randomly as Random Group-1 while maintaining the same proportion of survival events, while the other one thirds were Random Group-2.

Within Random Group-1, patients with lymph node or distant metastases had worse survival. Permeability surface area product from the perfusion images, unfiltered mean of the PET, kurtosis of the CT, skewness of the contrast-enhanced CT were prognosticators. However, compared to the whole cohort, only mean of the unfiltered PET images and kurtosis of the CT images remained significant in both (Table 6).

Within Random Group-2, those with older age, lymph node or distant metastases, higher MTV, glycolysis, TLG, CT size on the FDG-PET/CT images had worse survival. Kurtosis of the unfiltered PET images, SD & MPP of the intermediately-filtered CT images, as well as kurtosis of the CT images were prognosticators. Compared to the

whole cohort, glycolysis, TLG, CT size on the FDG-PET/CT images, SD and MPP of the intermediately-filtered CT images, kurtosis of the CT images, standard deviation, mean-positive pixels, and kurtosis of the coarsely-filtered contrast-enhanced CT images remained significant (Table 6). The complete list of parameters can be found in the table in the Appendix.

Thus, across the whole cohort, Random Group-1 and Random Group-2, only stage and the kurtosis of the finely and intermediately-filtered CT images were the stable prognosticator. The importance of kurtosis of CT images could be further confirmed in the Cox regression analysis showing both parameters significantly affected patients' survival independently (Table 7).

Table 6: Significant prognosticators from the Kaplan-Meier estimator & Log-Rank test. The texture parameters were listed as “texture parameter_filter level_image modality”. For example, skewness_6_VE meant the skewness calculated from the venous phase of contrast-enhanced CT after filtration with the 6-mm spatial scale filter.

Parameter	The Whole Cohort			Random Group-1			Random Group-2		
	Mean survival of patients with parameter > median (mean ± SE)	Mean survival of patients with parameter ≤ median (mean ± SE)	p-value (Log Rank test)	Mean survival of patients with parameter > median (mean ± SE)	Mean survival of patients with parameter ≤ median (mean ± SE)	p-value (Log Rank test)	Mean survival of patients with parameter > median (mean ± SE)	Mean survival of patients with parameter ≤ median (mean ± SE)	p-value (Log Rank test)
Age	73.46 ± 4.25	89.05 ± 3.83	0.025	81.40 ± 6.78	73.39 ± 6.12	0.905	64.39 ± 4.62	93.31 ± 4.37	0.004
Stage (3,4 vs 1,2)	65.94 ± 4.00	98.94 ± 4.27	< 0.001	62.79 ± 5.77	100.33 ± 6.26	< 0.001	65.45 ± 4.89	98.41 ± 5.76	< 0.001
PS	72.58 ± 5.15	81.45 ± 4.91	0.265	68.62 ± 8.24	84.29 ± 5.49	0.043	68.96 ± 5.61	76.67 ± 6.21	0.735
MTV	75.51 ± 4.56	82.49 ± 4.06	0.018	73.20 ± 5.97	79.31 ± 7.55	0.786	71.13 ± 6.55	84.78 ± 4.82	0.006
Glycolysis	75.93 ± 4.46	82.08 ± 4.18	0.021	82.76 ± 6.90	71.35 ± 6.19	0.861	73.06 ± 6.03	83.70 ± 4.99	0.014
TLG	71.85 ± 4.76	85.48 ± 3.93	0.001	78.45 ± 7.18	74.64 ± 6.09	0.425	67.39 ± 6.11	88.17 ± 4.82	0.001
CT size	75.24 ± 4.62	82.84 ± 4.19	0.026	79.64 ± 6.99	74.76 ± 6.22	0.481	69.89 ± 6.26	86.08 ± 4.89	0.006
Mean_0_PET	68.16 ± 4.85	88.82 ± 3.96	0.011	63.86 ± 6.99	90.28 ± 6.65	0.038	69.84 ± 5.85	87.14 ± 4.77	0.182
Mpp_0_PET	68.16 ± 4.85	88.82 ± 3.96	0.011	63.86 ± 6.99	90.28 ± 6.65	0.038	69.84 ± 5.85	87.14 ± 4.77	0.182
Skewness_0_PET	86.90 ± 4.10	67.37 ± 4.23	0.039	86.87 ± 6.83	67.31 ± 6.66	0.241	86.18 ± 5.16	67.65 ± 5.17	0.109
Skewness_2_PET	86.33 ± 4.23	67.20 ± 3.76	0.026	83.31 ± 6.88	70.40 ± 6.43	0.766	85.06 ± 5.37	65.36 ± 4.42	0.071
Kurtosis_0_PET	85.45 ± 4.14	72.83 ± 5.21	0.062	73.24 ± 6.25	80.63 ± 7.30	0.852	90.39 ± 4.56	62.56 ± 5.32	0.015
SD_3_CT	80.21 ± 3.53	72.61 ± 4.79	0.040	78.08 ± 5.57	75.35 ± 7.66	0.509	80.65 ± 4.41	70.51 ± 6.23	0.039
Mpp_3_CT	80.85 ± 3.32	72.90 ± 4.69	0.044	79.92 ± 5.44	74.07 ± 5.46	0.277	81.16 ± 4.12	70.28 ± 6.09	0.042
Kurtosis_0_CT	74.32 ± 4.49	79.37 ± 3.77	0.021	75.90 ± 7.32	77.97 ± 5.84	0.175	73.97 ± 5.43	79.18 ± 5.00	0.059
Kurtosis_2_CT	71.08 ± 4.50	88.42 ± 4.49	0.001	61.68 ± 6.43	93.78 ± 6.81	0.005	72.06 ± 5.53	76.88 ± 4.16	0.015
Kurtosis_3_CT	70.53 ± 4.56	82.96 ± 3.53	0.001	72.59 ± 7.84	79.71 ± 5.73	0.107	68.84 ± 5.70	83.81 ± 4.39	0.003

Kurtosis_4_CT	71.82 ± 4.65	81.56 ± 3.50	0.004	73.66 ± 7.13	80.36 ± 5.78	0.028	69.14 ± 5.94	83.15 ± 3.91	0.014
Kurtosis_5_CT	73.29 ± 4.55	80.66 ± 3.57	0.022	70.95 ± 7.28	82.24 ± 5.89	0.019	73.46 ± 5.84	79.70 ± 4.18	0.191
Kurtosis_6_CT	74.71 ± 4.55	79.22 ± 3.71	0.038	79.24 ± 7.10	74.53 ± 6.43	0.664	70.96 ± 6.00	81.11 ± 4.38	0.019
SD_4_VE	82.31 ± 5.13	72.51 ± 4.93	0.122	61.03 ± 4.28	78.08 ± 7.64	0.424	86.64 ± 5.26	60.08 ± 5.40	0.047
SD_5_VE	83.36 ± 4.85	70.93 ± 5.13	0.078	66.17 ± 6.92	83.96 ± 7.60	0.741	86.74 ± 5.21	59.04 ± 5.43	0.029
SD_6_VE	85.27 ± 4.69	68.92 ± 5.17	0.024	70.64 ± 6.90	78.55 ± 7.91	0.445	86.20 ± 5.17	59.41 ± 5.47	0.047
Mpp_4_VE	80.73 ± 5.23	73.78 ± 4.88	0.207	66.50 ± 7.38	84.87 ± 7.44	0.700	85.01 ± 5.64	60.02 ± 5.43	0.046
Mpp_5_VE	85.39 ± 4.66	68.00 ± 5.41	0.012	72.64 ± 6.63	81.30 ± 7.81	0.707	90.21 ± 5.19	54.24 ± 5.08	0.001
Mpp_6_VE	85.10 ± 4.59	68.16 ± 5.44	0.025	72.62 ± 6.70	81.61 ± 7.69	0.758	89.36 ± 5.06	54.77 ± 5.09	0.004
Skewness_6_VE	74.05 ± 5.32	80.01 ± 4.77	0.375	53.10 ± 5.05	94.72 ± 6.19	0.026	77.23 ± 6.40	68.26 ± 5.47	0.961
Kurtosis_3_VE	74.00 ± 4.91	75.09 ± 4.39	0.213	86.54 ± 7.30	54.87 ± 4.96	0.249	67.76 ± 6.41	76.61 ± 5.34	0.040
Kurtosis_4_VE	71.74 ± 4.86	76.94 ± 4.35	0.010	85.19 ± 7.66	68.47 ± 6.96	0.630	65.30 ± 6.07	79.15 ± 5.57	0.001
Kurtosis_5_VE	71.47 ± 5.10	77.94 ± 4.09	0.008	86.54 ± 7.85	70.26 ± 6.25	0.740	65.17 ± 6.67	80.18 ± 5.21	0.002
Kurtosis_6_VE	68.29 ± 5.54	78.49 ± 3.92	0.039	82.25 ± 8.04	73.96 ± 6.11	0.529	61.60 ± 6.28	81.54 ± 4.71	0.037

Table 7: Cox regression analysis examined the interaction between stage and CT kurtosis. Both parameters were significantly influence patients' survival.

Parameter	Hazard Ratio (HR)	95% confidence interval of HR		p-value
		Upper	Lower	
Stage	2.835	2.138	3.759	< 0.001
CT Kurtosis	0.603	0.392	0.927	0.021

3.2.3 Subgroup analysis by site

Of the 210 colon cancer patients, 58 died during follow-up. Significant prognosticators were listed in Table 8. After Benjamin-Hochberg procedure to control the false discovery rate at 0.05, stage, TLG, entropy of PET images, kurtosis of CT images were likely factors influencing the overall survival of colon cancer patients.

Table 8: Significant prognosticators from Kaplan-Meier mean survival & Log-Rank test in colon cancer patients

Parameter	Mean survival of patients with parameter > median (mean \pm SE)	Mean survival of patients with parameter \leq median (mean \pm SE)	p-value (Log Rank test)
Stage (3,4 vs 1,2)	63.79 \pm 5.30	103.41 \pm 3.75	< 0.001
MTV	73.40 \pm 5.95	89.15 \pm 5.08	0.012
TLG	70.91 \pm 5.91	89.62 \pm 4.78	0.002
CT size	75.92 \pm 5.59	87.17 \pm 5.07	0.036
Mean_0_PET	55.50 \pm 3.35	92.88 \pm 4.47	0.012
Entropy_0_ET	71.29 \pm 5.65	92.10 \pm 4.87	< 0.001
Entropy_2_PET	70.57 \pm 5.68	92.46 \pm 4.81	< 0.001
Entropy_3_PET	70.57 \pm 5.68	92.46 \pm 4.81	< 0.001
Entropy_4_PET	70.57 \pm 5.68	92.46 \pm 4.81	< 0.001
Entropy_5_PET	70.57 \pm 5.68	92.46 \pm 4.81	< 0.001

Entropy_6_PET	70.57 ± 5.68	92.46 ± 4.81	< 0.001
MPP_0_PET	55.50 ± 3.35	92.88 ± 4.47	0.012
Kurtosis_0_PET	92.48 ± 4.76	68.44 ± 7.17	0.006
SD_3_CT	91.90 ± 4.52	72.82 ± 5.90	0.034
Kurtosis_4_CT	71.34 ± 5.75	86.53 ± 3.99	0.001
Kurtosis_5_CT	71.89 ± 5.73	86.31 ± 3.86	0.005
Kurtosis_6_CT	74.39 ± 5.60	83.44 ± 4.49	0.018
Kurtosis_3_VE	70.15 ± 6.52	81.37 ± 5.24	0.020
Kurtosis_4_VE	68.47 ± 6.44	83.58 ± 5.06	0.004
Kurtosis_5_VE	69.86 ± 5.87	81.14 ± 5.10	0.012
Kurtosis_6_VE	65.63 ± 7.26	89.10 ± 5.48	0.037

38 deaths occurred during follow-up out of the 134 rectum cancer patients. Stage, MTV, BF/SUVmax ratio, MPP of unfiltered CT images, kurtosis of CT images, SD and skewness of contrast-enhanced CT images were prognosticators (Table 9). However, none of these remained significant after Benjamini-Hochberg procedure to control for multiple comparison at the false discovery rate of 0.05.

Table 9: Significant prognosticators from Kaplan-Meier mean survival & Log-Rank test in rectum cancer patients

Parameter	Mean survival of patients with parameter > median (mean ± SE)	Mean survival of patients with parameter ≤ median (mean ± SE)	p-value (Log Rank test)
Stage (3,4 vs 1,2)	63.87 ± 5.11	83.16 ± 6.32	0.003
MTV	64.54 ± 6.43	73.53 ± 5.50	0.048
BF/SUVmax	83.82 ± 5.43	54.50 ± 4.84	0.016
MPP_0_CT	80.03 ± 5.45	55.05 ± 5.00	0.030
Kurtosis_2_CT	56.79 ± 5.39	82.78 ± 5.30	0.006
Kurtosis_3_CT	55.08 ± 5.27	85.38 ± 4.94	0.003
SD_6_VE	69.88 ± 5.12	58.69 ± 6.82	0.017
Skewness_0_VE	52.46 ± 7.17	75.55 ± 5.85	0.044

3.2.4 Subgroup analysis by staging

Looking at the 266 patients with localized disease (stage 1-3), 48 deaths occurred during the follow-up period. The significant prognosticators were age, MTV, TLG, unfiltered skewness of the PET, mean-positive-pixels of intermediately-filtered CT image and kurtosis of unfiltered and finely-filtered CT images (Table 10). None of these remained significant after Benjamini-Hochberg procedure to control for multiple comparison at the false discovery rate of 0.05. Though these parameters were significant in the whole cohort.

Table 10: Significant prognosticators from Kaplan-Meier mean survival & Log-Rank test in patients with localized diseases

Parameter	Mean survival of patients with parameter > median (mean \pm SE)	Mean survival of patients with parameter \leq median (mean \pm SE)	p-value (Log Rank test)
Age	82.69 \pm 4.52	103.51 \pm 3.43	0.001
MTV	85.14 \pm 5.19	94.01 \pm 4.04	0.032
TLG	84.90 \pm 4.98	94.55 \pm 4.21	0.014
Skewness_0_PET	100.34 \pm 3.87	73.37 \pm 4.59	0.002
MPP_2_CT	89.45 \pm 3.74	84.75 \pm 5.05	0.034
MPP_3_CT	91.82 \pm 3.41	82.43 \pm 5.17	0.021
Kurtosis_0_CT	85.99 \pm 4.93	88.33 \pm 3.75	0.049
Kurtosis_2_CT	83.50 \pm 4.83	89.32 \pm 3.50	0.008
Kurtosis_3_CT	83.71 \pm 5.12	90.10 \pm 3.50	0.024

Among the 42 patients with stage 1 disease, only 3 died during the follow-up period. Significant prognosticators were SD of the intermediately and coarsely-filtered CT images, and MPP of the coarsely-filtered CT images (Table 11). None of these

remained significant after Benjamini-Hochberg procedure to control for multiple comparison at the false discovery rate of 0.05.

Table 11: Significant prognosticators in patients with stage 1 disease. No median survival was listed as the three dead patients were distributed in the same side when dichotomized by the median value of these parameters.

Parameter	p-value (Log Rank test)
SD_3_CT	0.049
SD_4_CT	0.049
SD_5_CT	0.043
SD_6_CT	0.049
MPP_5_CT	0.049

13 out of 90 patients with stage 2 disease died during the follow-up period.

Significant prognosticators were skewness of intermediately filtered CT images and kurtosis of unfiltered CT images (Table 12). None of these remained significant after Benjamini-Hochberg procedure to control for multiple comparison at the false discovery rate of 0.05.

Table 12: Significant prognosticators from Kaplan-Meier mean survival & Log-Rank test in patients with stage 2 diseases

Parameter	Mean survival of patients with parameter > median (mean \pm SE)	Mean survival of patients with parameter \leq median (mean \pm SE)	p-value (Log Rank test)
Skewness_3_CT	66.12 \pm 5.75	101.91 \pm 7.24	0.037
Kurtosis_0_CT	81.37 \pm 9.34	90.31 \pm 6.55	0.020

Among 134 patients with stage 3 disease, 32 died during the follow-up. Age, time to peak from CT perfusion images, entropy, MPP and kurtosis of CT images were prognosticators (Table 13). None of these remained significant after Benjamini-

Hochberg procedure to control for multiple comparison at the false discovery rate of 0.05.

Table 13: Significant prognosticators from Kaplan-Meier mean survival & Log-Rank test in patients with stage 3 diseases

Parameter	Mean survival of patients with parameter > median (mean \pm SE)	Mean survival of patients with parameter \leq median (mean \pm SE)	p-value (Log Rank test)
Age	65.55 \pm 5.95	97.34 \pm 5.04	0.002
Time to peak	60.33 \pm 5.36	90.67 \pm 5.01	0.002
Entropy_2_CT	90.32 \pm 4.80	69.43 \pm 6.79	0.014
MPP_0_CT	91.15 \pm 4.55	67.48 \pm 6.95	0.004
MPP_2_CT	90.00 \pm 4.82	70.04 \pm 6.80	0.008
MPP_3_CT	87.37 \pm 5.00	70.43 \pm 7.09	0.028
MPP_4_CT	87.49 \pm 4.96	70.22 \pm 7.11	0.026
Kurtosis_3_CT	72.48 \pm 7.11	84.96 \pm 5.81	0.017
Kurtosis_5_CT	72.38 \pm 6.53	89.73 \pm 4.69	0.029

As for the 78 patients with metastatic disease, 48 died during follow-up. The significant prognosticators included time to peak from the CT perfusion images, entropy of the PET images, SD and MPP of the contrast-enhanced CT. Among these, time to peak, PET volume and entropy of the PET images were unique to these stage 4 patients (Table 14). Again, none of these remained significant after Benjamini-Hochberg procedure to control for multiple comparison at the false discovery rate of 0.05.

Table 14: Significant prognosticators from Kaplan-Meier mean survival & Log-Rank test in patients with metastatic diseases

Parameter	Mean survival of patients with parameter > median (mean \pm SE)	Mean survival of patients with parameter \leq median (mean \pm SE)	p-value (Log Rank test)
-----------	---	--	-------------------------

Time to Peak	20.23 ± 2.27	31.65 ± 2.95	0.005
Entropy_0_PET	30.64 ± 6.62	35.51 ± 3.25	0.008
Entropy_2_PET	30.64 ± 6.62	35.51 ± 3.25	0.008
Entropy_3_PET	30.64 ± 6.62	35.51 ± 3.25	0.008
Entropy_4_PET	30.64 ± 6.62	35.51 ± 3.25	0.008
Entropy_5_PET	30.64 ± 6.62	35.51 ± 3.25	0.008
Entropy_6_PET	30.64 ± 6.62	35.51 ± 3.25	0.008
SD_4_VE	30.87 ± 3.20	21.46 ± 2.51	0.021
SD_5_VE	31.57 ± 3.06	20.83 ± 2.55	0.010
SD_6_VE	31.28 ± 2.99	20.48 ± 2.49	0.013
MPP_3_VE	31.52 ± 3.38	21.51 ± 2.46	0.020

3.2.5 Subgroup analysis by treatment modalities

213 patients went straight to surgery after the imaging studies, 103 of whom went on to have subsequent adjuvant chemotherapy, leaving 110 that had undergone primary surgery alone. 91 received curative-intend chemoradiotherapy upfront while 40 had palliative therapies.

43 out of 213 patients who received primary surgeries died during follow-up. Stage, MTV, glycolysis, TLG, CT size from FDG-PET/CT scans, mean and skewness of the unfiltered PET images, entropy of the PET images, SD & kurtosis of CT images were all prognosticators (Table 15). After Benjamini-Hochberg procedure to control the false discovery rate at 0.05, stage was the only prognosticator.

Table 15: Significant prognosticators from Kaplan-Meier mean survival & Log-Rank test in patients treated with primary surgery

Parameter	Mean survival of patients with parameter > median (mean ± SE)	Mean survival of patients with parameter ≤ median (mean ± SE)	p-value (Log Rank test)
Stage (3,4 vs 1,2)	74.44 ± 5.62	99.43 ± 4.66	< 0.001

MTV	83.68 ± 5.62	93.36 ± 4.50	0.014
Glycolysis	86.42 ± 4.95	91.47 ± 4.82	0.010
TLG	83.48 ± 5.51	93.23 ± 4.73	0.003
CT size	84.12 ± 5.61	92.80 ± 4.76	0.045
Mean_0_PET	61.89 ± 3.50	102.04 ± 3.84	0.001
Entropy_0_PET	85.57 ± 5.14	94.54 ± 4.80	0.022
Entropy_2_PET	85.55 ± 5.14	94.49 ± 4.81	0.023
Entropy_3_PET	85.34 ± 5.17	94.69 ± 4.77	0.019
Entropy_4_PET	85.57 ± 5.14	94.54 ± 4.80	0.022
Entropy_5_PET	85.34 ± 5.17	94.69 ± 4.77	0.019
Entropy_6_PET	85.34 ± 5.17	94.69 ± 4.77	0.019
MPP_0_PET	61.89 ± 3.50	102.04 ± 3.84	0.001
Skewness_0_PET	97.89 ± 4.34	75.23 ± 5.64	0.028
SD_3_CT	90.71 ± 3.56	80.66 ± 5.71	0.044
Kurtosis_2_CT	82.59 ± 5.39	98.09 ± 4.98	0.003
Kurtosis_4_CT	81.81 ± 5.62	91.53 ± 3.64	0.008
Kurtosis_3_VE	75.59 ± 6.16	94.55 ± 3.76	0.001
Kurtosis_4_VE	79.66 ± 6.19	89.66 ± 4.58	0.004
Kurtosis_5_VE	80.67 ± 6.64	88.89 ± 4.42	0.009
Kurtosis_6_VE	78.23 ± 6.79	89.68 ± 4.34	0.013

Among those patients treated with primary surgery, 110 were treated with surgery only without any adjuvant therapies. Of these, 17 died during the follow-up period. Stage, age, SUVmean, MTV, lesion glycolysis, TLG, CT size, entropy from PET images, skewness of PET and CT images as well as kurtosis of CT images were prognosticators (Table 16). After Benjamini-Hochberg procedure to control the false discovery rate at 0.05, stage, MTV, lesion glycolysis, TLG, kurtosis of CT images were prognosticators.

Table 16: Significant prognosticators from Kaplan-Meier mean survival & Log-Rank test in patients treated with only primary surgery without adjuvant treatments

Parameter	Mean survival of patients with parameter > median (mean \pm SE)	Mean survival of patients with parameter \leq median (mean \pm SE)	p-value (Log Rank test)
Stage (3,4 vs 1,2)	69.84 \pm 10.32	106.77 \pm 3.36	< 0.001
Age	90.59 \pm 6.01	107.01 \pm 4.33	0.025
SUVmean	88.67 \pm 6.50	104.42 \pm 4.04	0.017
MTV	87.18 \pm 6.81	105.39 \pm 3.57	0.002
Glycolysis	82.51 \pm 6.91	110.89 \pm 1.90	< 0.001
TLG	86.51 \pm 6.69	106.95 \pm 3.28	< 0.001
CT size	88.60 \pm 6.52	106.69 \pm 3.43	0.006
Entropy_0_PET	91.46 \pm 6.19	104.44 \pm 4.02	0.039
Entropy_2_PET	90.91 \pm 6.30	104.62 \pm 3.94	0.030
Entropy_3_PET	90.91 \pm 6.30	104.62 \pm 3.94	0.030
Entropy_4_PET	91.46 \pm 6.19	104.44 \pm 4.02	0.039
Entropy_5_PET	90.91 \pm 6.30	104.62 \pm 3.94	0.030
Entropy_6_PET	90.91 \pm 6.30	104.62 \pm 3.94	0.030
Skewness_0_PET	107.42 \pm 4.14	68.83 \pm 4.32	0.037
Skewness_3_CT	76.30 \pm 5.45	108.22 \pm 3.78	0.016
Kurtosis_2_CT	89.06 \pm 6.75	94.71 \pm 3.29	0.016
Kurtosis_3_VE	85.25 \pm 7.81	91.86 \pm 3.55	0.013
Kurtosis_4_VE	81.59 \pm 8.01	110.73 \pm 3.67	0.002
Kurtosis_5_VE	82.85 \pm 7.88	96.94 \pm 3.16	0.002
Kurtosis_6_VE	88.05 \pm 7.54	92.37 \pm 4.33	0.042

Of the 91 patients that received curative-intended chemoradiotherapy, 23 died during the follow-up period. MPP of unfiltered CT images, kurtosis of finely-filtered CT images, SD, MPP and entropy of coarsely filtered contrast-enhanced CT images were prognosticators (Table 17). After Benjamini-Hochberg procedure to control for multiple comparison at the false discovery rate of 0.05, none of these was significant.

Table 17: Significant prognosticators from Kaplan-Meier mean survival & Log-Rank test in patients treated with curative-intended chemoradiotherapy

Parameter	Mean survival of patients with parameter > median (mean \pm SE)	Mean survival of patients with parameter \leq median (mean \pm SE)	p-value (Log Rank test)
MPP_0_CT	87.00 \pm 6.44	56.27 \pm 5.72	0.018
Kurtosis_2_CT	59.71 \pm 6.38	85.15 \pm 6.37	0.037
SD_6_VE	76.66 \pm 5.45	54.85 \pm 7.75	0.016
Entropy_5_VE	80.07 \pm 5.40	55.16 \pm 7.51	0.007
Entropy_6_VE	76.08 \pm 5.60	55.76 \pm 7.85	0.020
MPP_6_VE	76.97 \pm 5.35	54.38 \pm 7.81	0.011

In 40 patients receiving palliative treatments, SUVmax, kurtosis of finely-filtered PET images, SD & entropy of coarsely-filtered contrast-enhanced CT were prognosticators (Table 18). None of these remained significant after Benjamini-Hochberg procedure to control the false discovery rate at 0.05.

Table 18: Significant prognosticators from Kaplan-Meier mean survival & Log-Rank test in patients treated with palliation

Parameter	Median survival of patients with parameter > median (mean \pm SE)	Median survival of patients with parameter \leq median (mean \pm SE)	p-value (Log Rank test)
SUVmax	14.60 \pm 2.67	23.64 \pm 2.83	0.030
Kurtosis_2_PET	24.40 \pm 3.42	14.04 \pm 1.56	0.006
Kurtosis_3_PET	26.04 \pm 4.01	14.60 \pm 1.61	0.004
SD_4_VE	22.62 \pm 3.30	12.99 \pm 3.23	0.040
SD_5_VE	26.04 \pm 3.73	12.99 \pm 2.94	0.014
Entropy_4_VE	26.04 \pm 3.28	14.60 \pm 2.67	0.016
Entropy_5_VE	26.04 \pm 3.65	12.99 \pm 3.23	0.008

3.3 Discussion

Angiogenesis is one of the corner stones of tumour biology [1]. Neovasculatures in tumours are immature, and prone to leakage compared to normal vessels. Perfusion images utilize intravenous contrast medium to study vascular delivery and local dispersion of the contrast medium, and reflect the transport capacity and leakiness of the vessels. [195]. In colorectal cancers, CT perfusion studies had been shown to correlate with tumour grading [178-181]. It seems well-differentiated tumours had higher blood flow, and higher blood flow might be indicative of better survival. As for direct comparison to microvascular density as shown by CD34 or CD105 staining, the results were less definite. While Goh *et al.* found moderate correlation [174, 175], others did not find this correlation [172, 178, 179].

In our whole cohort, we were unable to show that CT perfusion parameters predicted patients' survival. Previous reports by Hayano *et al.* [181] and Goh *et al.* [182] suggested higher blood flow was associated with better outcome in surgical patients. Compared to these reports, we had a considerably larger patient cohort and our patients underwent various treatments as determined in the multidisciplinary team discussion according to their respective clinical status. Therefore, CT perfusion parameters are probably not associated with patients overall survival in such a heterogeneous population. The relationship between the CT perfusion parameters and angiogenesis as demonstrated by histopathologic results are discussed in Chapter 4.

In patients with stage 3 and 4 disease we found those with shorter time-to-peak had longer survival. Although this parameter did not pass high statistical vigour, it was a recurrent feature that may suggest that it may be of true significance. Time to peak was positively correlated with tumour stage and high-grade tumour in 53 patients as reported by Xu *et al.* [180]. Sun *et al.* also reported poorly-differentiated tumour had a longer time-to-peak from 37 CRC patients [179]. Fraioli *et al.* in nonresectable non-small cell lung cancer patients treated with carboplatin, paclitaxel and bevacizumab revealed longer time to peak in non-responders [196]. Our results were compatible with these reports, implying that quicker contrast-enhancement suggests less aggressive tumours and better patient outcome.

FDG-PET was shown to predict survival in colorectal cancer patients. In surgical patients, Shi *et al.* found SUVmax and staging were independent prognosticators. Those with more advanced stage and higher SUVmax had shorter survival [136]. Ogawa *et al.* showed high total lesion glycolysis was a poor prognosis factor in rectal cancer patients treated with surgery. [137]. In metastatic patients treated with regorafenib, high pre-treatment total lesion glycolysis denoted worse survival [146].

In our entire cohort, total lesion glycolysis was a prognosticator in colorectal cancer, but when the population was divided into separate colon and rectal cancer patients, TLG was only prognostic in colon cancer patients. Colon cancer patients were more often treated with primary surgery, while rectal cancer patients were prone to have chemoradiotherapy upfront, which could have influenced the relationship between tumour metabolism and prognosis. In support of this theory, in this cohort higher TLG denoted a worse survival in patients treated with surgery, but not in

patients treated with chemoradiotherapy. SUVmax was a prognosticator in patients undergoing palliation. In the rectal group, those patients underwent heterogeneous treatment, different combination of chemotherapy, target drugs, and some of these has post therapy resection. These complicated and prolonged treatment courses might diminish the impact of initial FDG-PET uptake on survival.

In addition to conventional staging, CT and PET parameters, additional parameters such as textural analysis derived from both CT and PET were extracted. One can construct a histogram from the pixel values in a region of interest, and analyse the properties of the histogram such as mean, standard deviation, skewness, kurtosis. Ng *et al.* demonstrated entropy, kurtosis, skewness, SD of the pixel distribution histogram contrast-enhanced CT post fine filtration were predictive of the patient survival from 55 retrospectively collected patients. They used receiver operating characteristic (ROC) curve optimized thresholds for each parameter, and found the survival of patients with above and below the threshold had significantly different survival by Kaplan-Meier plots. [190]. These results might be over-optimistic as threshold values were calculated post hoc and whether these results could be applied to other patient cohorts is doubtful.

In our cohort, we found kurtosis was a stable prognosticator across the whole cohort after using both test and validation population analysis. Weiss *et al.* in 48 early non-small cell lung cancer found lower kurtosis was associated with worse survival. However, they sought the cut-off value by minimizing the p-value of the log-rank test, introducing bias [197]. In 73 oesophageal squamous cell carcinoma patients, Liu *et al.* found kurtosis of the non-contrast enhanced CT was correlated with T,N and overall

stage [198]. Though these results were from another oesophageal cancer rather than CRC, the findings were compatible i.e. higher kurtosis denoted a worse outcome. Kurtosis was reported to be of good reproducibility on repeated scans of a phantom [199] and on repeated scan of patients' lesions [200, 201]. It describes the shape of the histogram distribution by the width of distribution. A higher kurtosis indicates wider "tails" of the histogram distribution. In TexRAD software, the kurtosis decreased with the number of highlighted objects after filtering, and increased by the variation of intensity in these highlighted objects [187]. In our cohort, patients whose tumours had lower kurtosis had better survival. This might imply those tumours were more homogenous (less variation in CT numbers).

In the metastatic group of our cohort, those primary tumours with quicker contrast enhancement (shorter time to peak), higher SD & MPP of contrast-enhanced CT, lower entropy on PET, had longer survival. Ganeshan *et al.* prospectively injected 14 non-small cell lung cancer patients with pimonidazole 24 hours before surgery to compare the pimonidazole staining, a marker of hypoxia, from the surgical specimen with texture analysis results from the pre-operative contrast CT. They found SD and MPP of the contrast-enhanced CT were positively correlated with pimonidazole staining, suggesting higher SD & MPP could imply hypoxia in the tumour [202]. Though several groups reported hypoxic staining was associated with worse prognosis in colorectal cancers [58-61], a larger cohort consisting of 186 patients found no such correlation [62]. Whether high SD & MPP of contrast-enhanced CT reflected hypoxia in the primary tumour, and why that was a good prognosticator needs further investigation. Finally, entropy was shown to be one of the most stable parameters in

PET texture analysis [203-205]. Our data indicated in patients with stage 4 disease or in surgical patients, those with more homogenous primary tumours had better outcome.

For future work, the relationship between the texture parameters and underlying patho-physiologic properties could be interesting. Miles *et al.* showed that the texture parameter mean positive pixels from the primary colorectal patients in combination with FDG-PET scan and blood flow from CT perfusion could predict the status of KRAS mutation [134]. How kurtosis is related to the underlying genetic drive of the tumours and oncogene expression remains to be seen. Some of these is explored in the latter chapter.

In summary, out of the various parameters from FDG-PET and CT perfusion, it was found that metabolic parameters may have a role in prognosis of colorectal carcinoma, especially in colon cancer patients and probably in those treated with primary surgery. It was shown that there is a stable CRC prognosticator using textural analysis of the derived images. In the following chapters there will be examination of some of the colorectal cancer histological correlates as well as serum derived exosome proteins related with hypoxia that may give insight into the underlying mechanisms of how tumour textural measurements relate to prognosis.

4 What do these imaging parameters mean: Correlation with immunohistochemical staining results

This chapter investigates whether parameters derived from clinical images reflect the status of angiogenesis and other related biomarkers in the surgically resected colorectal tumours. The work was done with the kind assistance of Dr. Manuel Rodriguez-Justo and Dr. Saif U Rehman Khan.

4.1 Results

Out of the 344 patients, 213 were treated with primary surgery with no other therapy before resection. Histopathology specimens were obtained from 153 patients, and stained with VEGF, CD105, CA-IX, GLUT-1, HIF-1 α .

The significant findings are summarized in Table 19.

Table 19: Summary of significant correlations between IHC & image parameters

Parameters	Spearman's correlation coefficient	p-value
CD105 & VEGF	0.535	< 0.001
CD105 & HIF-1 α	-0.273	0.001
GLUT-1 & HIF-1 α	-0.264	0.001

VEGF & mean slope of increase	-0.365	< 0.001
VEGF & mean transit time	0.375	< 0.001

4.1.1 Associations between IHC parameters

Among these, CD105 was positively correlated with VEGF, while negatively correlated with HIF-1 α . HIF-1 α was negatively correlated with GLUT-1 (Table 20).

Table 20: Spearman's correlation coefficient and p-values of the histopathologic staining. Bold font denotes significant correlation after Bonferroni correction ($p < 0.004$).

ρ (p-value)	VEGF	CA-IX	GLUT-1	HIF-1 α
CD105	0.535 (<0.001)	0.177 (0.033)	0.099 (0.239)	-0.273 (0.001)
VEGF		0.157 (0.053)	0.140 (0.086)	-0.082 (0.311)
CA-IX			0.000 (0.999)	-0.012 (0.885)
GLUT-1				-0.264 (0.001)
HIF-1 α				

36 patients died during follow-up. CD105 was found to be a prognosticator.

Patients with higher microvascular density as counted by CD105 had worse outcome (Table 21)(Figure 6).

Table 21: Kaplan-Meier mean survival & Log-Rank test of the histopathologic staining results

Parameter	Mean survival of patients with parameter > median (mean \pm SE)	Mean survival of patients with parameter < median (mean \pm SE)	p-value (Log Rank test)
CD105	81.96 \pm 5.34	64.33 \pm 2.26	0.035
VEGF	83.29 \pm 6.45	68.29 \pm 3.99	0.377
CA-IX	87.36 \pm 6.33	85.33 \pm 5.51	0.631
GLUT-1	84.60 \pm 5.52	86.05 \pm 4.55	0.469

HIF-1 α	84.06 \pm 8.16	82.42 \pm 4.47	0.633
----------------	------------------	------------------	-------

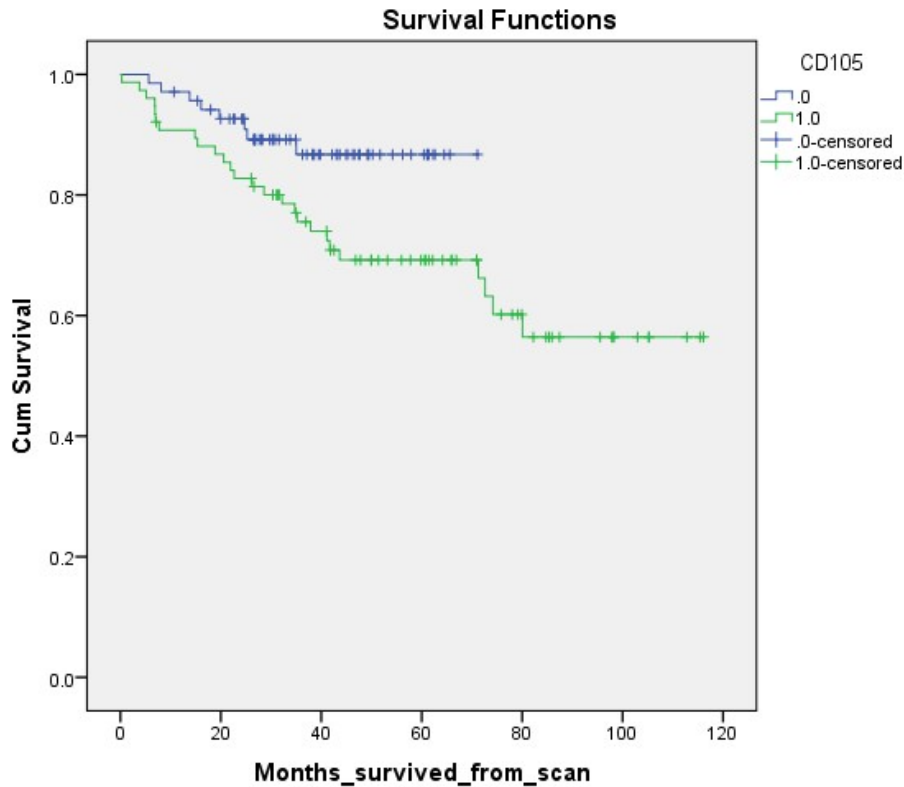


Figure 6. Kaplan-Meier survival curves comparing patients with high (1.0, lower curve) and low (.0, higher curve) CD105. Patients with higher microvascular density as counted by CD105 had worse outcome (mean survival 81.96 \pm 5.34 versus 64.33 \pm 2.26 months, $p = 0.035$).

4.1.2 Associations between CT perfusion and IHC

The correlation between the IHC results and CT perfusion revealed VEGF was negatively correlated with mean slope of contrast enhancement, and positively correlated with mean transit time. The correlations of other pairs did not reach a significance level after stringent correction for multiple-comparison. Thus the following might be false positive: CD105 was negatively associated with mean slope of increase, and positively with blood volume as well as mean transit time; VEGF positively correlated with time to peak; CA-IX negatively correlates with mean slope of increase and PS (Table 22).

Table 22: Spearman's correlation coefficient and p-values of the histopathologic staining and CT perfusion parameters. Bold font denotes significant correlation after Bonferroni correction ($p < 0.00167$).

ρ (p-value)	Time to Peak	Mean slope of increase	Blood volume	Blood flow	Mean transit time	PS
CD105	0.023 (0.807)	-0.207 (0.025)	0.221 (0.017)	0.129 (0.164)	0.218 (0.018)	0.011 (0.907)
VEGF	0.262 (0.003)	-0.365 (<0.001)	0.124 (0.173)	-0.073 (0.422)	0.375 (<0.001)	0.004 (0.968)
CA-IX	0.040 (0.661)	-0.186 (0.038)	-0.159 (0.079)	-0.103 (0.255)	-0.009 (0.925)	-0.239 (0.007)
GLUT-1	0.057 (0.530)	-0.055 (0.548)	-0.056 (0.540)	-0.020 (0.831)	0.086 (0.345)	0.000 (0.998)
HIF-1 α	-0.071 (0.436)	0.025 (0.783)	0.024 (0.795)	0.018 (0.840)	-0.114 (0.209)	0.030 (0.742)

4.1.3 Associations between PET parameters and IHC

None of the FDG-PET parameters were significantly correlated with the IHC results after Bonferroni correction for multiplicity. Disregarding the multiplicity, CD105 was positively correlated with TLG, and VEGF was positively correlated with SUV_{mean} (Table 23).

Table 23: Spearman's correlation coefficient and p-values of the histopathologic staining and FDG-PET parameters. None had the significance level below 0.0025 (the significance level after Bonferroni correction).

ρ (p-value)	SUVmax	SUVmean	MTV	Lesion glycolysis	TLG
CD105	0.081 (0.339)	0.066 (0.437)	0.162 (0.055)	0.164 (0.052)	0.201 (0.016)
VEGF	0.151 (0.066)	0.165 (0.044)	0.027 (0.743)	0.095 (0.252)	0.127 (0.124)
CA-IX	0.008 (0.925)	0.004 (0.963)	0.136 (0.097)	0.076 (0.357)	0.075 (0.366)
GLUT-1	0.036 (0.661)	0.062 (0.451)	-0.074 (0.3728)	-0.039 (0.639)	-0.032 (0.700)
HIF-1 α	-0.047 (0.572)	-0.078 (0.345)	-0.062 (0.450)	-0.102 (0.215)	-0.138 (0.092)

4.1.4 Associations between textural parameters (CT and PET) and IHC

There was no significant correlation between texture parameters and the IHC results after Bonferroni correction for multiplicity ($p < 0.000278$). Several pairs did have $p < 0.01$: entropy of finely-filtered CT with VEGF, SD & MPP of finely-filtered contrast-enhanced CT with CD105 (both negative), kurtosis and skewness of intermediately-filtered PET image with CD105, skewness of coarsely-filtered PET with VEGF, mean of filtered PET with VEGF (negative), SD of unfiltered PET with HIF-1 α (negative), kurtosis of unfiltered PET images with HIF-1 α (Table 24). A complete list of correlations is found in the Appendix.

Table 24: Correlations between texture parameters and IHC results with p-value less than 0.01

Parameters	Spearman's correlation	p-value

	coefficient	
Entropy_2_CT & VEGF	0.221	0.007
SD_2_VE & CD105	-0.290	0.002
MPP_2_VE & CD105	-0.283	0.002
Kurtosis_3_PET & CD105	0.225	0.008
Kurtosis_4_PET & CD105	0.241	0.004
Kurtosis_5_PET & CD105	0.239	0.004
Skewness_4_PET & CD105	0.237	0.005
Skewness_5_PET & CD105	0.238	0.005
Skewness_4_PET & VEGF	0.222	0.007
Skewness_5_PET & VEGF	0.252	0.002
Skewness_6_PET & VEGF	0.243	0.003
Mean_2_PET & VEGF	-0.229	0.005
Mean_3_PET & VEGF	-0.228	0.006
Mean_4_PET & VEGF	-0.233	0.005
Mean_5_PET & VEGF	-0.223	0.007
SD_0_PET & HIF-1 α	-0.257	0.002
Kurtosis_0_PET & HIF-1 α	0.239	0.004

4.2 Discussion

Tumours require vessel formation to supply oxygen and nutrients. Cells distant to the vascular supply may become hypoxic. Hypoxia stabilizes HIF-1 α to dimerize with

HIF-1 β and bind to hypoxia response elements. The targets of HIF-1 include VEGF and GLUT-1 are implicated in angiogenesis, glucose metabolism, cell proliferation, invasion and metastasis [56]. Carbonic anhydrase IX (CA-IX) is also a target of HIF-1 pathway as it has hypoxia response elements (HRE) in its promoter [206]. As angiogenesis and hypoxia are closely linked, we calculated microvascular density and the expression of related proteins in histopathologic specimens to represent angiogenesis, and investigated if the parameters from clinical images could infer the tissue status.

Different antibodies were used to identify endothelium cells. Minhajat *et al.* showed CD31 was a pan-endothelium marker that was expressed on endothelial cells of both cancerous and non-cancerous regions, but CD105 was preferably expressed in cancerous tissues [207]. CD105 is a receptor of TGF- β expressed on proliferating endothelial cells. It is thus a marker for neovascularization [208]. In 150 resected CRC specimens, Saad *et al.* found both CD31 and CD105 counts were correlated with lymph node metastases, but only CD105 was correlated with liver metastases. CD31 but not CD105 was correlated with tumour size [209]. In our patient samples, we used CD105 for microvascular density calculation.

In our cohort, microvascular density as counted by CD105 was positively correlated with VEGF. This is compatible with the role of VEGF promoting angiogenesis. CD105 was negatively correlated with HIF-1 α . Goethals *et al.* showed MVD is negatively correlated with pimonidazole staining in 20 CRC samples. They found carbonic anhydrase IX colocalized with pimonidazole in 30% of cases, and there was no correlation between pimonidazole staining and VEGF, EGFR [210].

In our cohort, HIF-1 α was negatively correlated with GLUT-1. Lee-Kong *et al.* investigated the biopsy samples of 85 rectal cancer patients before neoadjuvant

chemoradiotherapy. They found though HIF-1 α correlated with VEGF and GLUT-1, but it did not correlate with patients' outcome. Instead, high CA-IX expression was associated with worse overall survival [211]. However, there were reports that hypoxia and GLUT-1 were not related. In the report by Rajaganeshan *et al.* in 55 CRC patient samples they had positive correlation between VEGF and HIF-1 α but no correlation between HIF-1 α and GLUT-1 or CA-IX [212]. Verstraete *et al.* found no correlation between pimonidazole staining and CA-IX or GLUT-1 expression in 20 CRC patients. In their report, GLUT-1 expression was associated with advanced stages, and low CA-IX expression with better disease-free survival [213]. Thus, there seemed no consensus on the relationship between HIF-1 α and GLUT-1 on the tissue IHC.

It was reported that angiogenesis as reflected by microvascular density is a prognosticator in colorectal cancer. Higher MVD was predictive of poor recurrence-free survival and overall survival [214]. Similarly, VEGF expression was associated with worse survival [214]. For example, in 127 surgical treated CRC patients, Choi *et al.* demonstrated higher MVD as measured by factor VIII was associated with lymphovascular invasion, lymph node metastases, and hematogenous metastases. It was also an independent prognosticator in Cox multivariate analysis [215]. Another report by Kaio *et al.* indicated that the presence of VEGF staining in the deepest invasive margin of the surgical specimens was a bad prognosticator in 152 CRC patients. The presence was associated with histologic grading, lymphovascular invasion, lymph node and liver metastases. [216]. In our cohort, high CD105 expression had worse survival compatible with the previous reports.

Various attempts to correlate with CT perfusion parameters and microvascular density have been made. Goh *et al.* revealed moderate correlation between blood

volume ($r = 0.59$, $P = .002$), permeability surface-area product ($r = 0.46$, $P = .03$) and CD34 in 23 patients [174]. In another cohort, Goh *et al.* found mild correlation between blood flow and CD105 ($r = 0.33$, $p = 0.05$) in 35 patients, while there was no correlation between CD105 and FDG parameters (SUVmax or SUVmean) [175]. Kim *et al.* found no correlation between CT perfusion parameters and CD34 in 27 CRC patients [178]. In our cohort, which was substantially larger than these previous reports, we found possible evidence that CD105 negatively correlated with mean slope of increase and positively with mean transit time. This may suggest that the intravenous contrast medium took longer to flow through the tissues with more newly-formed vessels. This finding is compatible with Torri *et al.*, who measured the breast cancer cell line MDAMB231 in mice xenografts and found longer mean transit time in tumour compared to normal tissue [217]. It implies less efficient transport resulting from flow resistance of immature vessel architecture as well as increased interstitial pressure from leaky vessels [218].

CD105 was positively correlated with TLG in our cohort. High TLG was shown to be associated with worse survival [137] [139]. This result was compatible with a higher MVD as a predictor of poor survival as discussed above.

Similar to CD105, VEGF was negatively associated with the mean slope of contrast enhancement, positively with mean transit time and probably time to peak. This was not unexpected as VEGF is implied in endothelial proliferation and thus the formation of new vessels, which are often immature and leaky [77], resulting in increased mean transit time as discussed above. Furthermore, VEGF correlated with SUVmean in our cohort. VEGF is thought to be associated with migration and invasion of cancer cells. Bhattacharya *et al.* found knocking VEGF out of CRC cell lines decreased their

migration and invasion [219]. The serum level of VEGF was higher in patients with positive FDG uptake [135]. Our finding that VEGF correlated with SUVmean is compatible with these reports.

We found CA-IX was negatively correlated with mean slope of contrast enhancement and PS. Carbonic anhydrase catalyzes the conversion of carbon dioxide and water into bicarbonic acid, which dissociates into bicarbonate ions and protons. It helps maintain the acid-base balance [220]. PS describes the speed of contrast medium moving from capillary into the interstitium in a volume of tissue [221]. Our results showed tumours with higher CA-IX expression had slower rate of contrast enhancement and diffusion into the tissues. CA-IX expression has been shown to be controlled by HIF-1 activity [206] and thus could be a marker of hypoxia. The result confirmed that hypoxic tumours had inefficient transport from the vessels, including the delivery of chemotherapy agents [222].

In the previous chapter, we showed in patients with metastatic diseases, those that had higher SD & MPP of contrast-enhanced CT and lower entropy of the FDG-PET images had shorter overall survival. SD & MPP of contrast-enhanced CT were negatively correlated with CD-105 and CA-IX. This result is concordant with Ganeshan *et al.*, who found these two parameters were associated with hypoxia staining by pimonidazole [202]. High microvascular density and CA-IX expression were poor prognosticators as discussed above.

Although we found higher kurtosis of non-contrast CT images was associated with worse overall survival in the whole cohort, we did not find definite correlation between kurtosis and IHC results. There was mild correlation between kurtosis of unfiltered CT image and CA-IX ($p = 0.189$, $p = 0.035$), kurtosis of intermediately-filtered

contrast-enhanced CT images and CD105 ($\rho = 0.215$, $p = 0.020$), as well as negative correlation between kurtosis of unfiltered non-contrast CT image and GLUT-1 ($\rho = -0.181$, $p = 0.046$). Although kurtosis of non-contrast CT was found to be a significant prognosticator in our cohort, its biologic foundation was not clearly elucidated.

Unlike in the CT textural data, there was no correlation between entropy of FDG-PET images and IHC findings. Perhaps the entropy of FDG PET images reflects glucose metabolism per se rather than angiogenesis or hypoxia. Our prognostic findings however indicate that tumours with a more heterogeneous distribution of glycolysis had worse outcome.

In summary, we found tumours with slower contrast passage (mean transit time) had higher microvascular density as calculated by CD105 and angiogenesis as reflected by VEGF. The texture parameters SD and MPP of contrast-enhanced CT were mildly related to CD105 expression. These two texture parameters were also found to be prognosticators in patients with metastatic diseases. We revealed possible biologic rationale of the CT perfusion and CT textural findings.

5 What messages are there in serial exosomal proteins

5.1 Introduction

Angiogenesis is a hallmark of cancer. As tumour grows away from the vessels, the tissue becomes hypoxic [4]. Hypoxia activates hypoxia-inducible factor 1 (HIF-1), which controls genes related to angiogenesis, metabolism, epithelial-to-mesenchymal transition (EMT), proliferation, stemness, and often confers worse prognosis to patients [223, 224]. Thus, angiogenesis and hypoxia are closely related. In colorectal cancers, HIF-1 α was shown to correlate with patients' outcome [58-61]. It would be desirable to investigate hypoxia by in vivo imaging to look into the prognostic information.

The classic in vivo imaging agent for hypoxia is F-18 fluoromisonidazole (F-MISO). In the absence of oxygen, the tracer is reduced and trapped within the cells by binding to other intracellular macromolecules [225]. In clinical practice, the time required for the tracer to be accumulated in areas of hypoxia takes more than two hours. Furthermore, the physiologic uptake in the bowels precludes the effective use of F-MISO on colorectal cancers [226]. Other radiotracers for hypoxia are developing, but none reaches routine clinical use yet. Blood oxygenation level-dependent MR (BOLD)

measures the proportion of oxyhemoglobin and deoxyhemoglobin to provide a readout of tissue oxygenation. The bowel movement (motion artefact) and intraluminal air (susceptibility artefact) make it difficult to apply to colorectal cancers [227].

One way to overcome the cumbersome procedures and cost related to in vivo imaging is liquid biopsy. Exosomes could be isolated from body fluids including the blood. They are known to be involved in cell proliferation, metastases, angiogenesis and immunosuppression [14]. The contents of exosomes change in response to cell differentiation [228] and pharmacologic treatment [116]. Hypoxia has been shown to increase exosome release in breast cancer [12] and prostate cancer cell lines [13]. Isolating exosomes from the blood might be able to reflect status of hypoxia of the tumours.

Another way to investigate hypoxia might be achieved by radiomics. Radiomics refers to extracting high-dimension image features from clinical images to infer biologic information and to support clinical decision making [229]. For example, Grossmann *et al.* showed some distinct image features correlated with immune pathways [230]. Ganeshan *et al.* found standard deviation and mean positive pixels from the histogram analysis of the contrast-enhanced CT images after Laplace of Gaussian operation correlated with hypoxia staining by immunohistochemical staining of the tumour tissues from non-small cell lung cancer [202]. We have assessed applying the same texture analysis method to images of colorectal cancers would also provide information on tumour hypoxia.

By investigating the exosomes from the serum of patients and image parameters from the CT scans, we aim to shed light on the status of hypoxia and thus provide

prognostic information that could ultimately be used for early diagnosis, patient stratification, disease progression, and possible more clinically relevant parameters.

5.2 Results

5.2.1 Antibody specificity test

Dotblot is a biochemical technique useful to assess protein levels in a sample of either denatured or native origin [115]. For our purposes of studying native exosomal proteins, the dotblot technique offers a great advantage over conventional western blot, which is due to the fact that western blot requires very large amounts of exosomal lysates to be performed (minimal 10 μg), whereas the amount of samples required for a dotblot is considerably minor (0.5-1 μg). Due to clinical patient serum availability, using the minimum amounts of exosomes that would provide a good biochemical readout is essential. However, because the whole sample is dotted on a nitrocellulose membrane, there is a risk that the readout can be affected by nonspecific binding of the antibodies, which in western blot is ruled out because of the molecular weight separation rendered by electrophoresis. Therefore, specificity tests must be conducted prior to the use of each antibody in the dotblot assessment of proteins.

5.2.1.1 ALIX

The work was previously established in our Lab by Dr. James Monypenny of Pitmilley. A stable ALIX knock-down HCC1954 cell line was generated by using short hairpin RNA

(shRNA) with lentiviral transduction and clonal selection. The effectiveness of knock-down was demonstrated by western blot (Figure 7, left). Dotblot confirmed little signal in the knock-down lysate, demonstrating that this antibody (due to lack of nonspecific binding) can be used in dotblotting of exosomes.

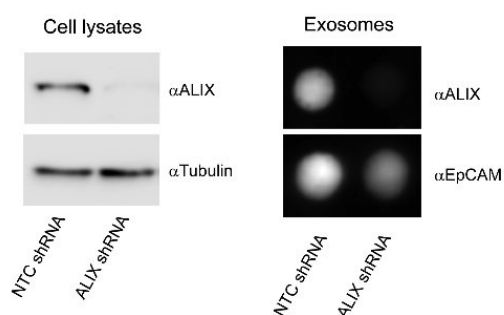


Figure 7. This work was done by by Dr. James Monypenny of Pitmilley. Western blot of the cell lysates of HCC1954 cells treated with control and ALIX shRNA respectively confirmed the knock-down of ALIX (left, upper row); tubulin control confirmed equal protein loading (left, lower row). Dotblot of the exosome confirmed there was little unspecific signals (right, upper row); despite equal protein loading, EpCAM was also decreased in exosomes derived from HCC1954 cells treated with ALIX shRNA as compared to those treated with control shRNA (right, lower row).

5.2.1.2 HER1

The work was done by Dr. James Monypenny of Pitmilley. EGFR knock-down H1975 cell line was established by using short hairpin RNA (shRNA). The bar chart at the right of Figure 8 confirmed the shRNA knock-down around 60% of the EGFR protein expression. On the left, EGFR in the exosomes isolated from the knock-down cell line was almost invisible on the dotblot, while CD63 confirmed the presence of exosome proteins.

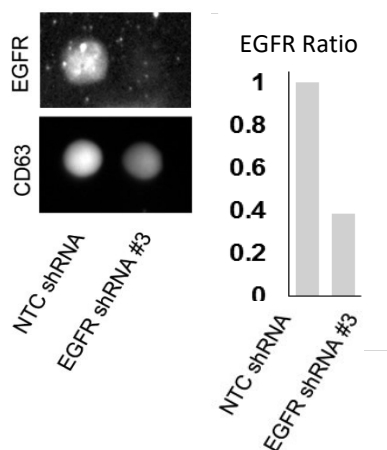


Figure 8. This work was done by Dr. James Monypenny of Pitmilly. Exosomes from the EGFR knock-down H1975 cell line had little signals from the anti-EGFR antibody on the dotblot (left, upper row), while the presence of exosome proteins was confirmed by CD63 staining (left, lower row). EGFR knock-down was confirmed by western blot (not shown). Those cells treated with EGFR shRNA had around 60% of the EGFR protein expression compared to those treated with control shRNA (right).

5.2.1.3 HER2

On the western blot (Figure 9, left), lysates from HER2 positive cell line HCC1954 bear a clear band at the expected length around 180 kDa. Tubulin staining confirmed slightly more loading of the MCF7 lysates. On the dotblot (Figure 9, right), the MCF7 dot was not clear on the HER2 strip, while HCC1954 was positive. GADPH demonstrated the loading of exosome proteins.

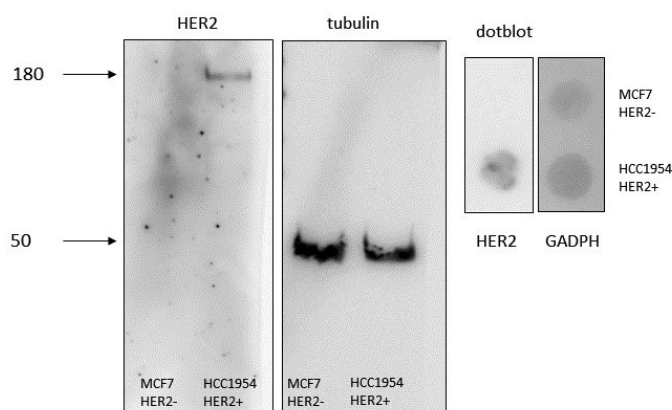


Figure 9. Western blots and dotblots of anti-HER2 antibody on the HER2 negative cell line MCF7 and HER2 positive cell line HCC1954 confirmed the specificity of anti-HER2 antibody. The presence and absence of HER2 proteins in HCC1954 and MCF7 cells were confirmed by western blot (left). On the dotblot of the anti-HER2 antibody, the exosomes from MCF7 had no signals, while those from HCC1954 were positive. GADPH confirmed the loading of exosome proteins.

5.2.1.4 HER3

Western blots by Dr. Myria Galazi confirmed absence of HER3 staining in the low-expressing prostate cancer cell line PC3 (Figure 10, left). Dotblots confirmed visibility of HER3 in the prostate cancer LNCaP cell line exosomes and no signal from the PC3 exosomes, in which GAPDH confirmed equal protein loading (Figure 10, right).

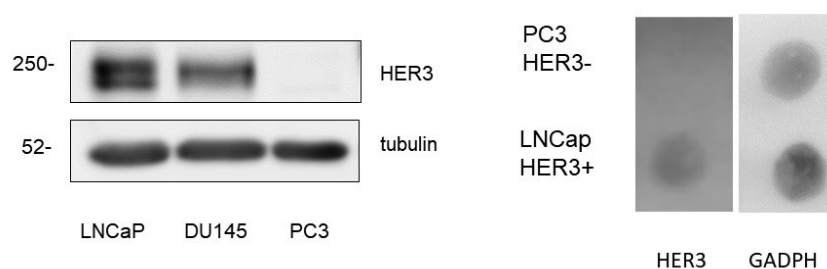


Figure 10. Western blot and dotblot of the anti-HER3 antibody on the HER3 negative cell line PC3 and HER3 positive cell line LNCaP confirmed the specificity of anti-HER3 antibody. The western blot done by Dr. Myria Galazi confirmed little HER3 expression in PC3 cells (left). Dotblot of the exosomes derived from the PC3 revealed almost invisible signals, confirming good specificity of the anti-HER3 antibody.

5.2.1.5 cMET

The work was done by Dr. James Monypenny of Pitmilley. cMET knock-down H1975 cell line was established by using shRNA. The bar chart at the right of Figure 11 confirmed almost complete knock-down of the cMET expression by the shRNA. On the left, cMET in the exosomes isolated from the knock-down cell line was invisible on the dotblot, while tubulin confirmed the presence of exosome proteins.

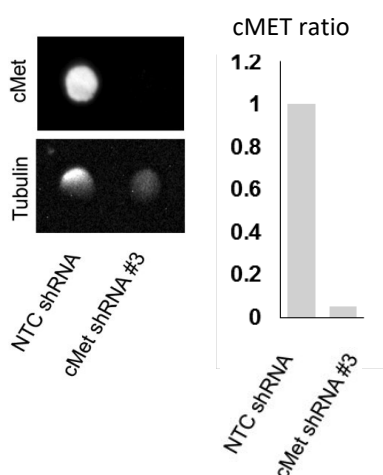


Figure 11. Exosomes from cMET knock-down H1975 cells had no visible signals from the anti-cMET antibody on the dotblot, while the presence of exosome proteins was confirmed by tubulin staining. The knock-down was confirmed by the western blot (not shown). The cells treated with cMET shRNA had less than 10% of cMET protein expression compared to those treated with control shRNA (right).

5.2.1.6 S100A9

An expected band was visible on the lysate of leukemic THP1 cells above 10 kDa.

These cells express S100A9 at high levels, while the lung cancer cell line H1975 express S100A9 poorly. While there was no signal on the H1975 lysate (Figure 12, left). On the dotblot (Figure 12, right), a weak signal could be seen on the H1975 exosomes, which might be explained by the enrichment of S100A9 in exosomes, also evident in THP1 exosomes.

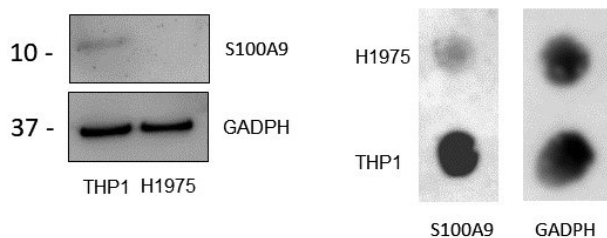


Figure 12. Western blot and dotblots of the anti-S100A9 antibody on THP1 and H1975 lysates and exosomes. Western blots revealed S100A9 signals in THP1 lysate, while little signals were detected in the lysate of H1975 (left). The dotblots showed strong signals from THP1 exosomes, but weak signals from H1975 exosomes were also detected (right). The weak signals might be the result of concentration of S100A9 in the exosomes.

5.2.1.7 P4HA1

The hepatocellular carcinoma HepG2 cell line was treated with 0.1 mM and 0.2 mM cobalt chloride overnight, which is known to induce chemical hypoxia. P4HA1 signal was very faint on control conditions, and visibly increased on those treated with CoCl_2 (Figure 13, left). Dotblot was performed on exosomes from SW48 cells treated with and without 0.2 mM CoCl_2 . A clear P4HA1 signal was detected on the treated cells. (Figure 13, right).

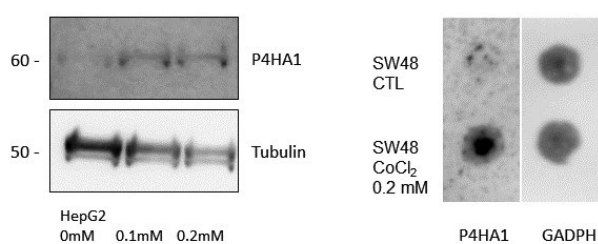


Figure 13. Western blot and dotblot of the anti-P4HA1 antibody. On the western blot, P4HA1 signals increased with the concentration of treated cobalt chloride (left). The exosomes from 0.2 mM cobalt chloride treated SW48 cells had a clear P4HA1 signals on the dotblot; while little signals were detected from the exosomes of control SW48 cells (right).

5.2.2 Cell line results

As shown in the following figure, we observed that P4HA1 as well as HIF-1 α increased in a variety of colorectal cell lines (Figure 14) after subjecting the latter to hypoxic conditions (1% oxygen) overnight. We harvested the exosomes from HCT-116 which showed the most striking response and confirmed that the exosomal protein assay also reproduced what was found in tumour cell lysates i.e. P4HA1 upregulation under hypoxia (Figure 18A).

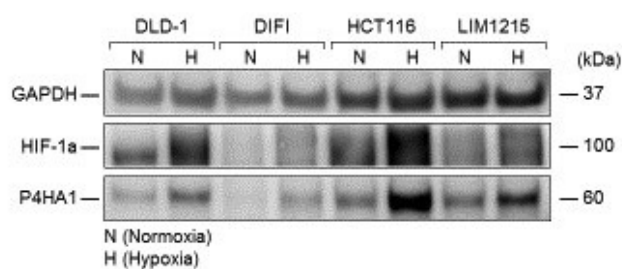


Figure 14. Several colorectal cell lines were cultured in McCoy's 5a Medium Modified supplemented with 10% fetal bovine serum, 1% glycine and penicillin/streptomycin. The normoxic control cells ('N') were incubated at 37 °C in a 5% CO₂ air atmosphere, while the hypoxia treated cells ('H') were incubated in a hypoxic incubator with 5% CO₂ and 1% O₂ at 37 °C overnight. Immunoblotting of cell lysates was performed for the detection of HIF-1 α and P4HA1, along with loading control (GAPDH).

5.2.3 Patient data

From May 2015 to Dec 2016, 54 patients recruited by the Institute of Nuclear Medicine at UCLH had their blood samples taken. Their age was between 42-83 years old (mean \pm SD: 64.83 \pm 11.19). There were 38 males, 16 females. 13 had metastatic disease. They were followed for 0.5-30.6 months (median: 21.5 months). 6 died during this period.

5.2.3.1 Patients Exosome results

Exosomes from the sera of these patients were purified and quantified by nanoparticle tracking analysis. The result showed in average there were 9.9×10^{11} particles per millilitre of the samples. The particle size was in average 89 nm (Figure 15), which complies with literature standards of exosomal quality. The exosomes from these patients were used for dotblot and probed with antibodies against ALIX, HER1, HER2, HER3, cMET, S100A9 and P4HA1 (Figure 16). The signal intensities of each protein were normalized by the signal intensity of the exosomal protein ALIX.

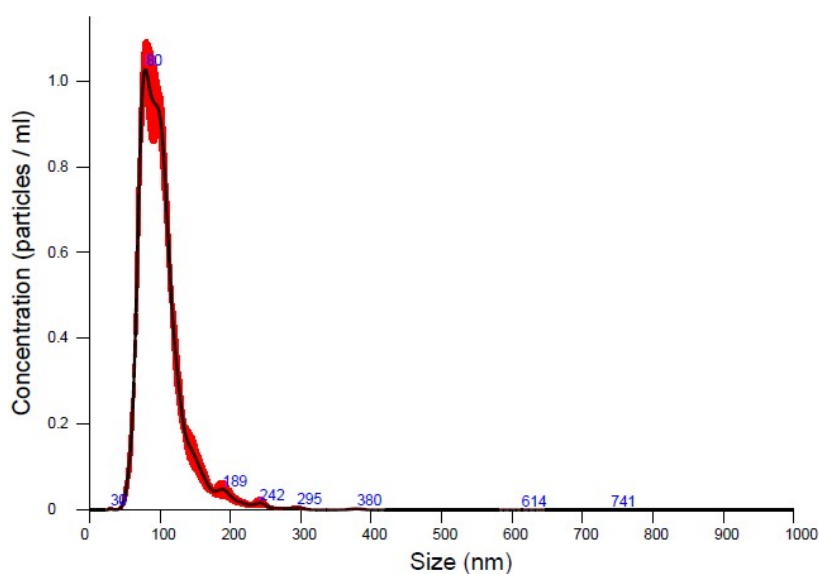


Figure 15. A sample of the nanoparticle tracking analysis result, showing the majority of the isolated particle was less than 100 nm in diameter.

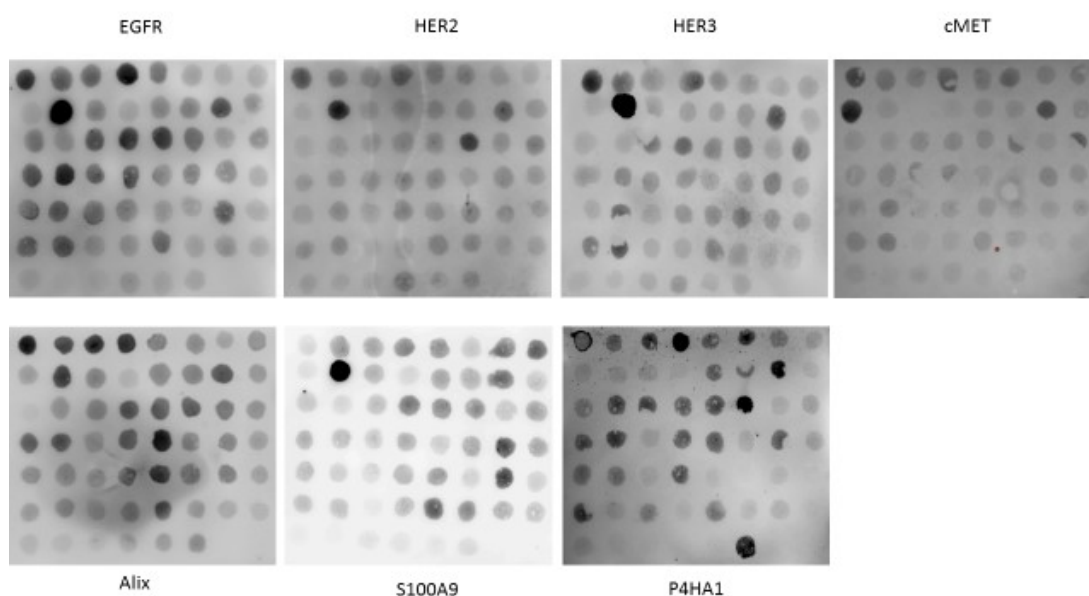


Figure 16. Dotblots of patient serum exosomes. Isolated exosomes from a total of 54 patients were stained with EGFR, HER2, HER3, cMET, Alix, S100A9 and P4HA1. Each dot contained 5 μ l of exosomes in PBS from a single patient. Every membrane was dotted in the same fashion, namely, the same position representing the exosome from the same patient. The signal intensities were quantified with a digital imaging platform (GE ImageQuant LAS 4000).

As shown in Figure 17, there was a positive correlation between HER1/HER3, HER2/HER3, HER1/S100A9, HER2/cMET and HER3/cMet. P4HA1 is increased in hypoxia as shown above (Figure 18A) and according to literature [67]. In addition, hypoxia plays a key role in tumour progression. Therefore, we decided to dichotomise the data

into two groups of low and high P4HA1 levels. When dichotomized by P4HA1 high and low groups by the median value of the intensity of P4HA1 normalized by ALIX, those patient samples with high P4HA1 also had higher normalized HER1 signals (Figure 18).

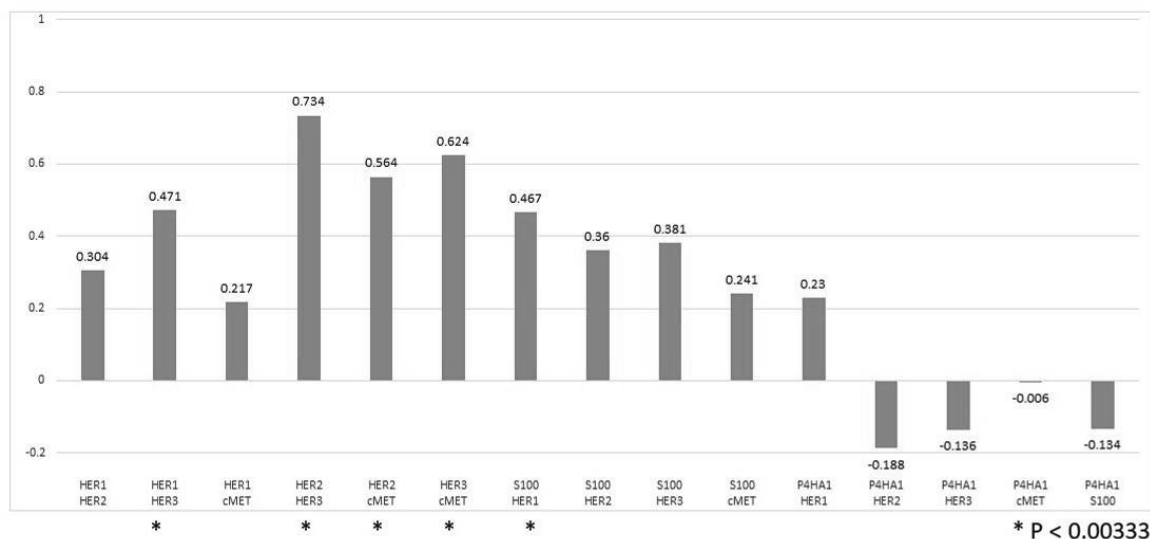


Figure 17. Separman correlation of the exosomal protein signals. The signals were normalized by the intensity of ALIX, a protein involved in the exosome synthesis. The correlation coefficients were listed above each bar. Significance level was adjusted by Bonferroni correction ($p < 0.00333$). There was a positive correlation between HER1/HER3, HER2/HER3, HER1/S100A9, HER2/cMET and HER3/cMet.

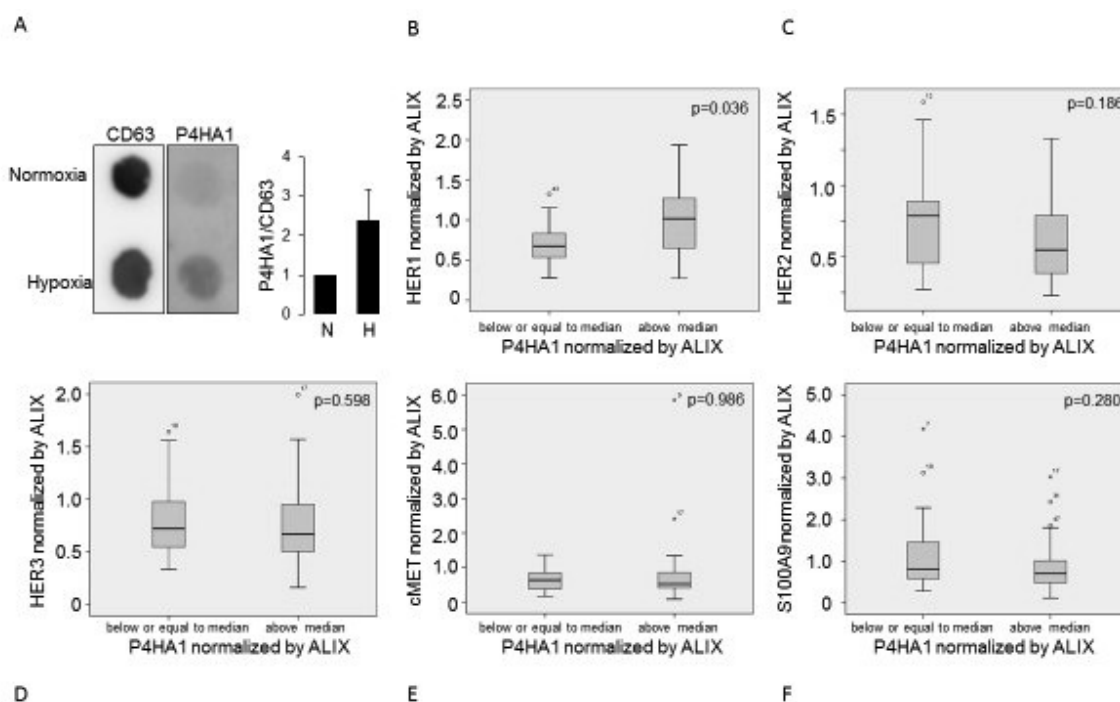


Figure 18 (A). Exosomes were isolated from the colorectal cancer cell line HCT116. The upper row showed the dotblots from the normoxic control exosomes. The lower row was from exosomes of cells subjected to 1% oxygen in a hypoxic incubator for 16 hours. Immunoblotting with anti-CD63, an exosomal marker, revealed similar loading of exosomes in each condition. P4HA1 was more than double (as indicated by the P4HA1/CD63 ratio) in exosomes after hypoxic treatment (H = hypoxia, N = normoxia). (B-F) Serum exosomes were isolated from 54 pre-treatment colorectal cancer patients (13 of whom were shown subsequently to have metastasis on staging images). The boxplot shows the median (the middle thick line), interquartile range (IQR, the difference between 75th and 25th percentile, the box), and 1.5x IQR above and below the box (the T-bars). The difference in the amount of exosomal EGFR/HER1, HER2, HER3, c-Met and S100A9 between patients whose exosomal marker for hypoxia (P4HA1) was $>$ vs \leq median, was compared for each of the proteins. The significance level by Mann-Whitney U test is indicated.

To understand the relationship between protein expression in the exosome and the tumour, tumour specimens were obtained in 18 patients. CD105, HIF-1 α and GLUT-1 were stained. Among these, GLUT-1 and HIF-1 α were negatively correlated. No correlation between the tumour protein expression and exosomal protein intensities was found (Figure 19).

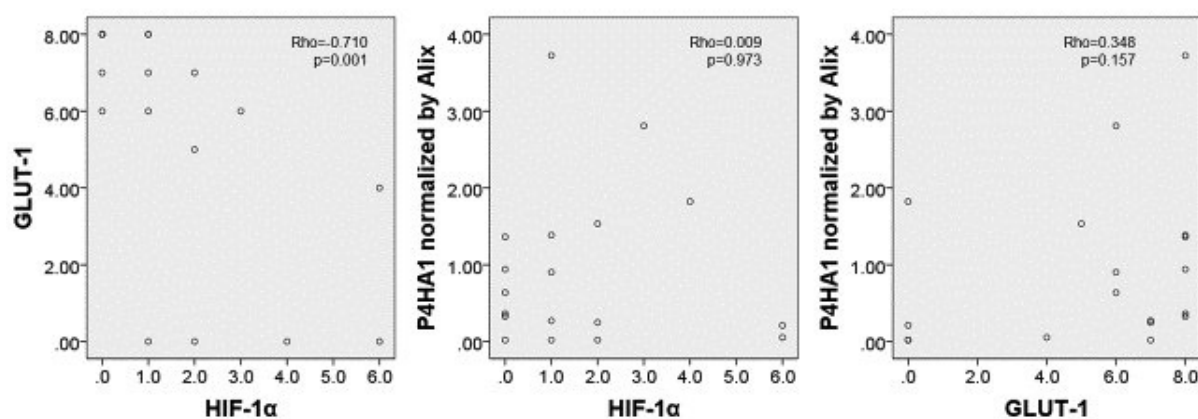


Figure 19. Scatter plot of HIF-1 α and GLUT-1 showed negative correlation between these two proteins on tumour specimens ($\rho = -0.710$, $p = 0.001$). No correlation was found between HIF-1 α on the tumour specimen and P4HA1 intensity in the exosomes ($\rho = 0.009$, $p = 0.973$), nor between GLUT1 on the tumour specimen and P4HA1 intensity in the exosomes ($\rho = 0.348$, $p = 0.157$).

5.2.3.2 Relationship between exosome, images and clinical status

Using the median value of each normalized protein signal intensities to group the patients into high and low groups, there was no survival difference by log-rank test. Namely, none of the exosomal proteins seemed to affect patients' overall survival.

Normalized HER1 intensity was negatively correlated with mean slope of increase from the CT perfusion study ($\rho = -0.424$, $p = 0.002$). There was no other correlation between the protein signal intensities and parameters from patients' images including blood volume (BV), blood flow (BF), mean transit time (MTT), permeability-surface area product (PS), time to peak, SUVmax, SUVmean, metabolic tumour volume (MTV), or lesion glycolysis as contoured by 40% of the SUVmax (TLG).

When dividing these patients into two groups by degrees of hypoxia using the median value of P4HA1 signals normalized by ALIX signals as the cut-off, the more hypoxic group (those with the signal > median) had a trend to have lower mean slope of increase from the CT perfusion images (Mann-Whitney U test, $p = 0.092$). This group also had higher EGFR signals in the exosomes (Mann-Whitney U test, $p = 0.036$) (Figure 20). A permutation test was performed to test the hypothesis that the mean-slope-of-increase is negatively correlated with both P4HA1 and HER1, and that additionally both P4HA1 and HER1 are positively correlated. The recorded values of these three variables were randomly permuted 100,000 times. The proportion of permutations in which a correlation equal or greater to the empirically observed correlations was used as a p-value. There is a significant inverse correlation between perfusion in the tumour and the exosomal hypoxia marker P4HA1 & EGFR ($p = 0.006$).

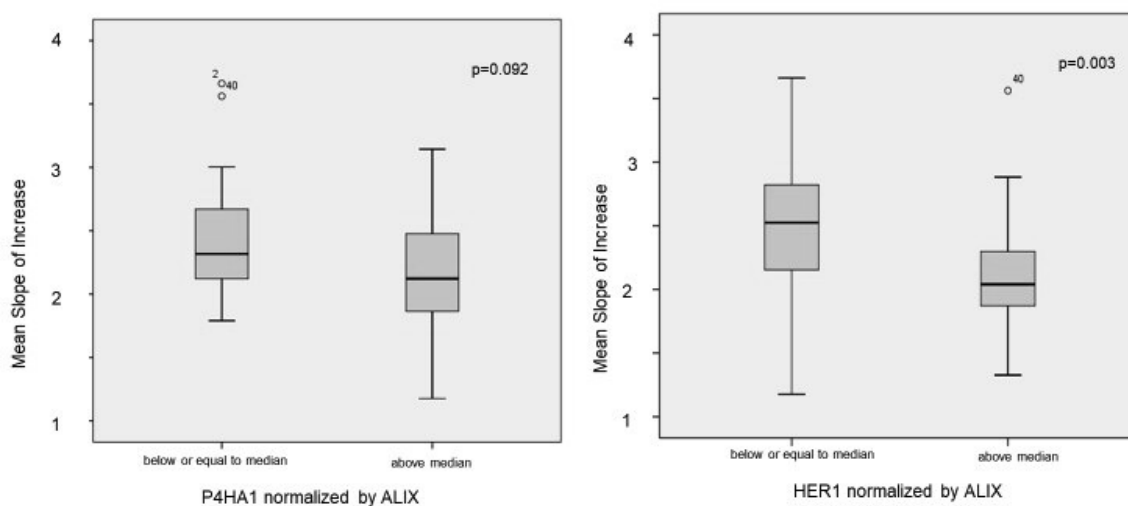


Figure 20. The boxplot shows the median (the middle thick line), interquartile range (IQR, the difference between 75th and 25th percentile, the box), and 1.5x IQR above and below the box (the T-bars). The difference in the CT perfusion parameter “mean slope of increase” between patients whose exosomal markers for hypoxia (P4HA1) and HER1 was > vs ≤ median, was compared. The significance level by Mann-Whitney U test is indicated.

The parameters derived from the texture analysis of clinical images including FDG-PET, non-contrast and contrast-enhanced CT, were compared to the protein intensities in the exosomes normalized by ALIX signals by Spearman's correlation. Among these, none were significant after Benferroni correction for multiplicity (Figure 16). However, if we explore the data using a less rigid criteria risking to err on the side of false positivity ($p < 0.05$), SD across various filter level of and MPP of intermediately-filtered PET was positively correlated with P4HA1, mean, SD and MPP of unfiltered PET were negatively correlated with S100A9, entropy of intermediately-filtered non-contrast CT was negatively correlated with cMET. For detailed numbers, please see the Appendix.

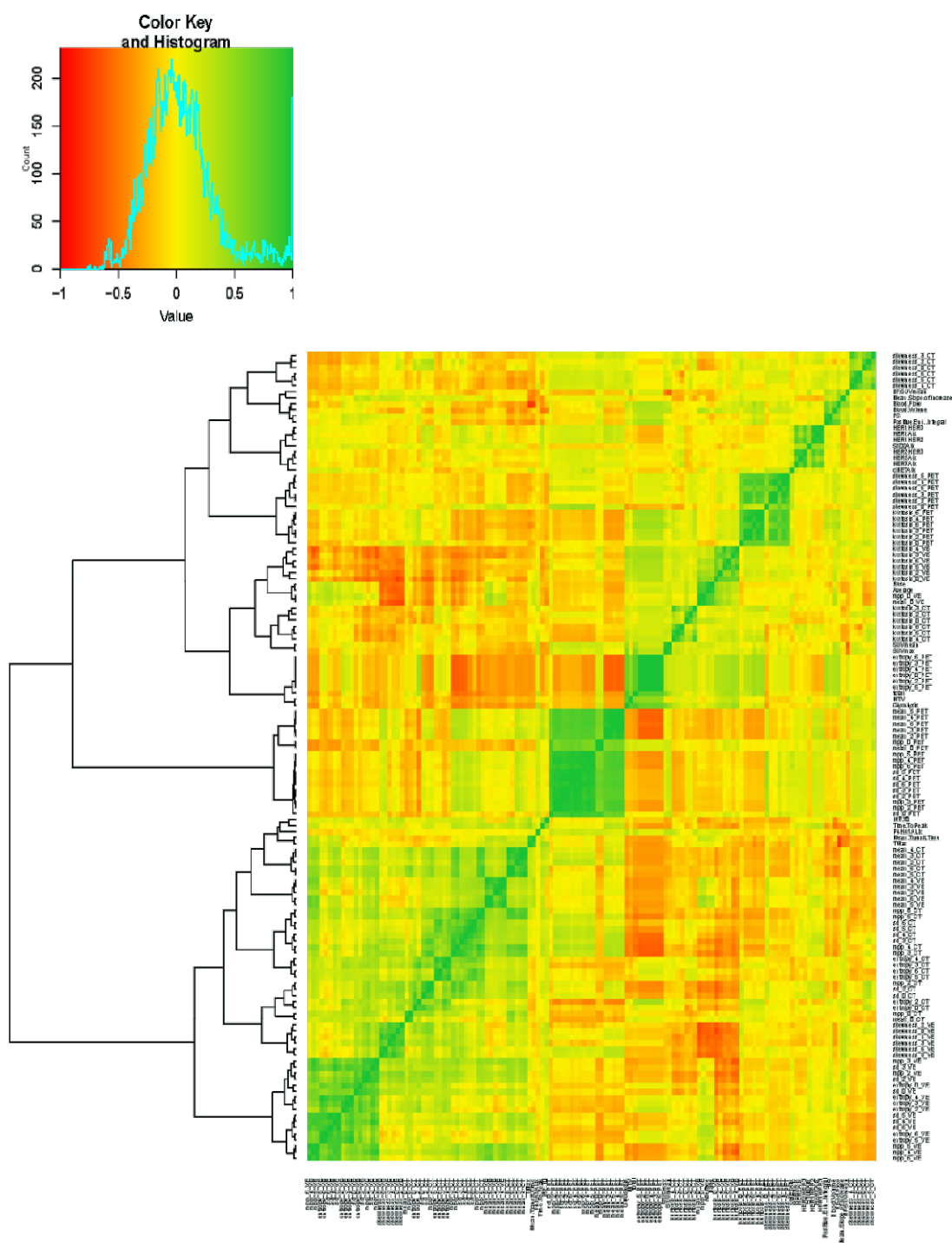


Figure 21. Heatmap of Spearman's correlation between image parameters and exosome protein intensities. The correlation coefficients were denoted by the color key as shown on the left upper corner. None of these were significant after Benferroni correction for multiplicity. The exact numbers are shown in the Appendix (Table 27-32).

13 out of these 54 patients had distant metastases. In those with localized disease and with metastatic disease, there were no differences in the exosomal protein quantities. On the clinical images, those with metastatic diseases had higher average and baseline Hounsfield unit, metabolic tumour volume. Texture analysis was performed on the FDG-PET, non-contrast CT and venous-phase of contrast-enhanced CT. SD & MPP of non-contrast CT images, MPP and kurtosis of contrast-enhanced CT images, as well as entropy of PET images were different in those with localized and metastatic diseases (Table 25).

Table 25: Significant different parameters between localized and metastatic tumours and their p-value by Mann-Whitney U test. Those with p-value < 0.05 were listed here.

parameter	p-value
Average	0.023
Base	0.039
MTV	0.016
SD_2_CT	0.040
SD_3_CT	0.022
SD_4_CT	0.034
Mpp_3_CT	0.036
MPP_0_VE	0.048
Kurtosis_0_VE	0.028
Kurtosis_4_VE	0.006
Kurtosis_5_VE	0.003
Kurtosis_6_VE	0.005
Entropy_0_PET	0.020
Entropy_2_PET	0.025

Entropy_3_PET	0.022
Entropy_4_PET	0.021
Entropy_5_PET	0.019
Entropy_6_PET	0.021

From the image dataset, we had performed a Principal Component Analysis on a total of 122 radiomic parameters, we were able to condense the number of dimensionalities down to 10 principal components which explain approximately 80% of the observed variability. Interestingly, PC1 was also able to distinguish metastatic from non-metastatic patients ($p = 0.041$) (Figure 22).

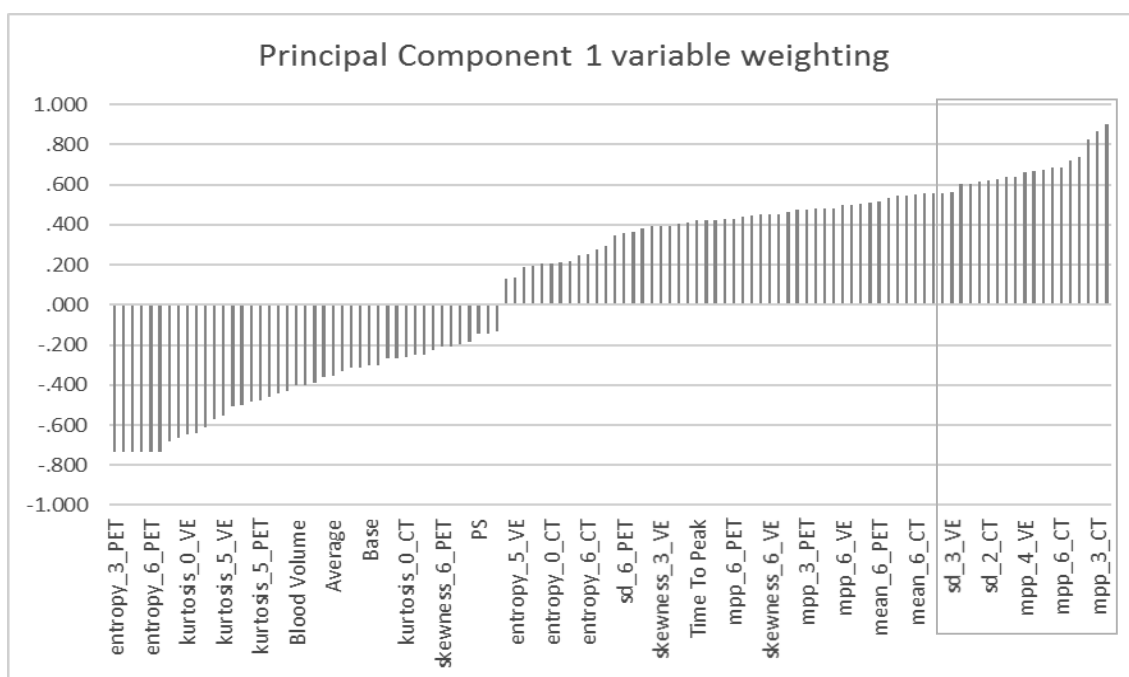


Figure 22. Radiomic analysis of image parameters from patients. The histogram shows Principal Component (PC)1 of 122 radiomic features. SD & MPP of CT, as well as entropy of PET were among the most weighted parameters constituting PC1, which was able to distinguish metastatic from non-metastatic patients ($p = 0.041$).

5.3 Discussion

Western blot separates proteins by their size and electronic charges with sodium dodecyl sulfate–polyacrylamide gel electrophoresis (SDS-PAGE), then transfers the protein onto a nitrocellulose or polyvinylidene difluoride (PVDF) membrane to be detected by antibodies [231]. Dotblot omits the electrophoresis, probing the target protein by the specificity of the recognized antigen [232]. It is quicker than the Western blot, and suitable for testing a large batch of samples. Where as in western blot the non-specific bands do not affect quantification, it is not possible to separate these signals in dot blots. Thus it is desirable to use highly specific antibody to minimize these unspecific bindings. We conducted a set of antibody validation experiments to ensure that the data we were obtaining by dotblot was a reliable and reproducible indication of exosomal protein quantities.

Through knock-out by shRNA and utilizing cell lines lacking the expression of the target protein, we confirmed specificities of the antibodies used against ALIX, HER1, HER2, HER3 and cMET. P4HA1 is induced by hypoxia through the hypoxia-response element (HRE) present in its promoter [67]. It is also reportedly present in exosomes [233]. We therefore chose to subject cells to hypoxic conditions and assess the P4HA1 signal. Our cell line work confirmed increased P4HA1 expression in hypoxic condition in the cell lysates. Remarkably, the increase was also noted in the isolated exosomes. This implies the P4HA1 signal in exosomes can reflect the hypoxic status of the cells.

The S100A9 antibody showed non-specific bands other than the expected one at 10 kDa when we conducted western blot tests. Accordingly, we observed a mild background on the dotblots. However, the S100A9 signal was higher in exosomes from

THP1 cells, which are high in S100A9 compared to those from H1975 cells, which are low, showing that it responds to biological changes as we expected. Additionally, exosomal quantities of S100A9 showed to be proportionally enriched in exosomes compared to cell lysates, rendering the influence of nonspecific binding insignificant. We conducted further tests using other S100A8 or S100A9 antibodies, however these exhibited higher background signals. We concluded that the signal intensity on the dotblot reliably reflects exosomal S100A9 expression.

We then moved on to apply this finding to patient samples. We isolated the exosomes from patients' sera by differential centrifugation followed by ultracentrifugation [192] and analysed the exosome quality with nanoparticle tracking analysis combined with biochemical tests [234]. Our isolates were mostly below 100 nm, and stained positive with ALIX, proving they contained exosomes by both optical and biochemical techniques. Due to the paucity of the clinical samples, no ultrastructural characterization by electronic microscopy was conducted. It is somewhat assumed that some impurities such as other kinds of microvesicles, or protein aggregates may contaminate the exosomal samples [235]. However, the nanoparticle tracking analysis data showed that particles above the 200 nm limit (microvesicles and other extracellular vesicles) were minimal from our exosomal purifications. Based on this, we went ahead to explore the relationship of the protein contents.

In our experiments, ALIX is used as a normalizer to compare the abundance of other proteins across patients to account for the difference of exosome abundance. ALIX is involved in the budding of membranes into endosome and exosomes. In association with endosome sorting complex required for transport (ESCRT), it also

helps sort proteins into the endosomes to be released as exosomes. It binds to syntenin and syndecan to control the numbers of exosomes formed [86]. We were unable to quantify the total protein amounts of the isolated exosomes, and the amounts of isolated exosomes differed in each patient. An intrinsic exosomal protein acting as a marker of the abundance of the exosomes served the purpose of normalizer.

We found positive correlations between HER1/HER3, HER1/S100A9, HER2/HER3, HER2/cMET, HER3/cMet in exosomes. The prognostic values of HER1, HER2, HER3 expressions in colorectal cancer are not well documented. Most reports did associate c-MET expression with worse survival. HER2/HER3 dimerization was shown to increase with cetuximab treatment [236]. C-MET activation was also shown to be conferring resistance to cetuximab in KRAS wild-type cells [49]. Increased S100A9 positive myeloid-derived suppressor cells in the blood of non-small cell lung cancer patients with mutant EGFR treated with tyrosine kinase inhibitors was associated with shorter progression-free survival [237]. Our results suggested these receptor tyrosine kinases and S100A9 were related as reported by others.

Using P4HA1 as a hypoxia marker, we found those with high P4HA1 expression also had higher EGFR expression. The increase of EGFR under hypoxic conditions was demonstrated in both the A431 human epidermoid carcinoma cell line [238] and breast cancer cell line [239]. The increase could be due to increased translation of EGFR mRNA mediated via HIF-2 α [240]. Another interaction between hypoxia and EGFR is through prolyl hydroxylase 2 (PHD2) which marks HIF-1 α for ubiquitination under normoxic conditions. PHD2 binds to EGFR and stabilizes it. [241]. In addition,

hypoxia induces caveolin-1 expression as it has HRE in its promoter. The formation of caveolae also leads to activation of EGFR by hetero-dimerization without ligands [242].

In another way, EGFR pathway can increase HIF-1. mTOR has been shown to stabilize HIF-1 α in the PC3 prostate cell line [243]. Zhong *et al.* also showed EGF increased HIF-1 α expression in DU145 and TSU prostate cell lines. The increase was blocked by the inhibition of PI3K/mTOR pathway. Thus HIF-1 α could be linked to EGFR pathway via PI3K/AKT/mTOR [244]. Furthermore, HER2 was shown to increase HIF-1 α expression via PI3K/AKT/mTOR pathway [245].

In our samples, there was no direct correlation between the intensities of exosomal proteins and protein expression on tumour specimens by IHC. Although hypoxia increased exosome release [12, 13], the amount of tumour-secreted exosomes might still constitute only a small proportion of the exosome in the sera, which we isolated. The exosomal proteins we investigated could represent a snapshot of the whole body status, but it might not be possible to reflect the exact status of the primary tumour. Furthermore, the histology specimen was only a single slice cut out of the whole tumour, which could be not representative as well.

We found normalized P4HA1 and EGFR intensities in exosomes were negatively correlated with mean slope of increase from the CT perfusion study ($\rho=-0.424$, $p=0.002$). Previously we found that the mean slope of increase was negatively associated with VEGF and CD105. Mean slope of increase is a semi-quantitative measurement from CT perfusion scans. It measures the change of tissue density curve over time, namely, the rate of contrast enhancement within the tumour during contrast medium flowing into the tissue [221]. Lower slope means slower change. This could be due to less efficient transport due to flow resistance of immature vessel architecture as well

as increased interstitial pressure from leaky vessels [218]. P4HA1 was indicative of hypoxia, which is a trigger for angiogenesis [56]. EGFR is also known to be involved in angiogenesis. Inhibition of EGFR by cetuximab decreased HIF-1 α expression and angiogenesis [246]. When human bronchial epithelial cell line BEAS-2B treated with a well-known carcinogen, hexavalent chromium, they promoted increased angiogenesis of human umbilical vein endothelial cells via EGFR, HIF-1 α and VEGF [247]. Our result is comparable with these findings, in that higher P4HA1 and EGFR would reflect angiogenesis, in which the newly-formed vessels are inefficient for transport and also correlate with the lower mean slope of increase that we observed.

We tried to find a relationship between texture analysis of the primary tumour and protein quantities in the exosomes. We found that SD across various filter level of and MPP of intermediately-filtered PET is positively correlated with P4HA1. Mean, SD and MPP of unfiltered PET were negatively correlated with S100A9. Entropy of intermediately-filtered non-contrast CT was negatively correlated with cMET. These correlations might be random as they disappeared after correction for multiplicity. More sophisticated methods such as machine learning might be able to provide more insights into whether additional information derived from routine clinical images could provide clues to the protein contents in exosomes.

From the clinical images of the primary tumour, those with higher baseline and average Hounsfield unit, metabolic tumour volume, entropy of PET images, kurtosis of contrast enhanced CT and lower SD & MPP of CT images were more likely to have metastatic diseases. The principal component analysis found a component consisted of SD and MPP of the CT images among other radiomic features was able to differentiate between metastatic and localized disease. As mentioned previously, SD & MPP were

associated with hypoxia. Our results confirmed the importance of perfusion and hypoxia in tumour metastasis.

It is difficult to directly visualize hypoxia by clinical images. In a glioma xenograft, the distance between perfused vessels and hypoxic regions was found to be 138-199 μm [248]. In a murine breast cancer model, the intensity of the hypoxic staining plateau after 120-130 μm . [249]. Current clinical PET/CT scanners with the pixel size and slice thickness between 2-4 mm [250] would have difficulty trying to provide reliable data with these subtle signals ten times below the scanner resolution. We found some indirect parameters, such as mean slope of increase from CT perfusion, SD & MPP of PET, might be suggestive of hypoxia of the tumour.

As hypoxia is also common in acute kidney injury and chronic kidney disease [251], pulmonary hypertension [252], inflammatory bowel disease [253]. The exosomal marker might also be of use to these benign diseases as well.

There were certain ways to improve our experiments. One area was the exosome isolation methods. Differential ultracentrifugation could not eliminate other extracellular vesicles of similar sizes to leave only exosomes [254]. Although methods such as density gradient and immunoisolation could provide purer exosomes, the reagents or antibodies involved in the isolation procedures might interfere with subsequent analysis of exosome function or receptor dimerization. We chose to accept a certain degree of impurities in our exosome preparation to enable the flexibility of downstream analysis.

Another aspect to improve is the analysis method. Artificial intelligence (AI) methods can handle not only the predefined features such as the histogram parameters generated here in our study, but also deep learning about the underlying

image features that might be important in tumour metastasis and patient survival.

Furthermore, in addition to the image features, AI algorithms can combine data from other sources to aid in the classification, such as patients demographics, blood test results, as well as the exosome protein quantifications [255].

In summary, we found a protein, P4HA1, in the circulating exosomes that increases with hypoxia. Those patients who had higher P4HA1 in their exosomes often had higher exosomal EGFR. Both proteins were negatively correlated with the mean slope of increase from our CT perfusion studies. SD & MPP from the texture analysis of clinical images were shown to correlate with hypoxia, and these parameters, along with components derived from the principal component analysis, were able to offer a distinguishment between patients with metastatic and local diseases, emphasizing the importance of hypoxia in cancer invasiveness and progression.

6 Summary and Conclusion

The main findings of this study and possible clinical relevance are summarized here.

6.1 FDG PET

- TLG was a prognosticator in colon cancer patients.
- MTV was higher in patients with metastatic diseases than those with localized diseases.

In current clinical practice, FDG-PET is used in staging as a problem-solving tool when CT or MR has equivocal findings. Our findings aid the interpretation of the FDG-PET images when a tumour has a high MTV. The finding that FDG-PET is prognostic in colon cancer patients might help in clinical decision making when patients and their doctors are unsure whether to receive adjunctive treatments. The outcome TLG data we show could be a potential factor to consider in the multidisciplinary team discussion and meeting with patients and family. Though the influence of the FDG-PET parameters did not apply to rectal cancer patients or patients already treated with chemoradiotherapy.

6.2 CT Perfusion

- Time to peak is a possible prognosticator in stage 3-4 patients
- The ratio of blood flow from CT perfusion scans and SUVmax of FDG-PET scans has potential as a prognosticator in rectal cancers.
- Mean slope of increase was negatively correlated with VEGF from the tissue specimens, P4HA1 & EGFR in exosomes.
- Mean transit time was positively correlated with VEGF from the tissue specimens.

Although both time to peak in stage 3-4 patients and the ratio of blood flow to SUVmax in rectal patients may be a type I statistical error as they did not pass correction for multiple comparisons, further research could clarify this. The possible usefulness of combination of the CT perfusion parameters with the metabolic marker from FDG-PET suggests the potential of looking beyond angiogenesis and taking other tumour features such as the metabolic flow relationship into consideration.

The mean slope of increase and mean transit time from the CT perfusion examinations were related to angiogenesis as reflected by the VEGF expression from tumour tissues. The finding could be used to monitor changes of vasculature post therapy, such as the impact of anti-angiogenic and other treatments.

6.3 Texture

- Kurtosis of non-contrast CT images was a stable prognosticator, along with clinical stages.

- Entropy of PET images was a prognosticator in colon cancer patients.
- SD, MPP of non-contrast CT images were lower in patients with metastatic diseases.

These textural data could provide additional information not demonstrated by conventional imaging metrics. However, the biologic meanings of such analysis need to be elucidated. The statistical methods we used to link the image parameters and biologic relevance were simple. More advanced modeling might be able to reveal hidden factors which may enlighten the interaction of biologic pathways reflected by the texture parameters. Furthermore, the use of modern methodologies such as artificial intelligence might be able to derive more parameters from the images and find better predictors of patient outcome by combining with the data from clinical demographics.

Currently in stage 3 colon cancer, the standard adjuvant chemotherapy is 6-month oxaliplatin-based regimens. Oxaliplatin exposure carries the risk of sensory neuropathy. It is desirable to identify low-risk patients and decrease the length of adjuvant chemotherapy to reduce the exposure to oxaliplatin and thus risk of sensory neuropathy [256]. The prognosticator we found did separate a group of lower risk patients within stage 3 colon cancer patients. Further research could test whether this group of patients could sustain the treatment response with a shortened chemotherapy course.

6.4 Exosomes

- P4HA1 in exosomes was a marker of hypoxia.

- P4HA1 & EGFR in exosomes were negatively correlated with mean slope of increase from CT perfusion scans.

Mean slope of increase from CT perfusion, in addition to indicating angiogenesis as suggested by its negative correlation with VEGF expression on tumour tissues, also hints at hypoxia and tumour proliferation as negatively correlated with P4HA1 and EGFR in exosomes. This evidence further substantiates a potential close link between hypoxia, angiogenesis and tumour proliferation.

Although no prognostic relationship was found between exosomal proteins in colorectal cancer patients, there are some interesting pointers for future research, e.g. the demonstration of a hypoxic marker from the sera exosomes. Going forward this could be applied to the early detection of colorectal cancer. Currently stool-based methods such as faecal occult blood test and colonoscopy are used for colon cancer screening. Faecal occult blood test, despite having a sensitivity > 70% and a specificity > 90%, requires the confirmation of colonoscopy for positive results. Colonoscopy is an invasive procedure uncomfortable to patients that often requires sedation. It is hoped that the addition of the blood exosome test to the screening could improve the stratification of patients as risk. As it is shown hypoxia-specific image probes could detect early tumours in mice [257], combining the ability to estimate degrees of hypoxia and further analysis of clinical parameters, it may be possible to develop an algorithm to predict patient outcome decreasing the necessity of follow-up investigations and diminishing patient anxieties during these follow-up periods, as well as potentially reducing the associated economical burdens to the health care system.

6.5 Conclusion

In conclusion, we have shown that the measurements from in vivo CT perfusion imaging of tumours from colorectal cancer patients is potentially associated with underlying angiogenesis. Further analysis of the clinical images using metabolic and textural parameters can be prognostic for colorectal cancer patients independent of their clinical stages, which has the potential to stratify patients into less intense treatment thus reducing side effects. In exosome proteins derived from the serum of colorectal cancer patients we found a hypoxic marker. Combining the imaging parameters and exosome analysis might pave the way for early tumour diagnosis and outcome stratification in the future.

7 Bibliography

1. Hanahan D, Weinberg RA: **Hallmarks of cancer: the next generation.** *Cell* 2011, **144**(5):646-674.
2. Raica M, Cimpean AM, Ribatti D: **Angiogenesis in pre-malignant conditions.** *European journal of cancer* 2009, **45**(11):1924-1934.
3. Del Monte U: **Does the cell number 10⁹ still really fit one gram of tumor tissue?** *Cell cycle* 2009, **8**(3):505-506.
4. Vaupel P, Kallinowski F, Okunieff P: **Blood flow, oxygen and nutrient supply, and metabolic microenvironment of human tumors: a review.** *Cancer research* 1989, **49**(23):6449-6465.
5. Zhang C, Cao S, Toole BP, Xu Y: **Cancer may be a pathway to cell survival under persistent hypoxia and elevated ROS: a model for solid-cancer initiation and early development.** *International journal of cancer Journal internationale du cancer* 2015, **136**(9):2001-2011.
6. Vander Heiden MG, Cantley LC, Thompson CB: **Understanding the Warburg effect: the metabolic requirements of cell proliferation.** *Science* 2009, **324**(5930):1029-1033.
7. Beckert S, Farrahi F, Aslam RS, Scheuenstuhl H, Konigsrainer A, Hussain MZ, Hunt TK: **Lactate stimulates endothelial cell migration.** *Wound Repair Regen* 2006, **14**(3):321-324.
8. Dong HJ, Jang GB, Lee HY, Park SR, Kim JY, Nam JS, Hong IS: **The Wnt/beta-catenin signaling/Id2 cascade mediates the effects of hypoxia on the hierarchy of colorectal-cancer stem cells.** *Scientific reports* 2016, **6**:22966.
9. Beck B, Blanpain C: **Unravelling cancer stem cell potential.** *Nature reviews Cancer* 2013, **13**(10):727-738.
10. Van Cutsem E, Tabernero J, Lakomy R, Prenen H, Prausova J, Macarulla T, Ruff P, van Hazel GA, Moiseyenko V, Ferry D *et al*: **Addition of aflibercept to fluorouracil, leucovorin, and irinotecan improves survival in a phase III randomized trial in patients with metastatic colorectal cancer previously treated with an oxaliplatin-based regimen.** *Journal of clinical oncology : official journal of the American Society of Clinical Oncology* 2012, **30**(28):3499-3506.
11. Price TJ, Segelov E, Burge M, Haller DG, Tebbutt NC, Karapetis CS, Punt CJ, Pavlakakis N, Arnold D, Gibbs P *et al*: **Current opinion on optimal systemic treatment for metastatic colorectal cancer: outcome of the ACTG/AGITG expert meeting ECCO 2013.** *Expert review of anticancer therapy* 2014, **14**(12):1477-1493.
12. King HW, Michael MZ, Gleadle JM: **Hypoxic enhancement of exosome release by breast cancer cells.** *BMC cancer* 2012, **12**:421.

13. Panigrahi GK, Praharaj PP, Peak TC, Long J, Singh R, Rhim JS, Elmagedd ZYA, Deep G: **Hypoxia-induced exosome secretion promotes survival of African-American and Caucasian prostate cancer cells.** *Scientific reports* 2018, **8**(1):3853.
14. Kahlert C, Kalluri R: **Exosomes in tumor microenvironment influence cancer progression and metastasis.** *J Mol Med (Berl)* 2013, **91**(4):431-437.
15. **GLOBOCAN 2012 v1.0, Cancer Incidence and Mortality Worldwide: IARC CancerBase No. 11** [<http://globocan.iarc.fr>]
16. **Cancer Research UK** [<http://www.cancerresearchuk.org/health-professional/cancer-statistics/statistics-by-cancer-type/bowel-cancer>]
17. van de Velde CJ, Boelens PG, Borrás JM, Coebergh JW, Cervantes A, Blomqvist L, Beets-Tan RG, van den Broek CB, Brown G, Van Cutsem E *et al*: **EURECCA colorectal: multidisciplinary management: European consensus conference colon & rectum.** *European journal of cancer* 2014, **50**(1):1 e1-1 e34.
18. Provenzale D, Gupta S, Ahnen DJ, Markowitz AJ, Chung DC, Mayer RJ, Regenbogen SE, Blanco AM, Bray T, Cooper G *et al*: **NCCN Guidelines Insights: Colorectal Cancer Screening, Version 1.2018.** *J Natl Compr Canc Netw* 2018, **16**(8):939-949.
19. Van Cutsem E, Cervantes A, Adam R, Sobrero A, Van Krieken JH, Aderka D, Aranda Aguilar E, Bardelli A, Benson A, Bodoky G *et al*: **ESMO consensus guidelines for the management of patients with metastatic colorectal cancer.** *Annals of oncology : official journal of the European Society for Medical Oncology / ESMO* 2016, **27**(8):1386-1422.
20. **Cancer survival in England: adult, stage at diagnosis and childhood – patients followed up to 2016**
[<https://www.ons.gov.uk/peoplepopulationandcommunity/healthandsocialcare/conditionsanddiseases/bulletins/cancersurvivalinengland/adultstageatdiagnosisandchildhoodpatientsfollowedupto2016>]
21. Grady WM, Markowitz SD: **The molecular pathogenesis of colorectal cancer and its potential application to colorectal cancer screening.** *Digestive diseases and sciences* 2015, **60**(3):762-772.
22. Guinney J, Dienstmann R, Wang X, de Reynies A, Schlicker A, Soneson C, Marisa L, Roepman P, Nyamundanda G, Angelino P *et al*: **The consensus molecular subtypes of colorectal cancer.** *Nature medicine* 2015, **21**(11):1350-1356.
23. Okita A, Takahashi S, Ouchi K, Inoue M, Watanabe M, Endo M, Honda H, Yamada Y, Ishioka C: **Consensus molecular subtypes classification of colorectal cancer as a predictive factor for chemotherapeutic efficacy against metastatic colorectal cancer.** *Oncotarget* 2018, **9**(27):18698-18711.
24. Le DT, Uram JN, Wang H, Bartlett BR, Kemberling H, Eyring AD, Skora AD, Luber BS, Azad NS, Laheru D *et al*: **PD-1 Blockade in Tumors with Mismatch-Repair Deficiency.** *The New England journal of medicine* 2015, **372**(26):2509-2520.
25. Wee P, Wang Z: **Epidermal Growth Factor Receptor Cell Proliferation Signaling Pathways.** *Cancers (Basel)* 2017, **9**(5).
26. Van Cutsem E, Kohne CH, Hitre E, Zaluski J, Chang Chien CR, Makhson A, D'Haens G, Pinter T, Lim R, Bodoky G *et al*: **Cetuximab and chemotherapy as initial treatment for metastatic colorectal cancer.** *The New England journal of medicine* 2009, **360**(14):1408-1417.

27. Van Cutsem E, Peeters M, Siena S, Humblet Y, Hendlisz A, Neyns B, Canon JL, Van Laethem JL, Maurel J, Richardson G *et al*: **Open-label phase III trial of panitumumab plus best supportive care compared with best supportive care alone in patients with chemotherapy-refractory metastatic colorectal cancer**. *Journal of clinical oncology : official journal of the American Society of Clinical Oncology* 2007, **25**(13):1658-1664.
28. Kountourakis P, Pavlakis K, Psyrri A, Rontogianni D, Xiros N, Patsouris E, Pectasides D, Economopoulos T: **Clinicopathologic significance of EGFR and Her-2/neu in colorectal adenocarcinomas**. *Cancer J* 2006, **12**(3):229-236.
29. Kountourakis P, Pavlakis K, Psyrri A, Rontogianni D, Xiros N, Patsouris E, Pectasides D, Economopoulos T: **Prognostic significance of HER3 and HER4 protein expression in colorectal adenocarcinomas**. *BMC cancer* 2006, **6**:46.
30. Molaie M, Pejhan S, Nayer BN, Moradi A, Ghiasi S, Zali MR: **Human epidermal growth factor receptor-2 family in colorectal adenocarcinoma: correlation with survival and clinicopathological findings**. *Eur J Gastroenterol Hepatol* 2009, **21**(3):289-293.
31. Sun SJ, Lin Q, Sun Q, Li J, Zhang XY, Tan ZG, Song Y, Guo YT, Li Y: **High HER-2 protein levels correlate with clinicopathological features in colorectal cancer**. *Journal of cancer research and therapeutics* 2016, **12**(1):323-333.
32. Richman SD, Southward K, Chambers P, Cross D, Barrett J, Hemmings G, Taylor M, Wood H, Hutchins G, Foster JM *et al*: **HER2 overexpression and amplification as a potential therapeutic target in colorectal cancer: analysis of 3256 patients enrolled in the QUASAR, FOCUS and PICCOLO colorectal cancer trials**. *The Journal of pathology* 2016, **238**(4):562-570.
33. Loree JM, Bailey AM, Johnson AM, Yu Y, Wu W, Bristow CA, Davis JS, Shaw KR, Broaddus R, Banks KC *et al*: **Molecular Landscape of ERBB2/ERBB3 Mutated Colorectal Cancer**. *Journal of the National Cancer Institute* 2018.
34. Jeong JH, Kim J, Hong YS, Kim D, Kim JE, Kim SY, Kim KP, Yoon YK, Kim D, Chun SM *et al*: **HER2 Amplification and Cetuximab Efficacy in Patients With Metastatic Colorectal Cancer Harboring Wild-type RAS and BRAF**. *Clin Colorectal Cancer* 2017, **16**(3):e147-e152.
35. Sawada K, Nakamura Y, Yamanaka T, Kuboki Y, Yamaguchi D, Yuki S, Yoshino T, Komatsu Y, Sakamoto N, Okamoto W *et al*: **Prognostic and Predictive Value of HER2 Amplification in Patients With Metastatic Colorectal Cancer**. *Clin Colorectal Cancer* 2018.
36. Seo AN, Kwak Y, Kim WH, Kim DW, Kang SB, Choe G, Lee HS: **HER3 protein expression in relation to HER2 positivity in patients with primary colorectal cancer: clinical relevance and prognostic value**. *Virchows Archiv : an international journal of pathology* 2015, **466**(6):645-654.
37. Ledel F, Stenstedt K, Hallstrom M, Ragnhammar P, Edler D: **HER3 expression in primary colorectal cancer including corresponding metastases in lymph node and liver**. *Acta Oncol* 2015, **54**(4):480-486.
38. Ledel F, Stenstedt K, Hallstrom M, Ragnhammar P, Edler D: **HER3 expression is correlated to distally located and low-grade colon cancer**. *Acta Oncol* 2016:1-6.
39. Scartozzi M, Mandolesi A, Giampieri R, Bittoni A, Pierantoni C, Zaniboni A, Galizia E, Giustini L, Silva RR, Bissoni R *et al*: **The role of HER-3 expression in the prediction of clinical outcome for advanced colorectal cancer patients receiving irinotecan and cetuximab**. *The oncologist* 2011, **16**(1):53-60.

40. Stahler A, Heinemann V, Neumann J, Crispin A, Schalhorn A, Stintzing S, Giessen-Jung C, Fischer von Weikersthal L, Vehling-Kaiser U, Stauch M *et al*: **Prevalence and influence on outcome of HER2/neu, HER3 and NRG1 expression in patients with metastatic colorectal cancer.** *Anti-cancer drugs* 2017, **28**(7):717-722.
41. Bradley CA, Salto-Tellez M, Laurent-Puig P, Bardelli A, Rolfo C, Taberero J, Khawaja HA, Lawler M, Johnston PG, Van Schaeybroeck S *et al*: **Targeting c-MET in gastrointestinal tumours: rationale, opportunities and challenges.** *Nat Rev Clin Oncol* 2017, **14**(9):562-576.
42. Raghav K, Morris V, Tang C, Morelli P, Amin HM, Chen K, Manyam GC, Broom B, Overman MJ, Shaw K *et al*: **MET amplification in metastatic colorectal cancer: An acquired response to EGFR inhibition, not a de novo phenomenon.** *Oncotarget* 2016, **7**(34):54627-55463.
43. Gayyed MF, Abd El-Maqoud NM, El-Hameed El-Heeny AA, Mohammed MF: **c-MET expression in colorectal adenomas and primary carcinomas with its corresponding metastases.** *Journal of gastrointestinal oncology* 2015, **6**(6):618-627.
44. Lee SJ, Lee J, Park SH, Park JO, Lim HY, Kang WK, Park YS, Kim ST: **c-MET Overexpression in Colorectal Cancer: A Poor Prognostic Factor for Survival.** *Clin Colorectal Cancer* 2018.
45. Shoji H, Yamada Y, Taniguchi H, Nagashima K, Okita N, Takashima A, Honma Y, Iwasa S, Kato K, Hamaguchi T *et al*: **Clinical impact of c-MET expression and genetic mutational status in colorectal cancer patients after liver resection.** *Cancer science* 2014, **105**(8):1002-1007.
46. Al-Maghrabi J, Emam E, Gomaa W, Saggaf M, Buhmeida A, Al-Qahtani M, Al-Ahwal M: **c-MET immunostaining in colorectal carcinoma is associated with local disease recurrence.** *BMC cancer* 2015, **15**:676.
47. Senetta R, Duregon E, Sonetto C, Spadi R, Mistrangelo M, Racca P, Chiusa L, Munoz FH, Ricardi U, Arezzo A *et al*: **YKL-40/c-Met expression in rectal cancer biopsies predicts tumor regression following neoadjuvant chemoradiotherapy: a multi-institutional study.** *PLoS ONE* 2015, **10**(4):e0123759.
48. Schweiger T, Starkl V, Glueck O, Glogner C, Traxler D, Jedamzik J, Liebmann-Reindl S, Birner P, Streubel B, Klepetko W *et al*: **Clinical impact of c-MET expression and mutational status in patients with colorectal cancer lung metastases.** *European journal of cardio-thoracic surgery : official journal of the European Association for Cardio-thoracic Surgery* 2016, **49**(4):1103-1111.
49. Bardelli A, Corso S, Bertotti A, Hobor S, Valtorta E, Siravegna G, Sartore-Bianchi A, Scala E, Cassingena A, Zecchin D *et al*: **Amplification of the MET receptor drives resistance to anti-EGFR therapies in colorectal cancer.** *Cancer discovery* 2013, **3**(6):658-673.
50. Takahashi N, Yamada Y, Furuta K, Honma Y, Iwasa S, Takashima A, Kato K, Hamaguchi T, Shimada Y: **Serum levels of hepatocyte growth factor and epiregulin are associated with the prognosis on anti-EGFR antibody treatment in KRAS wild-type metastatic colorectal cancer.** *British journal of cancer* 2014, **110**(11):2716-2727.
51. Mira A, Morello V, Cespedes MV, Perera T, Comoglio PM, Manges R, Michieli P: **Stroma-derived HGF drives metabolic adaptation of colorectal cancer to angiogenesis inhibitors.** *Oncotarget* 2017, **8**(24):38193-38213.

52. Matsumura A, Kubota T, Taiyoh H, Fujiwara H, Okamoto K, Ichikawa D, Shiozaki A, Komatsu S, Nakanishi M, Kuriu Y *et al*: **HGF regulates VEGF expression via the c-Met receptor downstream pathways, PI3K/Akt, MAPK and STAT3, in CT26 murine cells.** *International journal of oncology* 2013, **42**(2):535-542.
53. Jia Y, Dai G, Wang J, Gao X, Zhao Z, Duan Z, Gu B, Yang W, Wu J, Ju Y *et al*: **c-MET inhibition enhances the response of the colorectal cancer cells to irradiation and.** *Oncology letters* 2016, **11**(4):2879-2885.
54. Li F, Zhu YT: **HGF-activated colonic fibroblasts mediates carcinogenesis of colonic epithelial cancer cells via PKC-cMET-ERK1/2-COX-2 signaling.** *Cellular signalling* 2015, **27**(4):860-866.
55. Wong CC, Kai AK, Ng IO: **The impact of hypoxia in hepatocellular carcinoma metastasis.** *Frontiers of medicine* 2014, **8**(1):33-41.
56. Luo D, Wang Z, Wu J, Jiang C: **The role of hypoxia inducible factor-1 in hepatocellular carcinoma.** *BioMed research international* 2014, **2014**:409272.
57. Mees G, Dierckx R, Vangestel C, Van de Wiele C: **Molecular imaging of hypoxia with radiolabelled agents.** *European journal of nuclear medicine and molecular imaging* 2009, **36**(10):1674-1686.
58. Cao D, Hou M, Guan YS, Jiang M, Yang Y, Gou HF: **Expression of HIF-1alpha and VEGF in colorectal cancer: association with clinical outcomes and prognostic implications.** *BMC cancer* 2009, **9**:432.
59. Rasheed S, Harris AL, Tekkis PP, Turley H, Silver A, McDonald PJ, Talbot IC, Glynne-Jones R, Northover JM, Guenther T: **Hypoxia-inducible factor-1alpha and -2alpha are expressed in most rectal cancers but only hypoxia-inducible factor-1alpha is associated with prognosis.** *British journal of cancer* 2009, **100**(10):1666-1673.
60. Shioya M, Takahashi T, Ishikawa H, Sakurai H, Ebara T, Suzuki Y, Saitoh J, Ohno T, Asao T, Kuwano H *et al*: **Expression of hypoxia-inducible factor 1alpha predicts clinical outcome after preoperative hyperthermo-chemoradiotherapy for locally advanced rectal cancer.** *Journal of radiation research* 2011, **52**(6):821-827.
61. Shimomura M, Hinoi T, Kuroda S, Adachi T, Kawaguchi Y, Sasada T, Takakura Y, Egi H, Okajima M, Tashiro H *et al*: **Overexpression of hypoxia inducible factor-1 alpha is an independent risk factor for recurrence after curative resection of colorectal liver metastases.** *Annals of surgical oncology* 2013, **20 Suppl 3**:S527-536.
62. Saka B, Ekinci O, Dursun A, Akyurek N: **Clinicopathologic and prognostic significance of immunohistochemical expression of HIF-1alpha, CXCR4 and CA9 in colorectal carcinoma.** *Pathology, research and practice* 2017, **213**(7):783-792.
63. Kaidi A, Qualtrough D, Williams AC, Paraskeva C: **Direct transcriptional up-regulation of cyclooxygenase-2 by hypoxia-inducible factor (HIF)-1 promotes colorectal tumor cell survival and enhances HIF-1 transcriptional activity during hypoxia.** *Cancer research* 2006, **66**(13):6683-6691.
64. Ahn GO, Seita J, Hong BJ, Kim YE, Bok S, Lee CJ, Kim KS, Lee JC, Leeper NJ, Cooke JP *et al*: **Transcriptional activation of hypoxia-inducible factor-1 (HIF-1) in myeloid cells promotes angiogenesis through VEGF and S100A8.** *Proceedings of the National Academy of Sciences of the United States of America* 2014, **111**(7):2698-2703.

65. Imamura T, Kikuchi H, Herraiz MT, Park DY, Mizukami Y, Mino-Kenduson M, Lynch MP, Rueda BR, Benita Y, Xavier RJ *et al*: **HIF-1alpha and HIF-2alpha have divergent roles in colon cancer**. *International journal of cancer Journal international du cancer* 2009, **124**(4):763-771.
66. Gorres KL, Raines RT: **Prolyl 4-hydroxylase**. *Critical reviews in biochemistry and molecular biology* 2010, **45**(2):106-124.
67. Gilkes DM, Bajpai S, Chaturvedi P, Wirtz D, Semenza GL: **Hypoxia-inducible factor 1 (HIF-1) promotes extracellular matrix remodeling under hypoxic conditions by inducing P4HA1, P4HA2, and PLOD2 expression in fibroblasts**. *The Journal of biological chemistry* 2013, **288**(15):10819-10829.
68. Gilkes DM, Chaturvedi P, Bajpai S, Wong CC, Wei H, Pitcairn S, Hubbi ME, Wirtz D, Semenza GL: **Collagen prolyl hydroxylases are essential for breast cancer metastasis**. *Cancer research* 2013, **73**(11):3285-3296.
69. Wu C, So J, Davis-Dusenbery BN, Qi HH, Bloch DB, Shi Y, Lagna G, Hata A: **Hypoxia potentiates microRNA-mediated gene silencing through posttranslational modification of Argonaute2**. *Molecular and cellular biology* 2011, **31**(23):4760-4774.
70. Shen J, Xia W, Khotskaya YB, Huo L, Nakanishi K, Lim SO, Du Y, Wang Y, Chang WC, Chen CH *et al*: **EGFR modulates microRNA maturation in response to hypoxia through phosphorylation of AGO2**. *Nature* 2013, **497**(7449):383-387.
71. Eisenblaetter M, Flores-Borja F, Lee JJ, Wefers C, Smith H, Hueting R, Cooper MS, Blower PJ, Patel D, Rodriguez-Justo M *et al*: **Visualization of Tumor-Immune Interaction - Target-Specific Imaging of S100A8/A9 Reveals Pre-Metastatic Niche Establishment**. *Theranostics* 2017, **7**(9):2392-2401.
72. Burke M, Choksawangkar W, Edwards N, Ostrand-Rosenberg S, Fenselau C: **Exosomes from myeloid-derived suppressor cells carry biologically active proteins**. *Journal of proteome research* 2014, **13**(2):836-843.
73. Grebhardt S, Veltkamp C, Strobel P, Mayer D: **Hypoxia and HIF-1 increase S100A8 and S100A9 expression in prostate cancer**. *International journal of cancer Journal international du cancer* 2012, **131**(12):2785-2794.
74. Bassorgun CI, Unal B, Erin N, Ozluk A, Uzun OC, Elpek GO: **S100A8 and S100A9 Positive Cells in Colorectal Carcinoma: Clinicopathological Analysis**. *Gastroenterology research and practice* 2014, **2014**:943175.
75. Duan L, Wu R, Ye L, Wang H, Yang X, Zhang Y, Chen X, Zuo G, Weng Y, Luo J *et al*: **S100A8 and S100A9 are associated with colorectal carcinoma progression and contribute to colorectal carcinoma cell survival and migration via Wnt/beta-catenin pathway**. *PLoS ONE* 2013, **8**(4):e62092.
76. Ji H, Greening DW, Barnes TW, Lim JW, Tauro BJ, Rai A, Xu R, Adda C, Mathivanan S, Zhao W *et al*: **Proteome profiling of exosomes derived from human primary and metastatic colorectal cancer cells reveal differential expression of key metastatic factors and signal transduction components**. *Proteomics* 2013, **13**(10-11):1672-1686.
77. Battaglin F, Puccini A, Intini R, Schirripa M, Ferro A, Bergamo F, Lonardi S, Zagonel V, Lenz HJ, Loupakis F: **The role of tumor angiogenesis as a therapeutic target in colorectal cancer**. *Expert review of anticancer therapy* 2018, **18**(3):251-266.
78. Kabbinnavar FF, Hambleton J, Mass RD, Hurwitz HI, Bergsland E, Sarkar S: **Combined analysis of efficacy: the addition of bevacizumab to fluorouracil/leucovorin improves survival for patients with metastatic**

- colorectal cancer.** *Journal of clinical oncology : official journal of the American Society of Clinical Oncology* 2005, **23**(16):3706-3712.
79. Giantonio BJ, Catalano PJ, Meropol NJ, O'Dwyer PJ, Mitchell EP, Alberts SR, Schwartz MA, Benson AB, 3rd, Eastern Cooperative Oncology Group Study E: **Bevacizumab in combination with oxaliplatin, fluorouracil, and leucovorin (FOLFOX4) for previously treated metastatic colorectal cancer: results from the Eastern Cooperative Oncology Group Study E3200.** *Journal of clinical oncology : official journal of the American Society of Clinical Oncology* 2007, **25**(12):1539-1544.
 80. Mesange P, Bouygues A, Ferrand N, Sabbah M, Escargueil AE, Savina A, Chibaudel B, Tournigand C, Andre T, de Gramont A *et al*: **Combinations of Bevacizumab and Erlotinib show activity in colorectal cancer independent of RAS status.** *Clinical cancer research : an official journal of the American Association for Cancer Research* 2018, **24**(11):2548-2558.
 81. Rahbari NN, Kedrin D, Incio J, Liu H, Ho WW, Nia HT, Edrich CM, Jung K, Daubriac J, Chen I *et al*: **Anti-VEGF therapy induces ECM remodeling and mechanical barriers to therapy in colorectal cancer liver metastases.** *Sci Transl Med* 2016, **8**(360):360ra135.
 82. Semenza GL: **HIF-1 mediates metabolic responses to intratumoral hypoxia and oncogenic mutations.** *The Journal of clinical investigation* 2013, **123**(9):3664-3671.
 83. Gatenby RA, Smallbone K, Maini PK, Rose F, Averill J, Nagle RB, Worrall L, Gillies RJ: **Cellular adaptations to hypoxia and acidosis during somatic evolution of breast cancer.** *British journal of cancer* 2007, **97**(5):646-653.
 84. Valadi H, Ekstrom K, Bossios A, Sjostrand M, Lee JJ, Lotvall JO: **Exosome-mediated transfer of mRNAs and microRNAs is a novel mechanism of genetic exchange between cells.** *Nature cell biology* 2007, **9**(6):654-659.
 85. Harding C, Heuser J, Stahl P: **Endocytosis and intracellular processing of transferrin and colloidal gold-transferrin in rat reticulocytes: demonstration of a pathway for receptor shedding.** *European journal of cell biology* 1984, **35**(2):256-263.
 86. Baietti MF, Zhang Z, Mortier E, Melchior A, Degeest G, Geeraerts A, Ivarsson Y, Depoortere F, Coomans C, Vermeiren E *et al*: **Syndecan-syntenin-ALIX regulates the biogenesis of exosomes.** *Nature cell biology* 2012, **14**(7):677-685.
 87. van Niel G, Porto-Carreiro I, Simoes S, Raposo G: **Exosomes: a common pathway for a specialized function.** *Journal of biochemistry* 2006, **140**(1):13-21.
 88. Thery C, Zitvogel L, Amigorena S: **Exosomes: composition, biogenesis and function.** *Nature reviews Immunology* 2002, **2**(8):569-579.
 89. Rana S, Yue S, Stadel D, Zoller M: **Toward tailored exosomes: the exosomal tetraspanin web contributes to target cell selection.** *The international journal of biochemistry & cell biology* 2012, **44**(9):1574-1584.
 90. Lawson C, Vicencio JM, Yellon DM, Davidson SM: **Microvesicles and exosomes: new players in metabolic and cardiovascular disease.** *J Endocrinol* 2016, **228**(2):R57-71.
 91. Demory Beckler M, Higginbotham JN, Franklin JL, Ham AJ, Halvey PJ, Imasuen IE, Whitwell C, Li M, Liebler DC, Coffey RJ: **Proteomic analysis of exosomes from mutant KRAS colon cancer cells identifies intercellular transfer of mutant KRAS.** *Molecular & cellular proteomics : MCP* 2013, **12**(2):343-355.

92. Cha DJ, Franklin JL, Dou Y, Liu Q, Higginbotham JN, Demory Beckler M, Weaver AM, Vickers K, Prasad N, Levy S *et al*: **KRAS-dependent sorting of miRNA to exosomes.** *eLife* 2015, **4**:e07197.
93. Soldevilla B, Rodriguez M, San Millan C, Garcia V, Fernandez-Perianez R, Gil-Calderon B, Martin P, Garcia-Grande A, Silva J, Bonilla F *et al*: **Tumor-derived exosomes are enriched in DeltaNp73, which promotes oncogenic potential in acceptor cells and correlates with patient survival.** *Human molecular genetics* 2014, **23**(2):467-478.
94. Wang X, Ding X, Nan L, Wang Y, Wang J, Yan Z, Zhang W, Sun J, Zhu W, Ni B *et al*: **Investigation of the roles of exosomes in colorectal cancer liver metastasis.** *Oncology reports* 2015, **33**(5):2445-2453.
95. Hu Y, Yan C, Mu L, Huang K, Li X, Tao D, Wu Y, Qin J: **Fibroblast-Derived Exosomes Contribute to Chemoresistance through Priming Cancer Stem Cells in Colorectal Cancer.** *PLoS One* 2015, **10**(5):e0125625.
96. Wang Z, von Au A, Schnolzer M, Hackert T, Zoller M: **CD44v6-competent tumor exosomes promote motility, invasion and cancer-initiating cell marker expression.** *Oncotarget* 2016, **7**(34):55409-55436.
97. Lugini L, Valtieri M, Federici C, Cecchetti S, Meschini S, Condello M, Signore M, Fais S: **Exosomes from human colorectal cancer induce a tumor-like behavior in colonic mesenchymal stromal cells.** *Oncotarget* 2016, **7**(31):50086-50098.
98. Song M, Wang Y, Shang ZF, Liu XD, Xie DF, Wang Q, Guan H, Zhou PK: **Bystander autophagy mediated by radiation-induced exosomal miR-7-5p in non-targeted human bronchial epithelial cells.** *Scientific reports* 2016, **6**:30165.
99. Silva J, Garcia V, Rodriguez M, Compte M, Cisneros E, Veguillas P, Garcia JM, Dominguez G, Campos-Martin Y, Cuevas J *et al*: **Analysis of exosome release and its prognostic value in human colorectal cancer.** *Genes, chromosomes & cancer* 2012, **51**(4):409-418.
100. Fang S, Tian H, Li X, Jin D, Li X, Kong J, Yang C, Yang X, Lu Y, Luo Y *et al*: **Clinical application of a microfluidic chip for immunocapture and quantification of circulating exosomes to assist breast cancer diagnosis and molecular classification.** *PLoS One* 2017, **12**(4):e0175050.
101. Menck K, Bleckmann A, Wachter A, Hennies B, Ries L, Schulz M, Balkenhol M, Pukrop T, Schatlo B, Rost U *et al*: **Characterisation of tumour-derived microvesicles in cancer patients' blood and correlation with clinical outcome.** *Journal of extracellular vesicles* 2017, **6**(1):1340745.
102. Matsumura T, Sugimachi K, Iinuma H, Takahashi Y, Kurashige J, Sawada G, Ueda M, Uchi R, Ueo H, Takano Y *et al*: **Exosomal microRNA in serum is a novel biomarker of recurrence in human colorectal cancer.** *British journal of cancer* 2015, **113**(2):275-281.
103. Ogata-Kawata H, Izumiya M, Kurioka D, Honma Y, Yamada Y, Furuta K, Gunji T, Ohta H, Okamoto H, Sonoda H *et al*: **Circulating exosomal microRNAs as biomarkers of colon cancer.** *PLoS One* 2014, **9**(4):e92921.
104. Ostenfeld MS, Jensen SG, Jeppesen DK, Christensen LL, Thorsen SB, Stenvang J, Hvam ML, Thomsen A, Mouritzen P, Rasmussen MH *et al*: **miRNA profiling of circulating EpCAM(+) extracellular vesicles: promising biomarkers of colorectal cancer.** *Journal of extracellular vesicles* 2016, **5**:31488.

105. Tauro BJ, Greening DW, Mathias RA, Mathivanan S, Ji H, Simpson RJ: **Two distinct populations of exosomes are released from LIM1863 colon carcinoma cell-derived organoids.** *Molecular & cellular proteomics : MCP* 2013, **12**(3):587-598.
106. Hong BS, Cho JH, Kim H, Choi EJ, Rho S, Kim J, Kim JH, Choi DS, Kim YK, Hwang D *et al*: **Colorectal cancer cell-derived microvesicles are enriched in cell cycle-related mRNAs that promote proliferation of endothelial cells.** *BMC genomics* 2009, **10**:556.
107. Yoon YJ, Kim DK, Yoon CM, Park J, Kim YK, Roh TY, Gho YS: **Egr-1 activation by cancer-derived extracellular vesicles promotes endothelial cell migration via ERK1/2 and JNK signaling pathways.** *PLoS One* 2014, **9**(12):e115170.
108. Huang Z, Feng Y: **Exosomes derived from hypoxic colorectal cancer cells promotes angiogenesis through Wnt4 induced beta-catenin signaling in endothelial cells.** *Oncology research* 2016, **25**(5):651-661.
109. Luga V, Zhang L, Vitoria-Petit AM, Ogunjimi AA, Inanlou MR, Chiu E, Buchanan M, Hosein AN, Basik M, Wrana JL: **Exosomes mediate stromal mobilization of autocrine Wnt-PCP signaling in breast cancer cell migration.** *Cell* 2012, **151**(7):1542-1556.
110. Peinado H, Aleckovic M, Lavotshkin S, Matei I, Costa-Silva B, Moreno-Bueno G, Hergueta-Redondo M, Williams C, Garcia-Santos G, Ghajar C *et al*: **Melanoma exosomes educate bone marrow progenitor cells toward a pro-metastatic phenotype through MET.** *Nature medicine* 2012, **18**(6):883-891.
111. Grange C, Tapparo M, Collino F, Vitillo L, Damasco C, Derigibus MC, Tetta C, Bussolati B, Camussi G: **Microvesicles released from human renal cancer stem cells stimulate angiogenesis and formation of lung premetastatic niche.** *Cancer research* 2011, **71**(15):5346-5356.
112. Robbins PD, Morelli AE: **Regulation of immune responses by extracellular vesicles.** *Nature reviews Immunology* 2014, **14**(3):195-208.
113. Huber V, Fais S, Iero M, Lugini L, Canese P, Squarcina P, Zaccheddu A, Colone M, Arancia G, Gentile M *et al*: **Human colorectal cancer cells induce T-cell death through release of proapoptotic microvesicles: role in immune escape.** *Gastroenterology* 2005, **128**(7):1796-1804.
114. Yamada N, Kuranaga Y, Kumazaki M, Shinohara H, Taniguchi K, Akao Y: **Colorectal cancer cell-derived extracellular vesicles induce phenotypic alteration of T cells into tumor-growth supporting cells with transforming growth factor-beta1-mediated suppression.** *Oncotarget* 2016, **7**(19):27033-27043.
115. Monypenny J, Milewicz H, Flores-Borja F, Weitsman G, Cheung A, Chowdhury R, Burgoyne T, Arulappu A, Lawler K, Barber PR *et al*: **ALIX Regulates Tumor-Mediated Immunosuppression by Controlling EGFR Activity and PD-L1 Presentation.** *Cell reports* 2018, **24**(3):630-641.
116. Ragusa M, Statello L, Maugeri M, Barbagallo C, Passanisi R, Alhamdani MS, Li Destri G, Cappellani A, Barbagallo D, Scalia M *et al*: **Highly skewed distribution of miRNAs and proteins between colorectal cancer cells and their exosomes following Cetuximab treatment: biomolecular, genetic and translational implications.** *Oncoscience* 2014, **1**(2):132-157.
117. Gillies RJ, Gatenby RA: **Adaptive landscapes and emergent phenotypes: why do cancers have high glycolysis?** *J Bioenerg Biomembr* 2007, **39**(3):251-257.

118. Mankoff DA, Eary JF, Link JM, Muzi M, Rajendran JG, Spence AM, Krohn KA: **Tumor-specific positron emission tomography imaging in patients: [18F] fluorodeoxyglucose and beyond.** *Clinical cancer research : an official journal of the American Association for Cancer Research* 2007, **13**(12):3460-3469.
119. Dierckx RA, Van de Wiele C: **FDG uptake, a surrogate of tumour hypoxia?** *European journal of nuclear medicine and molecular imaging* 2008, **35**(8):1544-1549.
120. Patel S, McCall M, Ohinmaa A, Bigam D, Dryden DM: **Positron emission tomography/computed tomographic scans compared to computed tomographic scans for detecting colorectal liver metastases: a systematic review.** *Annals of surgery* 2011, **253**(4):666-671.
121. Lubezky N, Metser U, Geva R, Nakache R, Shmueli E, Klausner JM, Even-Sapir E, Figer A, Ben-Haim M: **The role and limitations of 18-fluoro-2-deoxy-D-glucose positron emission tomography (FDG-PET) scan and computerized tomography (CT) in restaging patients with hepatic colorectal metastases following neoadjuvant chemotherapy: comparison with operative and pathological findings.** *Journal of gastrointestinal surgery : official journal of the Society for Surgery of the Alimentary Tract* 2007, **11**(4):472-478.
122. Carnaghi C, Tronconi MC, Rimassa L, Tondulli L, Zuradelli M, Rodari M, Doci R, Luttmann F, Torzilli G, Rubello D *et al*: **Utility of 18F-FDG PET and contrast-enhanced CT scan in the assessment of residual liver metastasis from colorectal cancer following adjuvant chemotherapy.** *Nuclear medicine review Central & Eastern Europe* 2007, **10**(1):12-15.
123. Metser U, Halankar J, Langer D, Mohan R, Hussey D, Hadas M, Tamir S: **Effect of chemotherapy on the impact of FDG-PET/CT in selection of patients for surgical resection of colorectal liver metastases: single center analysis of PET-CAM randomized trial.** *Annals of nuclear medicine* 2017, **31**(2):153-162.
124. Choi YJ, Kim MJ, Lee BH, Kwon MJ, Hwang HS: **Relationship between Preoperative (1)(8)F-Fluorodeoxyglucose Uptake and Epidermal Growth Factor Receptor Status in Primary Colorectal Cancer.** *Yonsei medical journal* 2016, **57**(1):232-237.
125. Oner AO, Budak ES, Yildirim S, Aydin F, Sezer C: **The value of (18)FDG PET/CT parameters, hematological parameters and tumor markers in predicting KRAS oncogene mutation in colorectal cancer.** *Hell J Nucl Med* 2017, **20**(2):160-165.
126. Krikelis D, Skoura E, Kotoula V, Rondogianni P, Pianou N, Samartzis A, Xanthakis I, Fountzilias G, Datseris IE: **Lack of association between KRAS mutations and 18F-FDG PET/CT in Caucasian metastatic colorectal cancer patients.** *Anticancer research* 2014, **34**(5):2571-2579.
127. Kawada K, Nakamoto Y, Kawada M, Hida K, Matsumoto T, Murakami T, Hasegawa S, Togashi K, Sakai Y: **Relationship between 18F-fluorodeoxyglucose accumulation and KRAS/BRAF mutations in colorectal cancer.** *Clinical cancer research : an official journal of the American Association for Cancer Research* 2012, **18**(6):1696-1703.
128. Kawada K, Toda K, Nakamoto Y, Iwamoto M, Hatano E, Chen F, Hasegawa S, Togashi K, Date H, Uemoto S *et al*: **Relationship Between 18F-FDG PET/CT Scans and KRAS Mutations in Metastatic Colorectal Cancer.** *Journal of*

- nuclear medicine : official publication, Society of Nuclear Medicine* 2015, **56**(9):1322-1327.
129. Chen SW, Lin CY, Ho CM, Chang YS, Yang SF, Kao CH, Chang JG: **Genetic Alterations in Colorectal Cancer Have Different Patterns on 18F-FDG PET/CT.** *Clinical nuclear medicine* 2015, **40**(8):621-626.
 130. Cho A, Jo K, Hwang SH, Lee N, Jung M, Yun M, Hwang HS: **Correlation between KRAS mutation and (18)F-FDG uptake in stage IV colorectal cancer.** *Abdom Radiol (NY)* 2017, **42**(6):1621-1626.
 131. Lovinfosse P, Koopmansch B, Lambert F, Jodogne S, Kustermans G, Hatt M, Visvikis D, Seidel L, Polus M, Albert A *et al*: **(18)F-FDG PET/CT imaging in rectal cancer: relationship with the RAS mutational status.** *The British journal of radiology* 2016, **89**(1063):20160212.
 132. Lee JH, Kang J, Baik SH, Lee KY, Lim BJ, Jeon TJ, Ryu YH, Sohn SK: **Relationship Between 18F-Fluorodeoxyglucose Uptake and V-Ki-Ras2 Kirsten Rat Sarcoma Viral Oncogene Homolog Mutation in Colorectal Cancer Patients: Variability Depending on C-Reactive Protein Level.** *Medicine* 2016, **95**(1):e2236.
 133. Iwamoto M, Kawada K, Nakamoto Y, Itatani Y, Inamoto S, Toda K, Kimura H, Sasazuki T, Shirasawa S, Okuyama H *et al*: **Regulation of 18F-FDG accumulation in colorectal cancer cells with mutated KRAS.** *Journal of nuclear medicine : official publication, Society of Nuclear Medicine* 2014, **55**(12):2038-2044.
 134. Miles KA, Ganeshan B, Rodriguez-Justo M, Goh VJ, Ziauddin Z, Engledow A, Meagher M, Endozo R, Taylor SA, Halligan S *et al*: **Multifunctional imaging signature for V-KI-RAS2 Kirsten rat sarcoma viral oncogene homolog (KRAS) mutations in colorectal cancer.** *Journal of nuclear medicine : official publication, Society of Nuclear Medicine* 2014, **55**(3):386-391.
 135. Kocael A, Vatankulu B, Simsek O, Cengiz M, Kemik A, Kocael P, Halac M, Sonmezoglu K, Ulualp K: **Comparison of (18)F-fluorodeoxyglucose PET/CT findings with vascular endothelial growth factors and receptors in colorectal cancer.** *Tumour biology : the journal of the International Society for Oncodevelopmental Biology and Medicine* 2016, **37**(3):3871-3877.
 136. Shi D, Cai G, Peng J, Li D, Li X, Xu Y, Cai S: **The preoperative SUVmax for (18)F-FDG uptake predicts survival in patients with colorectal cancer.** *BMC cancer* 2015, **15**:991.
 137. Ogawa S, Itabashi M, Kondo C, Momose M, Sakai S, Kameoka S: **Prognostic Value of Total Lesion Glycolysis Measured by 18F-FDG-PET/CT in Patients with Colorectal Cancer.** *Anticancer research* 2015, **35**(6):3495-3500.
 138. Lee JE, Kim SW, Kim JS, Choi KY, Kang WK, Oh ST, Yoo Ie R, Kim SH: **Prognostic value of 18-fluorodeoxyglucose positron emission tomography-computed tomography in resectable colorectal cancer.** *World journal of gastroenterology : WJG* 2012, **18**(36):5072-5077.
 139. Jo HJ, Kim SJ, Lee HY, Kim IJ: **Prediction of survival and cancer recurrence using metabolic volumetric parameters measured by 18F-FDG PET/CT in patients with surgically resected rectal cancer.** *Clinical nuclear medicine* 2014, **39**(6):493-497.
 140. Nakajo M, Kajiya Y, Tani A, Jinguji M, Nakajo M, Kitazono M, Yoshiura T: **A pilot study for texture analysis of (18)F-FDG and (18)F-FLT-PET/CT to predict tumor recurrence of patients with colorectal cancer who received**

- surgery. *European journal of nuclear medicine and molecular imaging* 2017, 44(13):2158-2168.**
141. Lee JW, Baek MJ, Ahn TS, Lee SM: **Fluorine-18-fluorodeoxyglucose uptake of bone marrow on PET/CT can predict prognosis in patients with colorectal cancer after curative surgical resection.** *Eur J Gastroenterol Hepatol* 2018, **30(2):187-194.**
 142. Huang J, Huang L, Zhou J, Duan Y, Zhang Z, Wang X, Huang P, Tan S, Hu P, Wang J *et al*: **Elevated tumor-to-liver uptake ratio (TLR) from (18)F-FDG-PET/CT predicts poor prognosis in stage IIA colorectal cancer following curative resection.** *European journal of nuclear medicine and molecular imaging* 2017, **44(12):1958-1968.**
 143. Bang JI, Ha S, Kang SB, Lee KW, Lee HS, Kim JS, Oh HK, Lee HY, Kim SE: **Prediction of neoadjuvant radiation chemotherapy response and survival using pretreatment [(18)F]FDG PET/CT scans in locally advanced rectal cancer.** *European journal of nuclear medicine and molecular imaging* 2016, **43(3):422-431.**
 144. Kim SJ, Chang S: **Volumetric parameters changes of sequential 18F-FDG PET/CT for early prediction of recurrence and death in patients with locally advanced rectal cancer treated with preoperative chemoradiotherapy.** *Clinical nuclear medicine* 2015, **40(12):930-935.**
 145. Liu FY, Yen TC, Wang JY, Yang TS: **Early Prediction by 18F-FDG PET/CT for Progression-Free Survival and Overall Survival in Patients With Metastatic Colorectal Cancer Receiving Third-Line Cetuximab-Based Therapy.** *Clinical nuclear medicine* 2015, **40(3):200-205.**
 146. Lim Y, Bang JI, Han SW, Paeng JC, Lee KH, Kim JH, Kang GH, Jeong SY, Park KJ, Kim TY: **Total lesion glycolysis (TLG) as an imaging biomarker in metastatic colorectal cancer patients treated with regorafenib.** *European journal of nuclear medicine and molecular imaging* 2017, **44(5):757-764.**
 147. Marcus C, Wray R, Taghipour M, Marashdeh W, Ahn SJ, Mena E, Subramaniam RM: **JOURNAL CLUB: Value of Quantitative FDG PET/CT Volumetric Biomarkers in Recurrent Colorectal Cancer Patient Survival.** *AJR American journal of roentgenology* 2016, **207(2):257-265.**
 148. Grut H, Dueland S, Line PD, Revheim ME: **The prognostic value of (18)F-FDG PET/CT prior to liver transplantation for nonresectable colorectal liver metastases.** *European journal of nuclear medicine and molecular imaging* 2018, **45(2):218-225.**
 149. Samim M, Prevoo W, de Wit-van der Veen BJ, Kuhlmann KF, Ruers T, van Hillegersberg R, van den Bosch M, Verkooijen HM, Lam M, Stokkel MPM: **(18)F-FDG PET as novel imaging biomarker for disease progression after ablation therapy in colorectal liver metastases.** *European journal of nuclear medicine and molecular imaging* 2017, **44(7):1165-1175.**
 150. Skougaard K, Johannesen HH, Nielsen D, Schou JV, Jensen BV, Hogdall EV, Hendel HW: **CT versus FDG-PET/CT response evaluation in patients with metastatic colorectal cancer treated with irinotecan and cetuximab.** *Cancer medicine* 2014, **3(5):1294-1301.**
 151. Li QW, Zheng RL, Ling YH, Wang QX, Xiao WW, Zeng ZF, Fan W, Li LR, Gao YH: **Prediction of tumor response after neoadjuvant chemoradiotherapy in rectal cancer using (18)fluorine-2-deoxy-D-glucose positron emission tomography-computed tomography and serum**

- carcinoembryonic antigen: a prospective study.** *Abdom Radiol (NY)* 2016, **41(8)**:1448-1455.
152. Kawai K, Nozawa H, Hata K, Tanaka T, Nishikawa T, Oba K, Watanabe T: **Optimal Interval for (18)F-FDG-PET After Chemoradiotherapy for Rectal Cancer.** *Clin Colorectal Cancer* 2018, **17(2)**:e163-e170.
153. Goshen E, Davidson T, Zwas ST, Aderka D: **PET/CT in the evaluation of response to treatment of liver metastases from colorectal cancer with bevacizumab and irinotecan.** *Technology in cancer research & treatment* 2006, **5(1)**:37-43.
154. De Bruyne S, Van Damme N, Smeets P, Ferdinande L, Ceelen W, Mertens J, Van de Wiele C, Troisi R, Libbrecht L, Laurent S *et al*: **Value of DCE-MRI and FDG-PET/CT in the prediction of response to preoperative chemotherapy with bevacizumab for colorectal liver metastases.** *British journal of cancer* 2012, **106(12)**:1926-1933.
155. Mertens J, De Bruyne S, Van Damme N, Smeets P, Ceelen W, Troisi R, Laurent S, Geboes K, Peeters M, Goethals I *et al*: **Standardized added metabolic activity (SAM) IN (1)(8)F-FDG PET assessment of treatment response in colorectal liver metastases.** *European journal of nuclear medicine and molecular imaging* 2013, **40(8)**:1214-1222.
156. Latoria S, Piccirillo MC, Caraco C, Nasti G, Aloj L, Arrichiello C, de Lutio di Castelguidone E, Tatangelo F, Ottaiano A, Iaffaioli RV *et al*: **Early PET/CT scan is more effective than RECIST in predicting outcome of patients with liver metastases from colorectal cancer treated with preoperative chemotherapy plus bevacizumab.** *Journal of nuclear medicine : official publication, Society of Nuclear Medicine* 2013, **54(12)**:2062-2069.
157. Bystrom P, Berglund A, Garske U, Jacobsson H, Sundin A, Nygren P, Frodin JE, Glimelius B: **Early prediction of response to first-line chemotherapy by sequential [18F]-2-fluoro-2-deoxy-D-glucose positron emission tomography in patients with advanced colorectal cancer.** *Annals of oncology : official journal of the European Society for Medical Oncology / ESMO* 2009, **20(6)**:1057-1061.
158. Maisonobe JA, Garcia CA, Necib H, Vanderlinden B, Hendlisz A, Flamen P, Buvat I: **Comparison of PET metabolic indices for the early assessment of tumour response in metastatic colorectal cancer patients treated by polychemotherapy.** *European journal of nuclear medicine and molecular imaging* 2013, **40(2)**:166-174.
159. Hendlisz A, Golfinopoulos V, Garcia C, Covas A, Emonts P, Ameye L, Paesmans M, Deleporte A, Machiels G, Toussaint E *et al*: **Serial FDG-PET/CT for early outcome prediction in patients with metastatic colorectal cancer undergoing chemotherapy.** *Annals of oncology : official journal of the European Society for Medical Oncology / ESMO* 2012, **23(7)**:1687-1693.
160. Woff E, Hendlisz A, Garcia C, Deleporte A, Delaunoit T, Marechal R, Holbrechts S, Van den Eynde M, Demolin G, Vierasu I *et al*: **Monitoring metabolic response using FDG PET-CT during targeted therapy for metastatic colorectal cancer.** *European journal of nuclear medicine and molecular imaging* 2016, **43(10)**:1792-1801.
161. Kim SH, Kamaya A, Willmann JK: **CT perfusion of the liver: principles and applications in oncology.** *Radiology* 2014, **272(2)**:322-344.

162. Chen BB, Shih TT: **DCE-MRI in hepatocellular carcinoma-clinical and therapeutic image biomarker.** *World journal of gastroenterology : WJG* 2014, **20**(12):3125-3134.
163. Ingrisich M, Sourbron S: **Tracer-kinetic modeling of dynamic contrast-enhanced MRI and CT: a primer.** *J Pharmacokinet Pharmacodyn* 2013, **40**(3):281-300.
164. Goh V, Bartram C, Halligan S: **Effect of intravenous contrast agent volume on colorectal cancer vascular parameters as measured by perfusion computed tomography.** *Clinical radiology* 2009, **64**(4):368-372.
165. Goh V, Halligan S, Hugill JA, Gartner L, Bartram CI: **Quantitative colorectal cancer perfusion measurement using dynamic contrast-enhanced multidetector-row computed tomography: effect of acquisition time and implications for protocols.** *J Comput Assist Tomogr* 2005, **29**(1):59-63.
166. Goh V, Halligan S, Hugill JA, Bassett P, Bartram CI: **Quantitative assessment of colorectal cancer perfusion using MDCT: inter- and intraobserver agreement.** *AJR American journal of roentgenology* 2005, **185**(1):225-231.
167. Goh V, Shastry M, Engledow A, Kozarski R, Peck J, Endozo R, Rodriguez-Justo M, Taylor SA, Halligan S, Groves AM: **Integrated (18)F-FDG PET/CT and perfusion CT of primary colorectal cancer: effect of inter- and intraobserver agreement on metabolic-vascular parameters.** *AJR American journal of roentgenology* 2012, **199**(5):1003-1009.
168. Goh V, Halligan S, Gartner L, Bassett P, Bartram CI: **Quantitative colorectal cancer perfusion measurement by multidetector-row CT: does greater tumour coverage improve measurement reproducibility?** *The British journal of radiology* 2006, **79**(943):578-583.
169. Goh V, Halligan S, Bartram CI: **Quantitative tumor perfusion assessment with multidetector CT: are measurements from two commercial software packages interchangeable?** *Radiology* 2007, **242**(3):777-782.
170. Goh V, Shastry M, Engledow A, Reston J, Wellsted DM, Peck J, Endozo R, Rodriguez-Justo M, Taylor SA, Halligan S *et al*: **Commercial software upgrades may significantly alter Perfusion CT parameter values in colorectal cancer.** *Eur Radiol* 2011, **21**(4):744-749.
171. Dighe S, Castellano E, Blake H, Jeyadevan N, Koh MU, Orten M, Swift I, Brown G: **Perfusion CT to assess angiogenesis in colon cancer: technical limitations and practical challenges.** *The British journal of radiology* 2012, **85**(1018):e814-825.
172. Dighe S, Blake H, Jeyadevan N, Castellano I, Koh DM, Orten M, Chandler I, Swift I, Brown G: **Perfusion CT vascular parameters do not correlate with immunohistochemically derived microvessel density count in colorectal tumors.** *Radiology* 2013, **268**(2):400-410.
173. Goh V, Halligan S, Gharpuray A, Wellsted D, Sundin J, Bartram CI: **Quantitative assessment of colorectal cancer tumor vascular parameters by using perfusion CT: influence of tumor region of interest.** *Radiology* 2008, **247**(3):726-732.
174. Goh V, Halligan S, Daley F, Wellsted DM, Guenther T, Bartram CI: **Colorectal tumor vascularity: quantitative assessment with multidetector CT--do tumor perfusion measurements reflect angiogenesis?** *Radiology* 2008, **249**(2):510-517.
175. Goh V, Rodriguez-Justo M, Engledow A, Shastry M, Endozo R, Peck J, Meagher M, Taylor SA, Halligan S, Groves AM: **Assessment of the metabolic**

- flow phenotype of primary colorectal cancer: correlations with microvessel density are influenced by the histological scoring method.** *Eur Radiol* 2012, **22**(8):1687-1692.
176. Goh V, Engledow A, Rodriguez-Justo M, Shastry M, Peck J, Blackman G, Endozo R, Taylor S, Halligan S, Ell P *et al*: **The flow-metabolic phenotype of primary colorectal cancer: assessment by integrated 18F-FDG PET/perfusion CT with histopathologic correlation.** *Journal of nuclear medicine : official publication, Society of Nuclear Medicine* 2012, **53**(5):687-692.
177. Tixier F, Groves AM, Goh V, Hatt M, Ingrand P, Le Rest CC, Visvikis D: **Correlation of intra-tumor 18F-FDG uptake heterogeneity indices with perfusion CT derived parameters in colorectal cancer.** *PLoS One* 2014, **9**(6):e99567.
178. Kim JW, Jeong YY, Chang NK, Heo SH, Shin SS, Lee JH, Hur YH, Kang HK: **Perfusion CT in colorectal cancer: comparison of perfusion parameters with tumor grade and microvessel density.** *Korean journal of radiology* 2012, **13** Suppl 1:S89-97.
179. Sun H, Xu Y, Yang Q, Wang W: **Assessment of tumor grade and angiogenesis in colorectal cancer: whole-volume perfusion CT.** *Acad Radiol* 2014, **21**(6):750-757.
180. Xu Y, Sun H, Song A, Yang Q, Lu X, Wang W: **Predictive Significance of Tumor Grade Using 256-Slice CT Whole-Tumor Perfusion Imaging in Colorectal Adenocarcinoma.** *Acad Radiol* 2015, **22**(12):1529-1535.
181. Hayano K, Shuto K, Koda K, Yanagawa N, Okazumi S, Matsubara H: **Quantitative measurement of blood flow using perfusion CT for assessing clinicopathologic features and prognosis in patients with rectal cancer.** *Dis Colon Rectum* 2009, **52**(9):1624-1629.
182. Goh V, Halligan S, Wellsted DM, Bartram CI: **Can perfusion CT assessment of primary colorectal adenocarcinoma blood flow at staging predict for subsequent metastatic disease? A pilot study.** *Eur Radiol* 2009, **19**(1):79-89.
183. Qi Q, Yeung TP, Lee TY, Bauman G, Crukley C, Morrison L, Hoffman L, Yartsev S: **Evaluation of CT Perfusion Biomarkers of Tumor Hypoxia.** *PLoS One* 2016, **11**(4):e0153569.
184. Varia MA, Calkins-Adams DP, Rinker LH, Kennedy AS, Novotny DB, Fowler WC, Jr., Raleigh JA: **Pimonidazole: a novel hypoxia marker for complementary study of tumor hypoxia and cell proliferation in cervical carcinoma.** *Gynecol Oncol* 1998, **71**(2):270-277.
185. Spira D, Neumeister H, Spira SM, Hetzel J, Spengler W, von Weyhern CH, Horgner M: **Assessment of tumor vascularity in lung cancer using volume perfusion CT (VPCT) with histopathologic comparison: a further step toward an individualized tumor characterization.** *J Comput Assist Tomogr* 2013, **37**(1):15-21.
186. Willett CG, Boucher Y, di Tomaso E, Duda DG, Munn LL, Tong RT, Chung DC, Sahani DV, Kalva SP, Kozin SV *et al*: **Direct evidence that the VEGF-specific antibody bevacizumab has antivascular effects in human rectal cancer.** *Nature medicine* 2004, **10**(2):145-147.
187. Miles KA, Ganeshan B, Hayball MP: **CT texture analysis using the filtration-histogram method: what do the measurements mean?** *Cancer Imaging* 2013, **13**(3):400-406.

188. Ganeshan B, Miles KA, Young RC, Chatwin CR: **Hepatic enhancement in colorectal cancer: texture analysis correlates with hepatic hemodynamics and patient survival.** *Acad Radiol* 2007, **14**(12):1520-1530.
189. Ganeshan B, Miles KA, Young RC, Chatwin CR: **Texture analysis in non-contrast enhanced CT: impact of malignancy on texture in apparently disease-free areas of the liver.** *Eur J Radiol* 2009, **70**(1):101-110.
190. Ng F, Ganeshan B, Kozarski R, Miles KA, Goh V: **Assessment of primary colorectal cancer heterogeneity by using whole-tumor texture analysis: contrast-enhanced CT texture as a biomarker of 5-year survival.** *Radiology* 2013, **266**(1):177-184.
191. Ganeshan B, Miles KA, Young RC, Chatwin CR: **In search of biologic correlates for liver texture on portal-phase CT.** *Acad Radiol* 2007, **14**(9):1058-1068.
192. They C, Amigorena S, Raposo G, Clayton A: **Isolation and characterization of exosomes from cell culture supernatants and biological fluids.** *Curr Protoc Cell Biol* 2006, **Chapter 3**:Unit 3 22.
193. Groves AM, Shastry M, Rodriguez-Justo M, Malhotra A, Endozo R, Davidson T, Kelleher T, Miles KA, Ell PJ, Keshtgar MR: **(1)(8)F-FDG PET and biomarkers for tumour angiogenesis in early breast cancer.** *European journal of nuclear medicine and molecular imaging* 2011, **38**(1):46-52.
194. Shrout PE, Fleiss JL: **Intraclass correlations: uses in assessing rater reliability.** *Psychol Bull* 1979, **86**(2):420-428.
195. Goh V, Glynn-Jones R: **Perfusion CT imaging of colorectal cancer.** *The British journal of radiology* 2014, **87**(1034):20130811.
196. Fraioli F, Anzidei M, Zaccagna F, Mennini ML, Serra G, Gori B, Longo F, Catalano C, Passariello R: **Whole-tumor perfusion CT in patients with advanced lung adenocarcinoma treated with conventional and antiangiogenic chemotherapy: initial experience.** *Radiology* 2011, **259**(2):574-582.
197. Weiss GJ, Ganeshan B, Miles KA, Campbell DH, Cheung PY, Frank S, Korn RL: **Noninvasive image texture analysis differentiates K-ras mutation from pan-wildtype NSCLC and is prognostic.** *PLoS One* 2014, **9**(7):e100244.
198. Liu S, Zheng H, Pan X, Chen L, Shi M, Guan Y, Ge Y, He J, Zhou Z: **Texture analysis of CT imaging for assessment of esophageal squamous cancer aggressiveness.** *J Thorac Dis* 2017, **9**(11):4724-4732.
199. Caramella C, Allorant A, Orhac F, Bidault F, Asselain B, Ammari S, Jaranowski P, Moussier A, Balleyguier C, Lassau N *et al*: **Can we trust the calculation of texture indices of CT images? A phantom study.** *Med Phys* 2018, **45**(4):1529-1536.
200. Fave X, Mackin D, Yang J, Zhang J, Fried D, Balter P, Followill D, Gomez D, Jones AK, Stingo F *et al*: **Can radiomics features be reproducibly measured from CBCT images for patients with non-small cell lung cancer?** *Med Phys* 2015, **42**(12):6784-6797.
201. Hunter LA, Krafft S, Stingo F, Choi H, Martel MK, Kry SF, Court LE: **High quality machine-robust image features: identification in nonsmall cell lung cancer computed tomography images.** *Med Phys* 2013, **40**(12):121916.
202. Ganeshan B, Goh V, Mandeville HC, Ng QS, Hoskin PJ, Miles KA: **Non-small cell lung cancer: histopathologic correlates for texture parameters at CT.** *Radiology* 2013, **266**(1):326-336.

203. Tixier F, Hatt M, Le Rest CC, Le Pogam A, Corcos L, Visvikis D: **Reproducibility of tumor uptake heterogeneity characterization through textural feature analysis in 18F-FDG PET.** *Journal of nuclear medicine : official publication, Society of Nuclear Medicine* 2012, **53**(5):693-700.
204. Leijenaar RT, Carvalho S, Velazquez ER, van Elmpt WJ, Parmar C, Hoekstra OS, Hoekstra CJ, Boellaard R, Dekker AL, Gillies RJ *et al*: **Stability of FDG-PET Radiomics features: an integrated analysis of test-retest and inter-observer variability.** *Acta Oncol* 2013, **52**(7):1391-1397.
205. Desseroit MC, Tixier F, Weber WA, Siegel BA, Cheze Le Rest C, Visvikis D, Hatt M: **Reliability of PET/CT Shape and Heterogeneity Features in Functional and Morphologic Components of Non-Small Cell Lung Cancer Tumors: A Repeatability Analysis in a Prospective Multicenter Cohort.** *Journal of nuclear medicine : official publication, Society of Nuclear Medicine* 2017, **58**(3):406-411.
206. Kaluz S, Kaluzova M, Liao SY, Lerman M, Stanbridge EJ: **Transcriptional control of the tumor- and hypoxia-marker carbonic anhydrase 9: A one transcription factor (HIF-1) show?** *Biochimica et biophysica acta* 2009, **1795**(2):162-172.
207. Minhajat R, Mori D, Yamasaki F, Sugita Y, Satoh T, Tokunaga O: **Organ-specific endoglin (CD105) expression in the angiogenesis of human cancers.** *Pathol Int* 2006, **56**(12):717-723.
208. Minhajat R, Mori D, Yamasaki F, Sugita Y, Satoh T, Tokunaga O: **Endoglin (CD105) expression in angiogenesis of colon cancer: analysis using tissue microarrays and comparison with other endothelial markers.** *Virchows Archiv : an international journal of pathology* 2006, **448**(2):127-134.
209. Saad RS, Liu YL, Nathan G, Celebrezze J, Medich D, Silverman JF: **Endoglin (CD105) and vascular endothelial growth factor as prognostic markers in colorectal cancer.** *Modern pathology : an official journal of the United States and Canadian Academy of Pathology, Inc* 2004, **17**(2):197-203.
210. Goethals L, Debucquoy A, Perneel C, Geboes K, Ectors N, De Schutter H, Penninckx F, McBride WH, Begg AC, Haustermans KM: **Hypoxia in human colorectal adenocarcinoma: comparison between extrinsic and potential intrinsic hypoxia markers.** *Int J Radiat Oncol Biol Phys* 2006, **65**(1):246-254.
211. Lee-Kong SA, Ruby JA, Chessin DB, Pucciarelli S, Shia J, Riedel ER, Nitti D, Guillem JG: **Hypoxia-related proteins in patients with rectal cancer undergoing neoadjuvant combined modality therapy.** *Dis Colon Rectum* 2012, **55**(9):990-995.
212. Rajaganeshan R, Prasad R, Guillou PJ, Scott N, Poston G, Jayne DG: **Expression patterns of hypoxic markers at the invasive margin of colorectal cancers and liver metastases.** *European journal of surgical oncology : the journal of the European Society of Surgical Oncology and the British Association of Surgical Oncology* 2009, **35**(12):1286-1294.
213. Verstraete M, Debucquoy A, Devos E, Sagaert X, Penninckx F, Begg A, Haustermans K: **Investigation of possible endogenous hypoxia markers in colorectal cancer.** *Int J Radiat Biol* 2013, **89**(1):9-15.
214. Des Guetz G, Uzzan B, Nicolas P, Cucherat M, Morere JF, Benamouzig R, Breau JL, Perret GY: **Microvessel density and VEGF expression are prognostic factors in colorectal cancer. Meta-analysis of the literature.** *British journal of cancer* 2006, **94**(12):1823-1832.

215. Choi HJ, Hyun MS, Jung GJ, Kim SS, Hong SH: **Tumor angiogenesis as a prognostic predictor in colorectal carcinoma with special reference to mode of metastasis and recurrence.** *Oncology* 1998, 55(6):575-581.
216. Kaio E, Tanaka S, Kitadai Y, Sumii M, Yoshihara M, Haruma K, Chayama K: **Clinical significance of angiogenic factor expression at the deepest invasive site of advanced colorectal carcinoma.** *Oncology* 2003, 64(1):61-73.
217. Torii M, Fukui T, Inoue M, Kanao S, Umetani K, Shirai M, Inagaki T, Tsuchimochi H, Pearson JT, Toi M: **Analysis of the microvascular morphology and hemodynamics of breast cancer in mice using SPring-8 synchrotron radiation microangiography.** *J Synchrotron Radiat* 2017, 24(Pt 5):1039-1047.
218. Fukumura D, Duda DG, Munn LL, Jain RK: **Tumor microvasculature and microenvironment: novel insights through intravital imaging in pre-clinical models.** *Microcirculation* 2010, 17(3):206-225.
219. Bhattacharya R, Fan F, Wang R, Ye X, Xia L, Boulbes D, Ellis LM: **Intracrine VEGF signalling mediates colorectal cancer cell migration and invasion.** *British journal of cancer* 2017, 117(6):848-855.
220. Pastorek J, Pastorekova S: **Hypoxia-induced carbonic anhydrase IX as a target for cancer therapy: from biology to clinical use.** *Semin Cancer Biol* 2015, 31:52-64.
221. Cuenod CA, Balvay D: **Perfusion and vascular permeability: basic concepts and measurement in DCE-CT and DCE-MRI.** *Diagn Interv Imaging* 2013, 94(12):1187-1204.
222. Minchinton AI, Tannock IF: **Drug penetration in solid tumours.** *Nature reviews Cancer* 2006, 6(8):583-592.
223. Gillies RJ, Gatenby RA: **Hypoxia and adaptive landscapes in the evolution of carcinogenesis.** *Cancer Metastasis Rev* 2007, 26(2):311-317.
224. Vadde R, Vemula S, Jinka R, Merchant N, Bramhachari PV, Nagaraju GP: **Role of hypoxia-inducible factors (HIF) in the maintenance of stemness and malignancy of colorectal cancer.** *Crit Rev Oncol Hematol* 2017, 113:22-27.
225. Krohn KA, Link JM, Mason RP: **Molecular imaging of hypoxia.** *Journal of nuclear medicine : official publication, Society of Nuclear Medicine* 2008, 49 Suppl 2:129S-148S.
226. Roels S, Slagmolen P, Nuyts J, Lee JA, Loeckx D, Maes F, Stroobants S, Penninckx F, Haustermans K: **Biological image-guided radiotherapy in rectal cancer: is there a role for FMISO or FLT, next to FDG?** *Acta Oncol* 2008, 47(7):1237-1248.
227. Garcia-Figueiras R, Baleato-Gonzalez S, Padhani AR, Marhuenda A, Luna A, Alcalá L, Carballo-Castro A, Alvarez-Castro A: **Advanced imaging of colorectal cancer: From anatomy to molecular imaging.** *Insights Imaging* 2016, 7(3):285-309.
228. Garnier D, Magnus N, Meehan B, Kislinger T, Rak J: **Qualitative changes in the proteome of extracellular vesicles accompanying cancer cell transition to mesenchymal state.** *Experimental cell research* 2013, 319(17):2747-2757.
229. Gillies RJ, Kinahan PE, Hricak H: **Radiomics: Images Are More than Pictures, They Are Data.** *Radiology* 2016, 278(2):563-577.
230. Grossmann P, Stringfield O, El-Hachem N, Bui MM, Rios Velazquez E, Parmar C, Leijenaar RT, Haibe-Kains B, Lambin P, Gillies RJ *et al*: **Defining the biological basis of radiomic phenotypes in lung cancer.** *eLife* 2017, 6:e23421.
231. Kurien BT, Scofield RH: **Western blotting.** *Methods* 2006, 38(4):283-293.

232. Heinicke E, Kumar U, Munoz DG: **Quantitative dot-blot assay for proteins using enhanced chemiluminescence.** *J Immunol Methods* 1992, **152**(2):227-236.
233. Park JE, Tan HS, Datta A, Lai RC, Zhang H, Meng W, Lim SK, Sze SK: **Hypoxic tumor cell modulates its microenvironment to enhance angiogenic and metastatic potential by secretion of proteins and exosomes.** *Molecular & cellular proteomics : MCP* 2010, **9**(6):1085-1099.
234. Soo CY, Song Y, Zheng Y, Campbell EC, Riches AC, Gunn-Moore F, Powis SJ: **Nanoparticle tracking analysis monitors microvesicle and exosome secretion from immune cells.** *Immunology* 2012, **136**(2):192-197.
235. Tauro BJ, Greening DW, Mathias RA, Ji H, Mathivanan S, Scott AM, Simpson RJ: **Comparison of ultracentrifugation, density gradient separation, and immunoaffinity capture methods for isolating human colon cancer cell line LIM1863-derived exosomes.** *Methods* 2012, **56**(2):293-304.
236. Bosch-Vilaro A, Jacobs B, Pomella V, Abbasi Asbagh L, Kirkland R, Michel J, Singh S, Liu X, Kim P, Weitsman G *et al*: **Feedback activation of HER3 attenuates response to EGFR inhibitors in colon cancer cells.** *Oncotarget* 2017, **8**(3):4277-4288.
237. Feng PH, Yu CT, Chen KY, Luo CS, Wu SM, Liu CY, Kuo LW, Chan YF, Chen TT, Chang CC *et al*: **S100A9(+) MDSC and TAM-mediated EGFR-TKI resistance in lung adenocarcinoma: the role of RELB.** *Oncotarget* 2018, **9**(7):7631-7643.
238. Misra A, Pandey C, Sze SK, Thanabalu T: **Hypoxia activated EGFR signaling induces epithelial to mesenchymal transition (EMT).** *PLoS One* 2012, **7**(11):e49766.
239. Alam MW, Persson CU, Reinbothe S, Kazi JU, Ronnstrand L, Wigerup C, Ditzel HJ, Lykkesfeldt AE, Pahlman S, Jogi A: **HIF2alpha contributes to antiestrogen resistance via positive bilateral crosstalk with EGFR in breast cancer cells.** *Oncotarget* 2016, **7**(10):11238-11250.
240. Franovic A, Gunaratnam L, Smith K, Robert I, Patten D, Lee S: **Translational up-regulation of the EGFR by tumor hypoxia provides a nonmutational explanation for its overexpression in human cancer.** *Proceedings of the National Academy of Sciences of the United States of America* 2007, **104**(32):13092-13097.
241. Kozlova N, Wottawa M, Katschinski DM, Kristiansen G, Kietzmann T: **Hypoxia-inducible factor prolyl hydroxylase 2 (PHD2) is a direct regulator of epidermal growth factor receptor (EGFR) signaling in breast cancer.** *Oncotarget* 2017, **8**(6):9885-9898.
242. Wang Y, Roche O, Xu C, Moriyama EH, Heir P, Chung J, Roos FC, Chen Y, Finak G, Milosevic M *et al*: **Hypoxia promotes ligand-independent EGF receptor signaling via hypoxia-inducible factor-mediated upregulation of caveolin-1.** *Proceedings of the National Academy of Sciences of the United States of America* 2012, **109**(13):4892-4897.
243. Hudson CC, Liu M, Chiang GG, Otterness DM, Loomis DC, Kaper F, Giaccia AJ, Abraham RT: **Regulation of hypoxia-inducible factor 1alpha expression and function by the mammalian target of rapamycin.** *Molecular and cellular biology* 2002, **22**(20):7004-7014.
244. Zhong H, Chiles K, Feldser D, Laughner E, Hanrahan C, Georgescu MM, Simons JW, Semenza GL: **Modulation of hypoxia-inducible factor 1alpha expression by the epidermal growth factor/phosphatidylinositol 3-**

- kinase/PTEN/AKT/FRAP pathway in human prostate cancer cells: implications for tumor angiogenesis and therapeutics.** *Cancer research* 2000, **60**(6):1541-1545.
245. Laughner E, Taghavi P, Chiles K, Mahon PC, Semenza GL: **HER2 (neu) signaling increases the rate of hypoxia-inducible factor 1alpha (HIF-1alpha) synthesis: novel mechanism for HIF-1-mediated vascular endothelial growth factor expression.** *Molecular and cellular biology* 2001, **21**(12):3995-4004.
246. Wang WM, Zhao ZL, Ma SR, Yu GT, Liu B, Zhang L, Zhang WF, Kulkarni AB, Sun ZJ, Zhao YF: **Epidermal growth factor receptor inhibition reduces angiogenesis via hypoxia-inducible factor-1alpha and Notch1 in head neck squamous cell carcinoma.** *PLoS One* 2015, **10**(2):e0119723.
247. Kim D, Dai J, Park YH, Fai LY, Wang L, Pratheeshkumar P, Son YO, Kondo K, Xu M, Luo J *et al*: **Activation of Epidermal Growth Factor Receptor/p38/Hypoxia-inducible Factor-1alpha Is Pivotal for Angiogenesis and Tumorigenesis of Malignantly Transformed Cells Induced by Hexavalent Chromium.** *The Journal of biological chemistry* 2016, **291**(31):16271-16281.
248. Rijken PF, Bernsen HJ, Peters JP, Hodgkiss RJ, Raleigh JA, van der Kogel AJ: **Spatial relationship between hypoxia and the (perfused) vascular network in a human glioma xenograft: a quantitative multi-parameter analysis.** *Int J Radiat Oncol Biol Phys* 2000, **48**(2):571-582.
249. Fenton BM, Paoni SF, Beauchamp BK, Ding I: **Zonal image analysis of tumour vascular perfusion, hypoxia, and necrosis.** *British journal of cancer* 2002, **86**(11):1831-1836.
250. Kaalep A, Sera T, Rijnsdorp S, Yaqub M, Talsma A, Lodge MA, Boellaard R: **Feasibility of state of the art PET/CT systems performance harmonisation.** *European journal of nuclear medicine and molecular imaging* 2018, **45**(8):1344-1361.
251. Ow CPC, Ngo JP, Ullah MM, Hilliard LM, Evans RG: **Renal hypoxia in kidney disease: Cause or consequence?** *Acta Physiol (Oxf)* 2018, **222**(4):e12999.
252. Dunham-Snary KJ, Wu D, Sykes EA, Thakrar A, Parlow LR, Mewburn JD, Parlow JL, Archer SL: **Hypoxic Pulmonary Vasoconstriction: From Molecular Mechanisms to Medicine.** *Chest* 2017, **151**(1):181-192.
253. Van Welden S, Selfridge AC, Hindryckx P: **Intestinal hypoxia and hypoxia-induced signalling as therapeutic targets for IBD.** *Nature reviews Gastroenterology & hepatology* 2017, **14**(10):596-611.
254. Tkach M, Kowal J, Thery C: **Why the need and how to approach the functional diversity of extracellular vesicles.** *Philos Trans R Soc Lond B Biol Sci* 2018, **373**(1737).
255. Hosny A, Parmar C, Quackenbush J, Schwartz LH, Aerts H: **Artificial intelligence in radiology.** *Nature reviews Cancer* 2018, **18**(8):500-510.
256. Grothey A, Sobrero AF, Shields AF, Yoshino T, Paul J, Taieb J, Souglakos J, Shi Q, Kerr R, Labianca R *et al*: **Duration of Adjuvant Chemotherapy for Stage III Colon Cancer.** *The New England journal of medicine* 2018, **378**(13):1177-1188.
257. Zheng X, Wang X, Mao H, Wu W, Liu B, Jiang X: **Hypoxia-specific ultrasensitive detection of tumours and cancer cells in vivo.** *Nature communications* 2015, **6**:5834.

8 Appendix



Cancer Institute
 Lab 407
 Avigayil Chalk
 72 Huntley Street
 London WC1E 6DD
 UNITED KINGDOM

24.11.2016

Certificate

Order

By order of Avigayil Chalk (Cancer Institute) we were requested to perform a cell line authentication test. Following samples were examined:

<u>Our sample number</u>	<u>Client sample name</u>
CL161121_017	CACO2
CL161121_018	DIFI
CL161121_019	HCT116
CL161121_020	HCT15
CL161121_021	HT29
CL161121_022	LIM1215
CL161121_023	LOVO
CL161121_024	LS174T
CL161121_025	SW48
CL161121_026	DLD1 WT
CL161121_027	DLD1 Kras mutant

Method:

DNA was isolated separately from the samples. Genetic characteristics were determined by PCR-single-locus-technology. 21 independent PCR-systems Amelogenin, D3S1358, D1S1656, D6S1043, D13S317, Penta E, D16S539, D18S51, D2S1338, CSF1PO, Penta D, TH01, vWA, D21S11, D7S820, D5S818, TPOX, D8S1179, D12S391, D19S433 and FGA were investigated (Promega, PowerPlex 21 PCR Kit). In parallel, positive and negative controls were carried out yielding correct results.

Eurofins Medigenomix Forensik GmbH Anzingerstr. 7a D-85560 Ebersberg	Tel. + 49 (0) 8092 8289 260 Fax. + 49 (0) 8092 8289 190 www.eurofins.de/forensik-de forensik@eurofins.com	Geschäftsführer Dr. Peter Persigehl Dr. Brigitte Obermaier Dr. Bruno Poddevin	HRB 20 12 60 Amtsgericht München	Ust.Id.Nr. DE 285161076 Steuernummer 114/116/00159
---	--	--	-------------------------------------	---



Genomics



Forensik



ISO 17025:2005 accredited

Results:

DNA-System	DNA-criteria CACO2 CL161121_017	DNA-criteria DIFI CL161121_018	DNA-criteria HCT116 CL161121_019	DNA-criteria HCT15 CL161121_020	DNA-criteria HT29 CL161121_021
AM	X, X	X, X	X, X	X, Y	X, X
D3S1358	14, 16, 17	17, 17	12, 17	17, 17	15, 17
D1S1656	15, 16, 17, 18.3	15, 15	13, 13	17.3, 19.3	15, 16
D6S1043	11, 12, 13	11, 12	13, 14	11, 13	12, 14
D13S317	11, 14	8, 11	10, 12	8, 11	11, 11
Penta E	7, 11	12, 18	12, 14	7, 14	14, 16
D16S539	11, 12, 13	12, 12	11, 12, 13	12, 13	11, 12
D18S51	12, 14, 17	13, ?	16, 17	11, 17	13, 13.1
D2S1338	17, 24, 25	18, 22, 24	16, 16	17, 25	19, 23
CSF1PO	10, 11, 12	10, 11	7, 10	12, 12	11, 12
Penta D	9, 9	12, 12	9, 13	9, 14	11, 13
TH01	6, 8, 9.3	7, 9.3	8, 9	7, 9.3	6, 9
vWA	14, 16, 18	17, 18	17, 22	18, 19	17, 19
D21S11	29, 30	32, 32	29, 30	29, 32.2	29, 30
D7S820	8, 11, 12	10, 12	11, 12	10, 12	10, 10
D5S818	11, 12, 13	11, 12	10, 11	13, 13	11, 12
TPOX	8, 9, 11	8, 9	8, 9	8, 11	8, 9
D8S1179	12, 13, 14	12, 12	10, 14, 15	15, 15	10, 16
D12S391	17, 18, 23	15, 18	17, 22	19, 22	19, 21
D19S433	13, 15	14, 14	12, 12	14, 16	14, 14
FGA	19, 23	27, 27	18, 23	22, 22	20, 22

DNA-System	DNA-criteria LIM1215 CL161121_022	DNA-criteria LOVO CL161121_023	DNA-criteria LS174T CL161121_024	DNA-criteria SW48 CL161121_025	DNA-criteria DLD1 WT CL161121_026
AM	X, X	X, Y	X, X	X, X	X, Y
D3S1358	15, 16	14, 16, 17, 18	15, 17	14, 15, 16	17, 17
D1S1656	15, 15.3, 16, 17, 18, 19	13, 14, 15, 16.3	13, 18.3, 19.3	11, 13, 14	17.3, 19.3
D6S1043	11, 12, 13	11, 12, 17, 18	12, 13, 14	11, 12, 18, 19	11, 13
D13S317	8, 11, 12	8, 11, 12	10, 11	11, 12, 13	8, 11
Penta E	7, 7	9, 10, 15, 16	15, 16	12, 13	7, 14
D16S539	9, 12	9, 12	11, 13	11, 13	12, 13
D18S51	12, 13, 17, 18, 19	13, 17, 18, 19	11, 13	13, 13	11, 17
D2S1338	16, 21	17, 18	18, 22	19, 25, 26	17, 25
CSF1PO	10, 11	10, 11, 13, 14	10, 13, 14	9, 10	12, 12
Penta D	11, 12, 13	10, 14	10, 10	10, 10	9, 14
TH01	9.3, 10	9.3, 9.3	6, 7	6, 9.3	7, 9.3
vWA	15, 16	17, 18, 19	15, 17	18, 19, 20, 21	18, 19
D21S11	29, 30, 31	29, 30, 31.2	29, 31, 32	28, 31, 32	29, 32.2
D7S820	9, 10.3	9.3, 10, 10.3, 11	10.3, 11	9, 10, 11	10, 12
D5S818	9, 13	11, 12, 13	11, 15, 16	10, 13, 14, 15	13, 13
TPOX	8, 8	8, 9	8, 9	8, 8	8, 11
D8S1179	13, 14	10, 10	12, 13, 16	13, 15	15, 15
D12S391	19, 20, 21, 22	20, 22, 23, 24	16, 18, 20, 21	20, 21	19, 22
D19S433	10, 11, 15.2, 16.2	14, 15	14, 15	14, 14	14, 16
FGA	21, 22, 24, 25	18, 20	21, 22	20, 20	22, 22

Eurofins Medigenomix
Forensik GmbH
Anzingerstr. 7a
D-85560 Ebersberg

Tel. + 49 (0) 8092 8289 260
Fax. + 49 (0) 8092 8289 190
www.eurofins.de/forensik-de
forensik@eurofins.com

Geschäftsführer
Dr. Peter Persigehl
Dr. Brigitte Obermaier
Dr. Bruno Poddevin

HRB 20 12 60
Amtsgericht München

Ust.-Id.Nr. DE 285161076
Steuernummer 114/116/00159



ISO 17025:2005 accredited

DNA-System	DNA-criteria DLD1 Kras mutant CL161121_027
AM	X, Y
D3S1358	17, 17
D1S1656	17.3, 19.3
D6S1043	11, 13
D13S317	8, 11
Penta E	7, 14
D16S539	12, 13
D18S51	11, 17
D2S1338	17, 25
CSF1PO	11, 12
Penta D	9, 14
TH01	7, 9.3
vWA	18, 19
D21S11	29, 32.2
D7S820	10, 12
D5S818	13, 13
TPOX	8, 11
D8S1179	15, 15
D12S391	19, 22
D19S433	14, 16
FGA	22, 22

Summary:

The following cell lines could be detected in the online database of the DSMZ (<http://www.dsmz.de/de/service/services-human-and-animal-cell-lines/online-str-analysis.html>):

Our sample number	Client sample name	DSMZ name
CL161121_017	CACO2	Cell line not found in DSMZ
CL161121_018	DIFI	Cell line not found in DSMZ
CL161121_019	HCT116	HCT 116
CL161121_020	HCT15	HCT-15
CL161121_021	HT29	HT-29
CL161121_022	LIM1215	Cell line not found in DSMZ
CL161121_023	LOVO	LoVo
CL161121_024	LS174T	LS-174T
CL161121_025	SW48	SW48
CL161121_026	DLD1 WT	HCT-15
CL161121_027	DLD1 Kras mutant	DLD-1

Dr. Burkhard Rolf
Director Forensic Services

Astrid Phillip, M. Sc.
Project Manager DNA-Forensics

Eurofins Medigenomix Forensik GmbH carries out all analyses with greatest care and on the basis of state of the art scientific knowledge. All results solely refer to the analysed samples. Our expert's reports must not be duplicated in extracts without consent of Eurofins Medigenomix Forensik GmbH. Cell_line-certificate_eng_V03_141211
Vorlage_Verwandschaftsanalyse_EUROFINS_v02_121127

Eurofins Medigenomix
Forensik GmbH
Anzingerstr. 7a
D-85560 Ebersberg

Tel. + 49 (0) 8092 8289 260
Fax. + 49 (0) 8092 8289 190
www.eurofins.de/forensik-de
forensik@eurofins.com

Geschäftsführer
Dr. Peter Persigehl
Dr. Brigitte Obermaier
Dr. Bruno Poddevin

HRB 20 12 60
Amtsgericht München

Ust.-Id.Nr. DE 285161076
Steuernummer 114/116/00159

Table 26: Mean survival from the Kaplan-Meier estimator & results of Log-Rank test. The texture parameters were listed as “texture parameter_filter level_image modality”. For example, skewness_6_VE meant the skewness calculated from the venous phase of contrast-enhanced CT after filtration with the 6-mm spatial scale filter.

Parameter	The Whole Cohort			Random Group-1			Random Group-2		
	Mean survival of patients with parameter > median (mean \pm SE)	Mean survival of patients with parameter \leq median (mean \pm SE)	p-value (Log Rank test)	Mean survival of patients with parameter > median (mean \pm SE)	Mean survival of patients with parameter \leq median (mean \pm SE)	p-value (Log Rank test)	Mean survival of patients with parameter > median (mean \pm SE)	Mean survival of patients with parameter \leq median (mean \pm SE)	p-value (Log Rank test)
Age	73.46 \pm 4.25	89.05 \pm 3.83	0.025	81.40 \pm 6.78	73.39 \pm 6.12	0.905	64.39 \pm 4.62	93.31 \pm 4.37	0.004
Stage (3,4 vs 1,2)	65.94 \pm 4.00	98.94 \pm 4.27	< 0.001	62.79 \pm 5.77	100.33 \pm 6.26	< 0.001	65.45 \pm 4.89	98.41 \pm 5.76	< 0.001
Site (Right vs Left)	87.70 \pm 5.27	77.37 \pm 3.70	0.391	81.71 \pm 7.52	77.94 \pm 5.97	0.414	86.02 \pm 6.58	71.84 \pm 3.98	0.654
Average	75.54 \pm 4.62	79.75 \pm 5.58	0.320	75.30 \pm 6.44	78.77 \pm 8.16	0.788	71.87 \pm 5.62	70.19 \pm 4.92	0.203
Base	69.75 \pm 3.82	81.76 \pm 5.74	0.197	69.83 \pm 6.65	87.00 \pm 7.76	0.302	74.10 \pm 5.39	63.37 \pm 3.87	0.361
Time to Peak	74.74 \pm 4.62	79.33 \pm 5.56	0.105	71.37 \pm 8.22	81.88 \pm 6.06	0.076	65.36 \pm 4.46	76.02 \pm 7.68	0.310
Mean Slope Increase	75.11 \pm 6.23	77.80 \pm 4.42	0.917	71.03 \pm 8.11	80.31 \pm 7.57	0.957	71.92 \pm 9.17	70.98 \pm 4.63	0.991
Blood Volume	79.38 \pm 4.78	67.20 \pm 3.84	0.271	83.70 \pm 7.57	67.52 \pm 6.86	0.413	75.39 \pm 6.11	68.17 \pm 4.66	0.534
Blood Flow	79.14 \pm 5.33	68.63 \pm 3.77	0.551	81.82 \pm 8.35	71.42 \pm 6.41	0.756	77.54 \pm 6.98	65.65 \pm 4.36	0.573
Mean Transit Time	78.76 \pm 4.38	67.36 \pm 4.39	0.645	84.17 \pm 7.35	66.87 \pm 6.99	0.511	75.98 \pm 5.37	50.36 \pm 2.75	0.896
PS	72.58 \pm 5.15	81.45 \pm 4.91	0.265	68.62 \pm 8.24	84.29 \pm 5.49	0.043	68.96 \pm 5.61	76.67 \pm 6.21	0.735
SUVmax	78.59 \pm 4.37	79.38 \pm 4.42	0.464	83.63 \pm 7.29	70.97 \pm 5.72	0.662	76.86 \pm 5.28	78.31 \pm 6.20	0.190
SUVmean	78.48 \pm 4.36	79.43 \pm 4.44	0.520	76.69 \pm 8.04	76.07 \pm 5.48	0.728	77.49 \pm 5.17	76.48 \pm 6.71	0.299
MTV	75.51 \pm 4.56	82.49 \pm 4.06	0.018	73.20 \pm 5.97	79.31 \pm 7.55	0.786	71.13 \pm 6.55	84.78 \pm 4.82	0.006
Glycolysis	75.93 \pm 4.46	82.08 \pm 4.18	0.021	82.76 \pm 6.90	71.35 \pm 6.19	0.861	73.06 \pm 6.03	83.70 \pm 4.99	0.014
TLG	71.85 \pm 4.76	85.48 \pm 3.93	0.001	78.45 \pm 7.18	74.64 \pm 6.09	0.425	67.39 \pm 6.11	88.17 \pm 4.82	0.001
BF/SUVmax	74.59 \pm 4.17	72.60 \pm 4.84	0.094	73.84 \pm 6.56	80.31 \pm 8.32	0.957	71.40 \pm 5.26	69.11 \pm 5.81	0.057

BF/SUVmean	72.99 ± 4.23	74.52 ± 4.80	0.394	72.76 ± 6.70	81.28 ± 8.23	0.860	69.43 ± 5.27	71.31 ± 5.83	0.241
CT size	75.24 ± 4.62	82.84 ± 4.19	0.026	79.64 ± 6.99	74.76 ± 6.22	0.481	69.89 ± 6.26	86.08 ± 4.89	0.006
Mean_0_PET	68.16 ± 4.85	88.82 ± 3.96	0.011	63.86 ± 6.99	90.28 ± 6.65	0.038	69.84 ± 5.85	87.14 ± 4.77	0.182
Mean_2_PET	78.33 ± 4.75	79.13 ± 4.35	0.572	69.36 ± 6.86	83.87 ± 6.84	0.572	79.96 ± 5.89	76.74 ± 5.53	0.296
Mean_3_PET	77.00 ± 4.95	80.15 ± 4.29	0.798	67.91 ± 6.85	85.75 ± 6.75	0.318	78.70 ± 6.40	77.20 ± 5.43	0.325
Mean_4_PET	77.91 ± 4.71	79.84 ± 4.34	0.745	68.23 ± 7.28	84.16 ± 6.78	0.517	80.00 ± 5.54	77.02 ± 5.69	0.412
Mean_5_PET	78.90 ± 4.71	78.91 ± 4.36	0.534	68.84 ± 7.27	83.69 ± 6.84	0.599	81.03 ± 5.56	75.96 ± 5.66	0.283
Mean_6_PET	78.97 ± 4.71	78.80 ± 4.36	0.523	68.84 ± 7.27	83.69 ± 6.84	0.599	81.06 ± 5.57	75.93 ± 5.66	0.295
SD_0_PET	81.67 ± 4.18	72.23 ± 4.15	0.963	83.29 ± 6.52	72.90 ± 6.28	0.876	80.23 ± 5.30	714.36 ± 5.2	0.926
SD_2_PET	81.44 ± 4.17	76.43 ± 4.70	0.392	76.79 ± 5.96	75.55 ± 7.86	0.469	81.40 ± 5.29	75.89 ± 5.84	0.385
SD_3_PET	80.75 ± 4.19	76.66 ± 4.81	0.571	74.59 ± 6.19	77.51 ± 7.86	0.826	79.47 ± 5.30	76.39 ± 6.12	0.744
SD_4_PET	80.31 ± 4.19	77.79 ± 4.72	0.700	74.64 ± 6.31	76.85 ± 7.91	0.745	79.57 ± 5.31	77.69 ± 5.87	0.803
SD_5_PET	81.24 ± 4.24	76.75 ± 4.62	0.433	73.84 ± 6.57	79.02 ± 7.33	0.881	81.26 ± 5.30	75.95 ± 5.83	0.430
SD_6_PET	79.33 ± 4.25	78.66 ± 4.65	0.887	71.46 ± 6.93	81.19 ± 7.16	0.735	80.20 ± 5.10	75.77 ± 6.47	0.584
Mpp_0_PET	68.16 ± 4.85	88.82 ± 3.96	0.011	63.86 ± 6.99	90.28 ± 6.65	0.038	69.84 ± 5.85	87.14 ± 4.77	0.182
Mpp_2_PET	77.40 ± 3.69	75.63 ± 4.80	0.288	77.95 ± 5.98	74.41 ± 7.77	0.319	76.91 ± 4.65	75.21 ± 6.04	0.379
Mpp_3_PET	76.34 ± 3.71	76.57 ± 4.82	0.500	74.97 ± 6.07	76.49 ± 7.96	0.731	76.38 ± 4.63	75.74 ± 6.09	0.471
Mpp_4_PET	81.26 ± 4.23	76.73 ± 4.64	0.337	77.34 ± 6.27	75.24 ± 7.41	0.285	79.81 ± 5.27	76.64 ± 6.14	0.650
Mpp_5_PET	81.13 ± 4.20	76.89 ± 4.68	0.229	74.94 ± 7.39	76.04 ± 7.31	0.275	81.15 ± 5.06	74.81 ± 6.48	0.306
Mpp_6_PET	78.26 ± 4.34	79.92 ± 4.58	0.970	68.70 ± 7.94	82.17 ± 7.16	0.803	80.45 ± 5.27	75.94 ± 6.13	0.404
Entropy_0_PET	76.39 ± 4.49	81.93 ± 4.31	0.085	79.33 ± 6.79	74.50 ± 6.60	0.413	74.35 ± 5.85	82.95 ± 5.14	0.122
Entropy_2_PET	76.77 ± 4.52	81.39 ± 4.30	0.102	79.33 ± 6.79	74.50 ± 6.60	0.413	74.35 ± 5.85	82.95 ± 5.14	0.122
Entropy_3_PET	76.39 ± 4.49	81.93 ± 4.31	0.085	79.33 ± 6.79	74.50 ± 6.60	0.413	74.35 ± 5.85	82.95 ± 5.14	0.122

Entropy_4_PET	76.39 ± 4.49	81.93 ± 4.31	0.085	79.33 ± 6.79	74.50 ± 6.60	0.413	74.35 ± 5.85	82.95 ± 5.14	0.122
Entropy_5_PET	76.39 ± 4.49	81.93 ± 4.31	0.085	79.33 ± 6.79	74.50 ± 6.60	0.413	74.35 ± 5.85	82.95 ± 5.14	0.122
Entropy_6_PET	76.39 ± 4.49	81.93 ± 4.31	0.085	79.33 ± 6.79	74.50 ± 6.60	0.413	74.35 ± 5.85	82.95 ± 5.14	0.122
Skewness_0_PET	86.90 ± 4.10	67.37 ± 4.23	0.039	86.87 ± 6.83	67.31 ± 6.66	0.241	86.18 ± 5.16	67.65 ± 5.17	0.109
Skewness_2_PET	86.33 ± 4.23	67.20 ± 3.76	0.026	83.31 ± 6.88	70.40 ± 6.43	0.766	85.06 ± 5.37	65.36 ± 4.42	0.071
Skewness_3_PET	83.22 ± 4.30	71.61 ± 3.96	0.228	85.52 ± 6.70	68.70 ± 6.51	0.389	82.93 ± 5.41	67.30 ± 4.37	0.269
Skewness_4_PET	79.79 ± 4.49	74.55 ± 3.76	0.918	81.33 ± 6.95	72.01 ± 6.35	0.966	79.21 ± 5.98	73.94 ± 4.53	0.752
Skewness_5_PET	82.61 ± 4.38	72.16 ± 3.88	0.302	82.66 ± 6.95	70.33 ± 6.53	0.697	79.73 ± 5.63	73.83 ± 4.76	0.879
Skewness_6_PET	84.13 ± 4.37	70.52 ± 3.94	0.115	84.81 ± 7.00	68.54 ± 6.42	0.337	85.71 ± 5.31	68.74 ± 4.94	0.187
Kurtosis_0_PET	85.45 ± 4.14	72.83 ± 5.21	0.062	73.24 ± 6.25	80.63 ± 7.30	0.852	90.39 ± 4.56	62.56 ± 5.32	0.015
Kurtosis_2_PET	81.74 ± 4.20	70.66 ± 3.85	0.705	75.94 ± 7.10	78.29 ± 6.25	0.274	82.65 ± 5.39	67.94 ± 4.32	0.489
Kurtosis_3_PET	80.37 ± 4.37	72.22 ± 3.63	0.773	77.57 ± 7.01	75.49 ± 6.32	0.479	81.61 ± 5.53	68.46 ± 4.27	0.433
Kurtosis_4_PET	80.28 ± 4.38	72.06 ± 3.67	0.777	75.67 ± 7.27	76.66 ± 6.04	0.315	81.89 ± 5.53	68.00 ± 4.29	0.359
Kurtosis_5_PET	78.59 ± 4.48	73.47 ± 3.55	0.761	74.97 ± 7.66	76.15 ± 5.85	0.377	81.42 ± 5.40	68.32 ± 4.32	0.546
Kurtosis_6_PET	79.94 ± 4.40	72.05 ± 3.73	0.875	77.73 ± 7.30	74.69 ± 6.21	0.558	81.43 ± 5.34	68.11 ± 4.46	0.629
Mean_0_CT	83.91 ± 4.42	74.78 ± 4.38	0.229	92.43 ± 6.45	64.99 ± 6.24	0.069	80.90 ± 5.36	76.13 ± 5.82	0.856
Mean_2_CT	82.08 ± 4.40	78.25 ± 4.49	0.805	73.69 ± 6.12	78.40 ± 7.79	0.897	82.80 ± 4.95	75.26 ± 5.70	0.862
Mean_3_CT	71.14 ± 3.68	81.30 ± 4.38	0.736	71.29 ± 6.29	80.86 ± 7.29	0.815	70.30 ± 4.14	79.16 ± 5.74	0.856
Mean_4_CT	70.86 ± 3.66	81.76 ± 4.39	0.596	69.51 ± 6.70	82.47 ± 7.01	0.610	69.32 ± 4.14	79.99 ± 5.92	0.808
Mean_5_CT	79.01 ± 4.52	80.90 ± 4.51	0.643	82.71 ± 7.60	71.19 ± 6.14	0.712	68.94 ± 4.21	80.28 ± 5.89	0.692
Mean_6_CT	80.73 ± 4.33	78.95 ± 4.76	0.920	82.99 ± 7.55	70.93 ± 6.19	0.671	74.54 ± 4.65	77.87 ± 6.13	0.820
SD_0_CT	77.88 ± 3.81	76.29 ± 4.43	0.075	80.21 ± 5.86	73.60 ± 7.57	0.145	73.14 ± 5.00	79.95 ± 5.44	0.780
SD_2_CT	78.15 ± 3.83	75.22 ± 4.57	0.107	82.39 ± 5.37	69.26 ± 7.74	0.095	74.50 ± 5.00	78.42 ± 5.52	0.450

SD_3_CT	80.21 ± 3.53	72.61 ± 4.79	0.040	78.08 ± 5.57	75.35 ± 7.66	0.509	80.65 ± 4.41	70.51 ± 6.23	0.039
SD_4_CT	85.18 ± 4.21	75.10 ± 4.60	0.184	87.07 ± 6.38	69.40 ± 6.33	0.478	78.04 ± 4.67	74.74 ± 5.75	0.256
SD_5_CT	77.77 ± 4.58	80.54 ± 4.21	0.389	75.52 ± 7.44	78.37 ± 5.83	0.280	79.10 ± 5.78	78.44 ± 5.30	0.765
SD_6_CT	78.36 ± 4.64	79.94 ± 4.21	0.504	76.11 ± 7.44	77.78 ± 5.93	0.321	78.79 ± 5.94	78.90 ± 5.24	0.689
Mpp_0_CT	83.48 ± 4.34	76.68 ± 4.61	0.275	91.30 ± 6.32	64.95 ± 6.53	0.150	74.51 ± 4.85	78.10 ± 5.73	0.753
Mpp_2_CT	77.42 ± 3.84	76.63 ± 4.44	0.113	79.54 ± 5.83	72.44 ± 7.73	0.144	75.10 ± 4.96	78.07 ± 5.55	0.361
Mpp_3_CT	80.85 ± 3.32	72.90 ± 4.69	0.044	79.92 ± 5.44	74.07 ± 5.46	0.277	81.16 ± 4.12	70.28 ± 6.09	0.042
Mpp_4_CT	85.92 ± 3.89	74.14 ± 4.76	0.194	86.41 ± 6.52	69.66 ± 6.30	0.516	79.63 ± 4.28	71.70 ± 6.09	0.136
Mpp_5_CT	83.30 ± 4.30	76.97 ± 4.56	0.403	80.21 ± 7.94	72.90 ± 6.09	0.950	72.95 ± 4.03	74.42 ± 5.90	0.338
Mpp_6_CT	82.61 ± 4.29	77.32 ± 4.63	0.612	80.91 ± 7.57	72.93 ± 6.13	0.997	71.13 ± 4.08	76.23 ± 5.94	0.733
Entropy_0_CT	74.17 ± 3.98	80.39 ± 4.25	0.844	79.67 ± 6.00	74.62 ± 7.31	0.185	72.31 ± 5.22	80.91 ± 5.26	0.939
Entropy_2_CT	80.66 ± 4.59	79.44 ± 4.43	0.974	89.92 ± 6.39	66.25 ± 6.49	0.290	69.45 ± 5.18	83.77 ± 5.27	0.321
Entropy_3_CT	83.13 ± 4.28	77.24 ± 4.55	0.499	84.09 ± 6.92	71.46 ± 6.15	0.863	74.85 ± 5.08	78.47 ± 5.41	0.895
Entropy_4_CT	82.71 ± 4.27	76.02 ± 4.45	0.748	81.93 ± 6.80	72.49 ± 6.51	0.886	84.14 ± 5.59	74.32 ± 5.32	0.394
Entropy_5_CT	80.01 ± 4.43	78.24 ± 4.35	0.528	80.82 ± 7.16	73.97 ± 6.01	0.580	78.69 ± 5.71	78.74 ± 5.31	0.516
Entropy_6_CT	78.71 ± 4.44	79.48 ± 4.38	0.478	74.33 ± 7.53	78.14 ± 6.07	0.229	79.6 ± 5.56	78.06 ± 5.42	0.648
Skewness_0_CT	73.61 ± 3.83	81.29 ± 4.40	0.893	76.60 ± 6.09	75.62 ± 7.98	0.523	69.68 ± 5.06	83.97 ± 5.40	0.312
Skewness_2_CT	72.87 ± 3.98	81.64 ± 4.30	0.921	73.08 ± 6.01	82.56 ± 7.03	0.806	70.44 ± 5.34	82.27 ± 5.34	0.711
Skewness_3_CT	74.43 ± 3.86	80.06 ± 4.44	0.782	75.46 ± 6.20	79.71 ± 6.74	0.324	76.16 ± 4.45	77.10 ± 5.73	0.750
Skewness_4_CT	76.05 ± 3.72	77.53 ± 4.68	0.771	77.07 ± 6.02	76.68 ± 7.46	0.332	77.21 ± 4.38	76.55 ± 5.67	0.935
Skewness_5_CT	75.87 ± 3.80	78.34 ± 4.52	0.523	75.85 ± 5.98	77.97 ± 7.18	0.431	77.17 ± 4.61	75.39 ± 5.94	0.443
Skewness_6_CT	76.66 ± 3.74	77.20 ± 4.62	0.379	73.98 ± 6.10	81.35 ± 7.10	0.908	78.26 ± 4.65	74.68 ± 5.73	0.267
Kurtosis_0_CT	74.32 ± 4.49	79.37 ± 3.77	0.021	75.90 ± 7.32	77.97 ± 5.84	0.175	73.97 ± 5.43	79.18 ± 5.00	0.059

Kurtosis_2_CT	71.08 ± 4.50	88.42 ± 4.49	0.001	61.68 ± 6.43	93.78 ± 6.81	0.005	72.06 ± 5.53	76.88 ± 4.16	0.015
Kurtosis_3_CT	70.53 ± 4.56	82.96 ± 3.53	0.001	72.59 ± 7.84	79.71 ± 5.73	0.107	68.84 ± 5.70	83.81 ± 4.39	0.003
Kurtosis_4_CT	71.82 ± 4.65	81.56 ± 3.50	0.004	73.66 ± 7.13	80.36 ± 5.78	0.028	69.14 ± 5.94	83.15 ± 3.91	0.014
Kurtosis_5_CT	73.29 ± 4.55	80.66 ± 3.57	0.022	70.95 ± 7.28	82.24 ± 5.89	0.019	73.46 ± 5.84	79.70 ± 4.18	0.191
Kurtosis_6_CT	74.71 ± 4.55	79.22 ± 3.71	0.038	79.24 ± 7.10	74.53 ± 6.43	0.664	70.96 ± 6.00	81.11 ± 4.38	0.019
Mean_0_VE	75.92 ± 4.74	79.92 ± 5.33	0.847	79.39 ± 8.03	65.22 ± 5.31	0.895	74.63 ± 5.99	66.22 ± 4.94	0.874
Mean_2_VE	72.50 ± 4.11	74.46 ± 4.96	0.244	75.93 ± 6.72	78.91 ± 7.80	0.465	69.05 ± 4.84	72.62 ± 6.30	0.480
Mean_3_VE	73.85 ± 4.15	74.14 ± 4.94	0.327	74.23 ± 6.93	79.72 ± 8.02	0.995	69.25 ± 4.91	72.32 ± 6.23	0.412
Mean_4_VE	74.62 ± 4.15	73.55 ± 4.90	0.263	72.32 ± 6.98	81.93 ± 7.97	0.626	71.62 ± 4.89	69.95 ± 6.13	0.163
Mean_5_VE	73.61 ± 4.09	74.31 ± 5.03	0.519	71.65 ± 7.08	82.81 ± 7.86	0.522	71.49 ± 4.70	69.36 ± 6.41	0.210
Mean_6_VE	73.13 ± 3.98	74.07 ± 5.22	0.615	70.37 ± 6.99	84.00 ± 7.99	0.371	70.65 ± 4.54	68.64 ± 6.82	0.327
SD_0_VE	78.36 ± 5.48	75.27 ± 4.80	0.363	59.56 ± 5.99	83.82 ± 6.97	0.802	78.41 ± 6.54	62.02 ± 4.52	0.422
SD_2_VE	79.50 ± 5.81	74.89 ± 4.64	0.412	68.13 ± 7.80	83.95 ± 7.33	0.513	82.47 ± 7.00	61.23 ± 4.26	0.114
SD_3_VE	79.89 ± 5.72	74.62 ± 4.70	0.346	54.56 ± 4.78	87.80 ± 6.79	0.272	79.04 ± 6.79	66.21 ± 5.28	0.143
SD_4_VE	82.31 ± 5.13	72.51 ± 4.93	0.122	61.03 ± 4.28	78.08 ± 7.64	0.424	86.64 ± 5.26	60.08 ± 5.40	0.047
SD_5_VE	83.36 ± 4.85	70.93 ± 5.13	0.078	66.17 ± 6.92	83.96 ± 7.60	0.741	86.74 ± 5.21	59.04 ± 5.43	0.029
SD_6_VE	85.27 ± 4.69	68.92 ± 5.17	0.024	70.64 ± 6.90	78.55 ± 7.91	0.445	86.20 ± 5.17	59.41 ± 5.47	0.047
Mpp_0_VE	79.23 ± 4.73	65.38 ± 3.85	0.629	80.10 ± 7.86	65.09 ± 5.32	0.832	77.51 ± 5.92	63.70 ± 4.76	0.857
Mpp_2_VE	77.22 ± 5.78	76.312 ± 4.70	0.757	65.71 ± 7.80	86.15 ± 7.22	0.233	80.00 ± 7.03	60.47 ± 4.02	0.196
Mpp_3_VE	79.09 ± 5.91	74.50 ± 4.65	0.263	72.57 ± 7.90	80.03 ± 7.39	0.807	78.09 ± 7.31	66.27 ± 5.19	0.202
Mpp_4_VE	80.73 ± 5.23	73.78 ± 4.88	0.207	66.50 ± 7.38	84.87 ± 7.44	0.700	85.01 ± 5.64	60.02 ± 5.43	0.046
Mpp_5_VE	85.39 ± 4.66	68.00 ± 5.41	0.012	72.64 ± 6.63	81.30 ± 7.81	0.707	90.21 ± 5.19	54.24 ± 5.08	0.001
Mpp_6_VE	85.10 ± 4.59	68.16 ± 5.44	0.025	72.62 ± 6.70	81.61 ± 7.69	0.758	89.36 ± 5.06	54.77 ± 5.09	0.004

Entropy_0_VE	74.57 ± 5.61	77.53 ± 4.86	0.960	65.06 ± 8.40	84.74 ± 6.82	0.665	81.87 ± 5.80	61.90 ± 5.82	0.209
Entropy_2_VE	75.06 ± 5.89	77.82 ± 4.64	0.619	58.04 ± 6.97	84.30 ± 6.98	0.443	77.44 ± 6.33	62.81 ± 4.58	0.642
Entropy_3_VE	72.67 ± 5.57	80.27 ± 4.60	0.574	59.79 ± 6.02	83.72 ± 7.00	0.784	75.12 ± 7.29	67.20 ± 4.38	0.784
Entropy_4_VE	80.71 ± 5.20	73.02 ± 5.04	0.143	55.18 ± 4.43	84.60 ± 7.13	0.624	74.51 ± 6.73	70.22 ± 5.24	0.896
Entropy_5_VE	78.30 ± 5.32	75.29 ± 4.96	0.397	65.86 ± 7.13	84.35 ± 7.22	0.748	81.18 ± 6.25	63.80 ± 5.83	0.071
Entropy_6_VE	79.32 ± 5.03	74.35 ± 5.18	0.424	65.80 ± 7.57	81.27 ± 7.47	0.756	80.11 ± 5.91	64.99 ± 6.03	0.141
Skewness_0_VE	74.76 ± 6.04	78.59 ± 4.55	0.406	68.47 ± 8.16	82.86 ± 7.23	0.744	70.95 ± 7.93	66.93 ± 4.09	0.576
Skewness_2_VE	75.82 ± 6.13	78.19 ± 4.58	0.528	60.71 ± 5.97	85.20 ± 7.35	0.231	75.49 ± 8.04	65.96 ± 4.38	0.831
Skewness_3_VE	79.76 ± 4.84	76.62 ± 4.80	0.477	72.68 ± 7.22	81.29 ± 7.86	0.578	80.11 ± 5.73	66.31 ± 4.43	0.706
Skewness_4_VE	75.66 ± 5.61	77.93 ± 4.71	0.616	65.76 ± 7.69	87.13 ± 7.45	0.241	76.24 ± 7.30	68.76 ± 5.13	0.799
Skewness_5_VE	73.23 ± 5.80	80.04 ± 4.63	0.372	64.72 ± 7.29	90.54 ± 6.89	0.192	76.41 ± 7.21	68.86 ± 5.18	0.828
Skewness_6_VE	74.05 ± 5.32	80.01 ± 4.77	0.375	53.10 ± 5.05	94.72 ± 6.19	0.026	77.23 ± 6.40	68.26 ± 5.47	0.961
Kurtosis_0_VE	77.09 ± 4.67	75.76 ± 5.81	0.960	85.51 ± 6.93	58.47 ± 5.99	0.519	63.30 ± 4.31	79.71 ± 6.10	0.604
Kurtosis_2_VE	77.74 ± 4.77	71.27 ± 4.69	0.811	82.56 ± 7.96	71.30 ± 7.34	0.663	72.32 ± 6.23	72.18 ± 6.01	0.588
Kurtosis_3_VE	74.00 ± 4.91	75.09 ± 4.39	0.213	86.54 ± 7.30	54.87 ± 4.96	0.249	67.76 ± 6.41	76.61 ± 5.34	0.040
Kurtosis_4_VE	71.74 ± 4.86	76.94 ± 4.35	0.010	85.19 ± 7.66	68.47 ± 6.96	0.630	65.30 ± 6.07	79.15 ± 5.57	0.001
Kurtosis_5_VE	71.47 ± 5.10	77.94 ± 4.09	0.008	86.54 ± 7.85	70.26 ± 6.25	0.740	65.17 ± 6.67	80.18 ± 5.21	0.002
Kurtosis_6_VE	68.29 ± 5.54	78.49 ± 3.92	0.039	82.25 ± 8.04	73.96 ± 6.11	0.529	61.60 ± 6.28	81.54 ± 4.71	0.037

Table 27: Spearman's correlation between histopathological results and texture analysis of the PET images. * p < 0.05; ** p < 0.01

		CD105	VEGF	CA-IX	GLUT	HiF1 α
mean_0_PET	Correlation Coefficient	-.059	-.155	-.034	-.062	-.025
	Sig. (2-tailed)	.488	.061	.685	.454	.768
sd_0_PET	Correlation Coefficient	.108	.117	-.006	.201*	-.257**
	Sig. (2-tailed)	.206	.160	.944	.015	.002
entropy_0_PET	Correlation Coefficient	.093	.144	.104	-.095	.110
	Sig. (2-tailed)	.274	.082	.212	.252	.184
mpp_0_PET	Correlation Coefficient	-.059	-.155	-.034	-.062	-.025
	Sig. (2-tailed)	.488	.061	.685	.454	.768
skewness_0_PET	Correlation Coefficient	.054	.210*	.050	.149	.018
	Sig. (2-tailed)	.523	.011	.547	.072	.833
kurtosis_0_PET	Correlation Coefficient	.039	.077	.002	-.102	.239**
	Sig. (2-tailed)	.644	.355	.977	.222	.004
mean_2_PET	Correlation Coefficient	-.158	-.229**	-.135	-.017	.029
	Sig. (2-tailed)	.063	.005	.104	.835	.725
sd_2_PET	Correlation Coefficient	-.040	-.013	-.099	.108	-.109
	Sig. (2-tailed)	.635	.871	.235	.196	.187
entropy_2_PET	Correlation Coefficient	.093	.143	.103	-.095	.108
	Sig. (2-tailed)	.272	.083	.216	.253	.193
mpp_2_PET	Correlation Coefficient	-.035	-.024	-.047	.105	-.169*
	Sig. (2-tailed)	.677	.772	.573	.209	.041
skewness_2_PET	Correlation Coefficient	.181*	.161	.112	.040	-.019
	Sig. (2-tailed)	.032	.051	.179	.631	.817
kurtosis_2_PET	Correlation Coefficient	.201*	.140	.072	-.047	.057
	Sig. (2-tailed)	.017	.091	.385	.577	.497
mean_3_PET	Correlation Coefficient	-.157	-.228**	-.127	-.015	.025
	Sig. (2-tailed)	.064	.006	.125	.856	.768
sd_3_PET	Correlation Coefficient	-.020	.001	-.083	.132	-.126
	Sig. (2-tailed)	.817	.989	.317	.111	.128
entropy_3_PET	Correlation Coefficient	.093	.144	.101	-.096	.108
	Sig. (2-tailed)	.273	.082	.222	.247	.191
mpp_3_PET	Correlation Coefficient	-.032	-.010	-.069	.126	-.169*
	Sig. (2-tailed)	.712	.902	.405	.130	.040
skewness_3_PET	Correlation Coefficient	.211*	.189*	.118	.071	-.028
	Sig. (2-tailed)	.012	.022	.156	.392	.736

kurtosis_3_PET	Correlation Coefficient	.225**	.175*	.086	-.020	.057
	Sig. (2-tailed)	.008	.034	.298	.813	.494
mean_4_PET	Correlation Coefficient	-.161	-.233**	-.120	-.012	.017
	Sig. (2-tailed)	.058	.005	.149	.883	.834
sd_4_PET	Correlation Coefficient	-.016	.019	-.085	.144	-.128
	Sig. (2-tailed)	.854	.824	.306	.082	.122
entropy_4_PET	Correlation Coefficient	.093	.144	.101	-.096	.108
	Sig. (2-tailed)	.276	.081	.224	.251	.192
mpp_4_PET	Correlation Coefficient	-.046	-.011	-.090	.146	-.143
	Sig. (2-tailed)	.589	.897	.278	.078	.083
skewness_4_PET	Correlation Coefficient	.237**	.222**	.122	.090	-.008
	Sig. (2-tailed)	.005	.007	.142	.281	.928
kurtosis_4_PET	Correlation Coefficient	.241**	.191*	.095	-.001	.089
	Sig. (2-tailed)	.004	.020	.251	.991	.284
mean_5_PET	Correlation Coefficient	-.154	-.223**	-.114	-.009	.007
	Sig. (2-tailed)	.069	.007	.169	.918	.932
sd_5_PET	Correlation Coefficient	-.007	.039	-.075	.154	-.139
	Sig. (2-tailed)	.933	.641	.367	.064	.094
entropy_5_PET	Correlation Coefficient	.093	.142	.103	-.096	.107
	Sig. (2-tailed)	.273	.087	.216	.250	.197
mpp_5_PET	Correlation Coefficient	-.069	-.036	-.105	.119	-.111
	Sig. (2-tailed)	.416	.663	.205	.154	.182
skewness_5_PET	Correlation Coefficient	.238**	.252**	.109	.116	.020
	Sig. (2-tailed)	.005	.002	.189	.165	.811
kurtosis_5_PET	Correlation Coefficient	.239**	.197*	.086	.003	.134
	Sig. (2-tailed)	.004	.017	.299	.971	.107
mean_6_PET	Correlation Coefficient	-.148	-.220**	-.102	-.004	-.001
	Sig. (2-tailed)	.080	.007	.219	.963	.989
sd_6_PET	Correlation Coefficient	.000	.048	-.076	.154	-.140
	Sig. (2-tailed)	.997	.561	.362	.064	.090
entropy_6_PET	Correlation Coefficient	.091	.143	.100	-.096	.109
	Sig. (2-tailed)	.283	.084	.227	.248	.189
mpp_6_PET	Correlation Coefficient	-.042	-.056	-.103	.127	-.124
	Sig. (2-tailed)	.623	.503	.216	.128	.135
skewness_6_PET	Correlation Coefficient	.187*	.243**	.080	.119	.049
	Sig. (2-tailed)	.027	.003	.338	.154	.557
kurtosis_6_PET	Correlation Coefficient	.202*	.180*	.063	-.015	.183*
	Sig. (2-tailed)	.017	.029	.447	.856	.027

total_6_PET	Correlation Coefficient	.091	.143	.100	-.096	.109
	Sig. (2-tailed)	.284	.085	.228	.250	.189

Table 28: Spearman's correlation between histopathological results and texture analysis of the non-contrast CT images. * $p < 0.05$; ** $p < 0.01$

		CD105	VEGF	CA-IX	GLUT	HiF1 α
mean_0_CT	Correlation Coefficient	.093	.065	.063	.076	.005
	Sig. (2-tailed)	.275	.436	.451	.360	.953
sd_0_CT	Correlation Coefficient	.105	.119	-.140	-.003	-.082
	Sig. (2-tailed)	.216	.150	.090	.969	.321
entropy_0_CT	Correlation Coefficient	.154	.191*	-.106	.015	-.101
	Sig. (2-tailed)	.069	.020	.202	.854	.224
mpp_0_CT	Correlation Coefficient	.149	.134	.002	.070	-.057
	Sig. (2-tailed)	.078	.107	.978	.399	.489
skewness_0_CT	Correlation Coefficient	.147	.022	-.118	-.092	-.066
	Sig. (2-tailed)	.083	.788	.156	.269	.427
kurtosis_0_CT	Correlation Coefficient	.022	-.053	.119	-.023	.118
	Sig. (2-tailed)	.793	.521	.151	.780	.155
mean_2_CT	Correlation Coefficient	-.134	-.001	-.050	.071	-.059
	Sig. (2-tailed)	.114	.988	.548	.397	.478
sd_2_CT	Correlation Coefficient	.095	.104	-.119	.037	.002
	Sig. (2-tailed)	.265	.210	.153	.656	.977
entropy_2_CT	Correlation Coefficient	.189*	.221**	-.018	.120	-.068
	Sig. (2-tailed)	.025	.007	.829	.150	.412
mpp_2_CT	Correlation Coefficient	.066	.091	-.122	.059	-.029
	Sig. (2-tailed)	.438	.275	.141	.480	.723
skewness_2_CT	Correlation Coefficient	.058	-.011	-.082	-.108	.093
	Sig. (2-tailed)	.494	.898	.321	.196	.263
kurtosis_2_CT	Correlation Coefficient	.097	.015	.045	-.088	.080
	Sig. (2-tailed)	.252	.857	.585	.293	.338
mean_3_CT	Correlation Coefficient	-.136	.021	-.053	.097	-.113
	Sig. (2-tailed)	.109	.800	.522	.244	.175
sd_3_CT	Correlation Coefficient	.024	.029	-.092	.036	.055
	Sig. (2-tailed)	.781	.729	.270	.662	.512
entropy_3_CT	Correlation Coefficient	.086	.150	-.017	.129	-.022
	Sig. (2-tailed)	.310	.070	.835	.122	.788
mpp_3_CT	Correlation Coefficient	-.019	.039	-.107	.075	.001
	Sig. (2-tailed)	.821	.639	.196	.365	.990

skewness_3_CT	Correlation Coefficient	.049	-.043	.027	-.045	.131
	Sig. (2-tailed)	.569	.606	.749	.586	.113
kurtosis_3_CT	Correlation Coefficient	.032	-.008	.104	-.104	.118
	Sig. (2-tailed)	.706	.925	.212	.213	.154
mean_4_CT	Correlation Coefficient	-.132	.034	-.039	.108	-.139
	Sig. (2-tailed)	.121	.685	.636	.197	.092
sd_4_CT	Correlation Coefficient	.017	-.002	-.046	.015	.081
	Sig. (2-tailed)	.843	.983	.576	.856	.331
entropy_4_CT	Correlation Coefficient	.070	.109	-.018	.109	.029
	Sig. (2-tailed)	.411	.188	.829	.189	.731
mpp_4_CT	Correlation Coefficient	-.066	.016	-.084	.043	.025
	Sig. (2-tailed)	.438	.850	.313	.605	.765
skewness_4_CT	Correlation Coefficient	.020	-.050	.001	-.043	.065
	Sig. (2-tailed)	.815	.551	.992	.605	.433
kurtosis_4_CT	Correlation Coefficient	.076	.007	.137	-.010	.038
	Sig. (2-tailed)	.371	.933	.098	.904	.650
mean_5_CT	Correlation Coefficient	-.123	.034	-.030	.107	-.152
	Sig. (2-tailed)	.148	.684	.716	.197	.066
sd_5_CT	Correlation Coefficient	.009	-.010	.012	-.012	.077
	Sig. (2-tailed)	.917	.904	.889	.883	.352
entropy_5_CT	Correlation Coefficient	.056	.082	.018	.048	.054
	Sig. (2-tailed)	.509	.324	.828	.562	.512
mpp_5_CT	Correlation Coefficient	-.065	.027	-.041	.004	-.005
	Sig. (2-tailed)	.445	.742	.618	.961	.947
skewness_5_CT	Correlation Coefficient	-.015	-.048	-.007	-.094	.046
	Sig. (2-tailed)	.858	.561	.929	.259	.577
kurtosis_5_CT	Correlation Coefficient	.118	.012	.145	.042	.004
	Sig. (2-tailed)	.167	.890	.080	.613	.965
mean_6_CT	Correlation Coefficient	-.094	.036	-.010	.097	-.162*
	Sig. (2-tailed)	.268	.662	.900	.246	.050
sd_6_CT	Correlation Coefficient	.030	-.003	.038	-.035	.018
	Sig. (2-tailed)	.728	.976	.649	.673	.833
entropy_6_CT	Correlation Coefficient	.084	.098	.057	.007	.002
	Sig. (2-tailed)	.324	.240	.492	.936	.978
mpp_6_CT	Correlation Coefficient	-.058	.017	-.002	-.021	-.046
	Sig. (2-tailed)	.498	.839	.980	.799	.578
skewness_6_CT	Correlation Coefficient	-.024	.010	.010	-.079	.056
	Sig. (2-tailed)	.778	.901	.901	.343	.499

kurtosis_6_CT	Correlation Coefficient	.105	.004	.103	.049	.022
	Sig. (2-tailed)	.218	.960	.215	.558	.793
total_6_CT	Correlation Coefficient	.203*	.168*	.080	.030	-.047
	Sig. (2-tailed)	.016	.042	.333	.718	.568

Table 29: Spearman's correlation between histopathological results and texture analysis of the contrast-enhanced CT images. * $p < 0.05$; ** $p < 0.01$

		CD105	VEGF	CA-IX	GLUT	HiF1 α
mean_0_VE	Correlation Coefficient	.145	.081	.162	-.083	-.057
	Sig. (2-tailed)	.120	.372	.072	.364	.528
sd_0_VE	Correlation Coefficient	-.114	-.042	-.186*	.007	-.070
	Sig. (2-tailed)	.221	.645	.039	.938	.445
entropy_0_VE	Correlation Coefficient	-.035	.004	-.165	.002	-.088
	Sig. (2-tailed)	.709	.966	.067	.983	.334
mpp_0_VE	Correlation Coefficient	.126	.065	.129	-.063	-.072
	Sig. (2-tailed)	.176	.473	.153	.489	.431
skewness_0_VE	Correlation Coefficient	-.146	-.109	-.202*	-.062	.031
	Sig. (2-tailed)	.117	.230	.024	.499	.731
kurtosis_0_VE	Correlation Coefficient	.145	.114	.189*	-.181*	.086
	Sig. (2-tailed)	.119	.210	.035	.046	.342
mean_2_VE	Correlation Coefficient	-.156	-.051	.012	-.085	.003
	Sig. (2-tailed)	.093	.576	.894	.353	.977
sd_2_VE	Correlation Coefficient	-.290**	-.183*	-.219*	-.077	.012
	Sig. (2-tailed)	.002	.043	.015	.402	.896
entropy_2_VE	Correlation Coefficient	-.051	-.024	-.143	-.085	.000
	Sig. (2-tailed)	.587	.796	.113	.351	.998
mpp_2_VE	Correlation Coefficient	-.283**	-.165	-.221*	-.111	.014
	Sig. (2-tailed)	.002	.069	.014	.224	.879
skewness_2_VE	Correlation Coefficient	-.103	.028	-.093	-.086	.029
	Sig. (2-tailed)	.268	.755	.306	.348	.747
kurtosis_2_VE	Correlation Coefficient	.168	.138	.093	-.045	.071
	Sig. (2-tailed)	.071	.129	.304	.623	.437
mean_3_VE	Correlation Coefficient	-.148	-.058	.066	-.098	-.018
	Sig. (2-tailed)	.110	.523	.466	.282	.846
sd_3_VE	Correlation Coefficient	-.178	-.068	-.022	.035	.019
	Sig. (2-tailed)	.054	.452	.804	.705	.832
entropy_3_VE	Correlation Coefficient	-.020	.059	-.006	.006	-.023
	Sig. (2-tailed)	.827	.517	.948	.944	.802

mpp_3_VE	Correlation Coefficient	-.221*	-.077	-.043	-.019	.006
	Sig. (2-tailed)	.017	.398	.635	.837	.947
skewness_3_VE	Correlation Coefficient	-.138	-.022	-.049	-.047	-.031
	Sig. (2-tailed)	.139	.809	.590	.608	.737
kurtosis_3_VE	Correlation Coefficient	.215*	.002	.148	-.097	.093
	Sig. (2-tailed)	.020	.984	.101	.290	.308
mean_4_VE	Correlation Coefficient	-.122	-.053	.086	-.085	-.040
	Sig. (2-tailed)	.190	.559	.343	.351	.657
sd_4_VE	Correlation Coefficient	-.066	.022	.094	.076	-.011
	Sig. (2-tailed)	.478	.811	.297	.406	.904
entropy_4_VE	Correlation Coefficient	.071	.131	.076	.046	-.069
	Sig. (2-tailed)	.448	.147	.401	.616	.448
mpp_4_VE	Correlation Coefficient	-.119	-.002	.062	.014	-.025
	Sig. (2-tailed)	.199	.986	.496	.882	.784
skewness_4_VE	Correlation Coefficient	-.150	-.048	-.032	-.011	-.050
	Sig. (2-tailed)	.105	.598	.727	.908	.585
kurtosis_4_VE	Correlation Coefficient	.208*	-.012	.121	-.083	.110
	Sig. (2-tailed)	.024	.892	.182	.363	.225
mean_5_VE	Correlation Coefficient	-.092	-.044	.102	-.068	-.065
	Sig. (2-tailed)	.321	.629	.259	.457	.475
sd_5_VE	Correlation Coefficient	.029	.062	.169	.089	-.040
	Sig. (2-tailed)	.758	.494	.060	.328	.657
entropy_5_VE	Correlation Coefficient	.149	.162	.157	.044	-.047
	Sig. (2-tailed)	.108	.074	.082	.630	.603
mpp_5_VE	Correlation Coefficient	-.028	.035	.127	.052	-.086
	Sig. (2-tailed)	.760	.698	.158	.573	.343
skewness_5_VE	Correlation Coefficient	-.131	-.037	-.041	.003	-.041
	Sig. (2-tailed)	.159	.688	.652	.972	.655
kurtosis_5_VE	Correlation Coefficient	.158	.022	.113	-.062	.042
	Sig. (2-tailed)	.090	.805	.213	.497	.641
mean_6_VE	Correlation Coefficient	-.078	-.036	.103	-.021	-.095
	Sig. (2-tailed)	.400	.696	.254	.820	.294
sd_6_VE	Correlation Coefficient	.113	.096	.208*	.096	-.058
	Sig. (2-tailed)	.224	.292	.021	.293	.525
entropy_6_VE	Correlation Coefficient	.209*	.180*	.168	.058	-.063
	Sig. (2-tailed)	.024	.047	.063	.523	.490
mpp_6_VE	Correlation Coefficient	.077	.068	.206*	.089	-.114
	Sig. (2-tailed)	.411	.453	.022	.328	.211

skewness_6_VE	Correlation Coefficient	-.064	.018	-.073	.008	-.009
	Sig. (2-tailed)	.495	.842	.418	.930	.922
kurtosis_6_VE	Correlation Coefficient	.024	-.044	.073	-.053	-.014
	Sig. (2-tailed)	.798	.630	.420	.560	.877
total_6_VE	Correlation Coefficient	.300**	.225*	.050	-.056	.037
	Sig. (2-tailed)	.001	.012	.581	.540	.686

Table 30: Correlation between protein signal intensities from the exosomes and texture parameters from the PET images. * $p < 0.05$; ** $p < 0.01$

		HER1	HER2	HER3	cMET	P4HA1	S100A9
mean_0_PET	Correlation Coefficient	0.078	0.009	0.137	-0.048	0.149	-.321*
	Sig. (2-tailed)	0.579	0.950	0.329	0.735	0.286	0.019
sd_0_PET	Correlation Coefficient	0.184	0.085	0.147	0.129	.368**	-.292*
	Sig. (2-tailed)	0.187	0.545	0.295	0.361	0.007	0.034
entropy_0_PET	Correlation Coefficient	-0.085	0.005	-0.035	0.075	0.056	-0.087
	Sig. (2-tailed)	0.547	0.971	0.804	0.597	0.689	0.534
mpp_0_PET	Correlation Coefficient	0.078	0.009	0.137	-0.048	0.149	-.321*
	Sig. (2-tailed)	0.579	0.950	0.329	0.735	0.286	0.019
skewness_0_PET	Correlation Coefficient	0.041	0.065	0.144	0.130	-0.019	0.086
	Sig. (2-tailed)	0.771	0.645	0.305	0.357	0.893	0.539
kurtosis_0_PET	Correlation Coefficient	-0.168	-0.071	-0.026	0.019	-0.113	0.120
	Sig. (2-tailed)	0.229	0.614	0.854	0.893	0.419	0.391
mean_2_PET	Correlation Coefficient	0.063	-0.051	0.063	-0.128	0.182	-0.154
	Sig. (2-tailed)	0.655	0.718	0.654	0.367	0.193	0.270
sd_2_PET	Correlation Coefficient	0.187	0.067	0.155	0.029	0.266	-0.129
	Sig. (2-tailed)	0.180	0.634	0.269	0.838	0.055	0.356
entropy_2_PET	Correlation Coefficient	-0.073	0.008	-0.037	0.075	0.064	-0.082
	Sig. (2-tailed)	0.602	0.953	0.792	0.598	0.650	0.561
mpp_2_PET	Correlation Coefficient	0.195	0.071	0.141	0.018	.276*	-0.151
	Sig. (2-tailed)	0.162	0.615	0.313	0.902	0.046	0.279
skewness_2_PET	Correlation Coefficient	-0.071	-0.064	-0.022	0.010	-0.100	-0.117
	Sig. (2-tailed)	0.611	0.651	0.878	0.943	0.477	0.404
kurtosis_2_PET	Correlation Coefficient	-0.112	-0.132	-0.040	0.080	-0.067	-0.080
	Sig. (2-tailed)	0.427	0.345	0.778	0.575	0.634	0.570
mean_3_PET	Correlation Coefficient	0.069	-0.037	0.075	-0.122	0.166	-0.141
	Sig. (2-tailed)	0.621	0.790	0.593	0.390	0.235	0.313
sd_3_PET	Correlation Coefficient	0.171	0.082	0.163	0.052	.281*	-0.151
	Sig. (2-tailed)	0.221	0.561	0.244	0.714	0.041	0.280

entropy_3_PET	Correlation Coefficient	-0.079	0.006	-0.030	0.078	0.059	-0.087
	Sig. (2-tailed)	0.574	0.965	0.830	0.583	0.676	0.535
mpp_3_PET	Correlation Coefficient	0.196	0.059	0.128	0.014	.273*	-0.165
	Sig. (2-tailed)	0.160	0.676	0.361	0.920	0.048	0.236
skewness_3_PET	Correlation Coefficient	0.000	-0.003	0.003	0.046	-0.082	-0.042
	Sig. (2-tailed)	0.998	0.985	0.984	0.745	0.558	0.766
kurtosis_3_PET	Correlation Coefficient	-0.130	-0.118	-0.060	0.095	-0.089	-0.070
	Sig. (2-tailed)	0.353	0.399	0.668	0.503	0.527	0.618
mean_4_PET	Correlation Coefficient	0.074	-0.013	0.104	-0.110	0.133	-0.135
	Sig. (2-tailed)	0.597	0.925	0.458	0.438	0.343	0.336
sd_4_PET	Correlation Coefficient	0.165	0.082	0.170	0.080	.285*	-0.181
	Sig. (2-tailed)	0.238	0.557	0.224	0.573	0.038	0.196
entropy_4_PET	Correlation Coefficient	-0.081	0.011	-0.028	0.084	0.057	-0.084
	Sig. (2-tailed)	0.564	0.940	0.841	0.553	0.685	0.549
mpp_4_PET	Correlation Coefficient	0.159	0.065	0.155	0.076	0.269	-0.168
	Sig. (2-tailed)	0.257	0.645	0.267	0.591	0.052	0.229
skewness_4_PET	Correlation Coefficient	0.023	0.072	0.041	0.134	-0.096	0.036
	Sig. (2-tailed)	0.870	0.608	0.769	0.343	0.494	0.796
kurtosis_4_PET	Correlation Coefficient	-0.126	-0.081	-0.041	0.118	-0.097	-0.049
	Sig. (2-tailed)	0.367	0.566	0.772	0.404	0.491	0.728
mean_5_PET	Correlation Coefficient	0.065	-0.002	0.121	-0.099	0.114	-0.139
	Sig. (2-tailed)	0.642	0.987	0.389	0.487	0.417	0.321
sd_5_PET	Correlation Coefficient	0.148	0.080	0.161	0.102	.290*	-0.202
	Sig. (2-tailed)	0.290	0.570	0.249	0.471	0.035	0.146
entropy_5_PET	Correlation Coefficient	-0.071	0.009	-0.030	0.078	0.062	-0.093
	Sig. (2-tailed)	0.612	0.948	0.833	0.584	0.659	0.506
mpp_5_PET	Correlation Coefficient	0.171	0.067	0.179	0.090	0.255	-0.157
	Sig. (2-tailed)	0.222	0.632	0.199	0.526	0.066	0.262
skewness_5_PET	Correlation Coefficient	0.030	0.100	0.078	0.197	-0.068	0.090
	Sig. (2-tailed)	0.829	0.478	0.579	0.161	0.629	0.520
kurtosis_5_PET	Correlation Coefficient	-0.118	-0.069	-0.034	0.131	-0.113	-0.005
	Sig. (2-tailed)	0.402	0.623	0.808	0.355	0.421	0.973
mean_6_PET	Correlation Coefficient	0.080	0.005	0.122	-0.092	0.100	-0.158
	Sig. (2-tailed)	0.568	0.973	0.383	0.518	0.478	0.259
sd_6_PET	Correlation Coefficient	0.153	0.078	0.168	0.100	.290*	-0.209
	Sig. (2-tailed)	0.273	0.579	0.228	0.482	0.035	0.133
entropy_6_PET	Correlation Coefficient	-0.080	0.009	-0.030	0.081	0.057	-0.086
	Sig. (2-tailed)	0.570	0.949	0.831	0.570	0.686	0.539

mpp_6_PET	Correlation Coefficient	0.160	0.070	0.188	0.113	0.244	-0.149
	Sig. (2-tailed)	0.251	0.616	0.178	0.425	0.078	0.286
skewness_6_PET	Correlation Coefficient	0.054	0.134	0.120	0.219	-0.021	0.101
	Sig. (2-tailed)	0.702	0.340	0.394	0.120	0.880	0.473
kurtosis_6_PET	Correlation Coefficient	-0.124	-0.050	-0.021	0.141	-0.150	0.020
	Sig. (2-tailed)	0.377	0.722	0.883	0.318	0.285	0.885
total_6_PET	Correlation Coefficient	-0.080	0.009	-0.030	0.081	0.057	-0.086
	Sig. (2-tailed)	0.568	0.950	0.830	0.568	0.685	0.540

Table 31: Correlation between protein signal intensities from the exosomes and texture parameters from the non-contrast CT images. * $p < 0.05$; ** $p < 0.01$

		HER1	HER2	HER3	cMET	P4HA1	S100A9
mean_0_CT	Correlation Coefficient	-0.008	-0.066	-0.026	0.048	0.155	0.206
	Sig. (2-tailed)	0.956	0.638	0.851	0.738	0.268	0.138
sd_0_CT	Correlation Coefficient	0.038	0.139	0.178	0.011	-0.045	0.043
	Sig. (2-tailed)	0.785	0.321	0.202	0.936	0.747	0.757
entropy_0_CT	Correlation Coefficient	-0.095	0.039	0.055	0.037	-0.098	-0.008
	Sig. (2-tailed)	0.496	0.779	0.696	0.794	0.485	0.953
mpp_0_CT	Correlation Coefficient	0.050	0.030	0.069	0.097	0.141	0.222
	Sig. (2-tailed)	0.725	0.831	0.624	0.495	0.315	0.111
skewness_0_CT	Correlation Coefficient	-0.173	-0.083	0.033	-0.183	-0.075	-0.158
	Sig. (2-tailed)	0.215	0.554	0.815	0.195	0.595	0.258
kurtosis_0_CT	Correlation Coefficient	0.009	-0.054	-0.048	-0.133	-0.001	0.122
	Sig. (2-tailed)	0.946	0.704	0.731	0.347	0.992	0.383
mean_2_CT	Correlation Coefficient	-0.097	-0.094	-0.109	-0.153	-0.002	0.023
	Sig. (2-tailed)	0.488	0.505	0.436	0.279	0.990	0.868
sd_2_CT	Correlation Coefficient	-0.019	-0.037	0.043	-0.084	-0.028	0.122
	Sig. (2-tailed)	0.895	0.790	0.758	0.555	0.843	0.382
entropy_2_CT	Correlation Coefficient	-0.174	-0.139	-0.058	-0.024	-0.083	0.056
	Sig. (2-tailed)	0.213	0.320	0.679	0.864	0.555	0.691
mpp_2_CT	Correlation Coefficient	-0.041	-0.016	0.070	-0.071	-0.033	0.113
	Sig. (2-tailed)	0.770	0.911	0.618	0.618	0.816	0.420
skewness_2_CT	Correlation Coefficient	-0.024	-0.016	0.109	-0.081	0.021	-0.110
	Sig. (2-tailed)	0.866	0.907	0.437	0.570	0.880	0.435
kurtosis_2_CT	Correlation Coefficient	0.181	0.006	-0.091	-0.215	0.039	0.088
	Sig. (2-tailed)	0.196	0.965	0.517	0.126	0.782	0.531
mean_3_CT	Correlation Coefficient	-0.129	-0.122	-0.127	-0.122	0.089	0.067
	Sig. (2-tailed)	0.357	0.382	0.367	0.389	0.525	0.632
sd_3_CT	Correlation Coefficient	0.016	0.010	0.012	-0.264	0.002	0.081

	Sig. (2-tailed)	0.912	0.943	0.930	0.058	0.989	0.565
entropy_3_CT	Correlation Coefficient	-0.108	-0.179	-0.118	-0.242	0.023	0.045
	Sig. (2-tailed)	0.441	0.199	0.399	0.083	0.870	0.747
mpp_3_CT	Correlation Coefficient	0.030	0.062	0.060	-0.171	0.026	0.159
	Sig. (2-tailed)	0.829	0.657	0.671	0.225	0.855	0.255
skewness_3_CT	Correlation Coefficient	0.043	0.059	0.244	-0.054	0.028	-0.035
	Sig. (2-tailed)	0.761	0.675	0.078	0.702	0.844	0.803
kurtosis_3_CT	Correlation Coefficient	0.100	0.084	0.005	-0.126	0.032	0.044
	Sig. (2-tailed)	0.477	0.548	0.973	0.375	0.819	0.753
mean_4_CT	Correlation Coefficient	-0.140	-0.132	-0.113	-0.070	0.095	0.106
	Sig. (2-tailed)	0.317	0.347	0.420	0.624	0.499	0.448
sd_4_CT	Correlation Coefficient	0.052	0.131	0.027	-0.255	0.071	0.074
	Sig. (2-tailed)	0.710	0.350	0.850	0.068	0.612	0.596
entropy_4_CT	Correlation Coefficient	-0.076	-0.107	-0.092	-.280*	0.051	0.019
	Sig. (2-tailed)	0.591	0.448	0.514	0.044	0.717	0.893
mpp_4_CT	Correlation Coefficient	0.060	0.112	0.048	-0.141	0.041	0.184
	Sig. (2-tailed)	0.670	0.425	0.730	0.320	0.769	0.187
skewness_4_CT	Correlation Coefficient	0.024	0.070	0.118	-0.135	-0.022	-0.040
	Sig. (2-tailed)	0.867	0.617	0.399	0.342	0.874	0.774
kurtosis_4_CT	Correlation Coefficient	-0.087	0.089	-0.021	-0.245	-0.050	-0.006
	Sig. (2-tailed)	0.538	0.525	0.880	0.080	0.724	0.966
mean_5_CT	Correlation Coefficient	-0.146	-0.100	-0.066	-0.014	0.055	0.158
	Sig. (2-tailed)	0.296	0.478	0.640	0.924	0.697	0.259
sd_5_CT	Correlation Coefficient	-0.014	0.192	0.019	-0.196	0.076	0.034
	Sig. (2-tailed)	0.918	0.169	0.892	0.163	0.590	0.809
entropy_5_CT	Correlation Coefficient	-0.127	-0.026	-0.119	-0.234	0.064	0.007
	Sig. (2-tailed)	0.366	0.851	0.395	0.095	0.651	0.959
mpp_5_CT	Correlation Coefficient	-0.018	0.163	0.031	-0.102	0.043	0.185
	Sig. (2-tailed)	0.898	0.243	0.824	0.470	0.761	0.184
skewness_5_CT	Correlation Coefficient	-0.073	0.003	-0.009	-0.241	-0.046	-0.083
	Sig. (2-tailed)	0.605	0.981	0.950	0.085	0.743	0.554
kurtosis_5_CT	Correlation Coefficient	-0.036	0.062	0.037	-0.159	-0.067	0.010
	Sig. (2-tailed)	0.799	0.659	0.793	0.261	0.636	0.946
mean_6_CT	Correlation Coefficient	-0.140	-0.045	-0.020	0.048	0.023	0.197
	Sig. (2-tailed)	0.317	0.749	0.888	0.733	0.869	0.158
sd_6_CT	Correlation Coefficient	-0.077	0.192	-0.025	-0.145	0.043	0.062
	Sig. (2-tailed)	0.586	0.169	0.860	0.305	0.759	0.660
entropy_6_CT	Correlation Coefficient	-0.145	0.046	-0.125	-0.189	0.038	0.038
	Sig. (2-tailed)	0.302	0.745	0.373	0.179	0.789	0.787

mpp_6_CT	Correlation Coefficient	-0.120	0.100	-0.023	-0.079	0.010	0.162
	Sig. (2-tailed)	0.392	0.476	0.868	0.578	0.941	0.246
skewness_6_CT	Correlation Coefficient	-0.151	0.019	-0.046	-0.260	-0.059	-0.095
	Sig. (2-tailed)	0.281	0.894	0.744	0.063	0.677	0.500
kurtosis_6_CT	Correlation Coefficient	0.105	0.106	0.216	0.032	-0.094	0.080
	Sig. (2-tailed)	0.456	0.451	0.120	0.822	0.503	0.571
total_6_CT	Correlation Coefficient	-0.126	0.011	0.021	0.067	-0.015	-0.061
	Sig. (2-tailed)	0.370	0.936	0.880	0.639	0.917	0.664

Table 32: Correlation between protein signal intensities from the exosomes and texture parameters from the contrast-enhanced CT images. * $p < 0.05$; ** $p < 0.01$

		HER1	HER2	HER3	cMET	P4HA1	S100A9
mean_0_VE	Correlation Coefficient	0.144	0.023	-0.087	0.040	0.148	0.002
	Sig. (2-tailed)	0.314	0.872	0.542	0.785	0.301	0.986
sd_0_VE	Correlation Coefficient	-0.158	-0.097	-0.233	-0.044	-0.102	0.063
	Sig. (2-tailed)	0.267	0.497	0.100	0.760	0.478	0.659
entropy_0_VE	Correlation Coefficient	-0.124	-0.018	-0.171	-0.058	-0.071	0.106
	Sig. (2-tailed)	0.385	0.902	0.230	0.688	0.620	0.460
mpp_0_VE	Correlation Coefficient	0.116	0.009	-0.130	0.013	0.104	0.009
	Sig. (2-tailed)	0.416	0.948	0.364	0.931	0.469	0.948
skewness_0_VE	Correlation Coefficient	-0.239	-0.097	-0.081	-0.036	-0.128	-0.046
	Sig. (2-tailed)	0.091	0.500	0.572	0.802	0.371	0.749
kurtosis_0_VE	Correlation Coefficient	0.154	-0.019	-0.029	0.035	0.198	-0.040
	Sig. (2-tailed)	0.281	0.894	0.838	0.812	0.165	0.778
mean_2_VE	Correlation Coefficient	-0.193	-0.099	-0.209	-0.063	-0.032	-0.001
	Sig. (2-tailed)	0.175	0.489	0.140	0.665	0.824	0.993
sd_2_VE	Correlation Coefficient	-0.063	-0.137	-0.195	-0.031	0.042	0.158
	Sig. (2-tailed)	0.658	0.339	0.169	0.831	0.769	0.268
entropy_2_VE	Correlation Coefficient	-0.052	0.019	-0.084	0.070	0.020	0.210
	Sig. (2-tailed)	0.715	0.894	0.560	0.627	0.889	0.140
mpp_2_VE	Correlation Coefficient	-0.123	-0.181	-0.229	-0.078	0.015	0.127
	Sig. (2-tailed)	0.389	0.205	0.106	0.588	0.918	0.375
skewness_2_VE	Correlation Coefficient	-0.103	-0.090	-0.099	-0.106	0.027	0.039
	Sig. (2-tailed)	0.472	0.532	0.488	0.464	0.850	0.784
kurtosis_2_VE	Correlation Coefficient	-0.091	0.015	-0.014	0.047	0.113	-0.241
	Sig. (2-tailed)	0.524	0.917	0.921	0.747	0.431	0.088
mean_3_VE	Correlation Coefficient	-0.101	-0.092	-0.191	-0.071	0.036	0.001
	Sig. (2-tailed)	0.482	0.519	0.180	0.626	0.799	0.992
sd_3_VE	Correlation Coefficient	-0.193	-0.147	-0.210	-0.015	0.143	0.033

	Sig. (2-tailed)	0.175	0.303	0.140	0.919	0.316	0.819
entropy_3_VE	Correlation Coefficient	-0.128	0.003	-0.094	0.065	0.080	0.116
	Sig. (2-tailed)	0.369	0.983	0.514	0.654	0.578	0.418
mpp_3_VE	Correlation Coefficient	-0.167	-0.154	-0.229	-0.047	0.122	0.042
	Sig. (2-tailed)	0.242	0.281	0.106	0.743	0.393	0.772
skewness_3_VE	Correlation Coefficient	-0.152	-0.227	-0.191	-0.159	-0.012	-0.009
	Sig. (2-tailed)	0.286	0.109	0.178	0.272	0.934	0.952
kurtosis_3_VE	Correlation Coefficient	-0.035	0.048	0.066	0.030	-0.002	-0.109
	Sig. (2-tailed)	0.809	0.739	0.645	0.838	0.990	0.446
mean_4_VE	Correlation Coefficient	-0.004	-0.098	-0.190	-0.078	0.077	0.021
	Sig. (2-tailed)	0.976	0.495	0.181	0.592	0.589	0.885
sd_4_VE	Correlation Coefficient	-0.167	-0.055	-0.156	0.047	0.147	-0.003
	Sig. (2-tailed)	0.241	0.699	0.273	0.746	0.302	0.981
entropy_4_VE	Correlation Coefficient	-0.155	0.022	-0.069	0.126	0.103	0.054
	Sig. (2-tailed)	0.279	0.876	0.630	0.383	0.474	0.705
mpp_4_VE	Correlation Coefficient	-0.132	-0.130	-0.217	-0.015	0.131	-0.005
	Sig. (2-tailed)	0.356	0.362	0.127	0.920	0.358	0.973
skewness_4_VE	Correlation Coefficient	-0.146	-0.207	-0.155	-0.141	-0.057	-0.077
	Sig. (2-tailed)	0.306	0.144	0.276	0.330	0.691	0.589
kurtosis_4_VE	Correlation Coefficient	0.047	0.097	0.119	0.006	0.025	-0.057
	Sig. (2-tailed)	0.744	0.497	0.407	0.969	0.864	0.691
mean_5_VE	Correlation Coefficient	0.081	-0.113	-0.203	-0.059	0.169	0.045
	Sig. (2-tailed)	0.570	0.428	0.154	0.685	0.237	0.756
sd_5_VE	Correlation Coefficient	-0.172	-0.013	-0.144	0.099	0.093	-0.009
	Sig. (2-tailed)	0.226	0.928	0.315	0.492	0.518	0.953
entropy_5_VE	Correlation Coefficient	-0.172	0.090	-0.034	0.184	0.015	0.061
	Sig. (2-tailed)	0.227	0.528	0.812	0.201	0.916	0.672
mpp_5_VE	Correlation Coefficient	-0.102	-0.093	-0.226	-0.012	0.096	0.034
	Sig. (2-tailed)	0.476	0.516	0.110	0.934	0.505	0.812
skewness_5_VE	Correlation Coefficient	-0.126	-0.099	-0.098	-0.089	-0.133	-0.152
	Sig. (2-tailed)	0.377	0.490	0.495	0.541	0.352	0.286
kurtosis_5_VE	Correlation Coefficient	0.057	0.060	0.112	0.060	0.074	-0.065
	Sig. (2-tailed)	0.691	0.674	0.436	0.680	0.606	0.648
mean_6_VE	Correlation Coefficient	0.119	-0.096	-0.205	-0.055	0.199	0.066
	Sig. (2-tailed)	0.404	0.505	0.148	0.705	0.161	0.644
sd_6_VE	Correlation Coefficient	-0.107	0.043	-0.098	0.146	0.014	0.095
	Sig. (2-tailed)	0.457	0.764	0.494	0.310	0.922	0.508
entropy_6_VE	Correlation Coefficient	-0.090	0.147	0.002	0.210	-0.026	0.152

	Sig. (2-tailed)	0.531	0.303	0.990	0.143	0.854	0.287
mpp_6_VE	Correlation Coefficient	-0.038	-0.054	-0.197	-0.006	0.024	0.106
	Sig. (2-tailed)	0.791	0.706	0.165	0.966	0.865	0.460
skewness_6_VE	Correlation Coefficient	-0.123	0.014	-0.085	-0.124	-0.141	-0.167
	Sig. (2-tailed)	0.389	0.924	0.552	0.392	0.323	0.242
kurtosis_6_VE	Correlation Coefficient	0.047	-0.072	0.015	0.110	0.167	-0.035
	Sig. (2-tailed)	0.744	0.616	0.918	0.445	0.242	0.805
total_6_VE	Correlation Coefficient	-0.001	0.183	0.230	0.256	-0.032	0.117
	Sig. (2-tailed)	0.993	0.200	0.105	0.073	0.824	0.412